

**Discovery of acoustic emission based biomarker
for quantitative assessment
of knee joint ageing and degeneration**

Hongzhi CHEN

Thesis submitted to the University of Central Lancashire
in partial fulfilment of the requirement for the degree of

DOCTOR OF PHILOSOPHY

The work presented in this thesis was carried out at
the Applied Digital Signal and Image Processing (ADSIP) Research Centre,
University of Central Lancashire in collaboration with
the School of Health and Medicine, Lancaster University.

August 2011

Student Declaration

Concurrent registration for two or more academic awards

- Either *I declare that while registered as a candidate for the research degree, I have not been a registered candidate or enrolled student for another award of the University or other academic or professional institution
- or *I declare that while registered for the research degree, I was with the University's specific permission, a registered candidate/enrolled student for the following award:
-

Material submitted for another award

- Either *I declare that no material contained in the thesis has been used in any other submission for an academic award and is solely my own work
- or *I declare that the following material contained in the thesis formed part of a submission for the award of
-

(state award and awarding body and list the material below):

* delete as appropriate

Collaboration

Where a candidate's research programme is part of a collaborative project, the thesis must indicate in addition clearly the candidate's individual contribution and the extent of the collaboration. Please state below:

The work presented in this thesis was carried out at the Applied Digital Signal and Image Processing (ADSIP) Research Centre, University of Central Lancashire in collaboration with the School of Health and Medicine, Lancaster University.

Signature of Candidate

Hongzhi Chen

Type of Award

DOCTORAL OF PHILOSOPHY

School

COMPUTING ENGINEERING AND PHYSICAL SCIENCE

TO MY DEAREST FAMILY

ACKNOWLEDGEMENTS

My special gratitude goes to my director of studies, Professor. Lik-Kwan Shark, for his guidance and encouragement over all these years. The work presented in this thesis could not possibly be done without his inspirational ideas, valuable insights and consistent enthusiasm.

My gratitude is also expressed to Professor John Goodacre, my second supervisor, for his continuous support throughout my work and for having given me the opportunity to work with the clinical department. It has been a wonderful experience.

Special thanks to my research advisor Dr. Benoit Mascaro and former team member Mr. James Prior for the technical and clinical support.

I would also like to extend my gratitude to all the people participating in the clinical studies.

Thanks to all colleagues in the Applied Digital Signal and Image Processing (ADSIP) Research Centre, and the School of Computing, Engineering, and Physical Science (CEPS) for other supports.

Finally, I would most like to thank my family, they are the best part in my life.

ABSTRACT

Discovery of acoustic emission based biomarker for quantitative assessment of knee joint ageing and degeneration

By Hongzhi Chen

Based on the study of 34 healthy and 19 osteoarthritic knees in three different age groups (early, middle and late adulthood), this thesis reports the discovery of the potential of knee acoustic emission (AE) as a biomarker for quantitative assessment of joint ageing and degeneration.

Signal processing and statistical analysis were conducted on the joint angle signals acquired using electronic goniometers attached to the lateral side of the legs during repeated sit-stand-sit movements. A four-phase movement model derived from joint angle measurement is proposed for statistical analysis, and it consists of the ascending-acceleration and ascending-deceleration phases in the sit-to-stand movement, followed by the descending-acceleration and descending-deceleration phases in the stand-to-sit movement. Through the quantitative assessment of joint angle signals based on the four-phase model established, statistical differences of different knee conditions related to age and degeneration were discovered based on cycle-by-cycle variations and movement symmetry.

For AE burst signals acquired from piezo-electric sensors attached to the knee joints during repeated sit-stand-sit movements, the statistical analysis started from the quantity of AE events in the proposed four movement phases and extended to waveform features extracted from AE signals. While the quantity of AE events was found to follow certain statistical trends related to age and degeneration in each movement phase, detail statistical analysis of AE waveform features yielded the peak amplitude value and average signal level of each AE burst as two most significant features.

An image based knee AE feature profile is presented based on 2D colour histograms formed by the peak amplitude value and average signal level in four movement phases. It provides not only a visual trend related to knee age and degeneration, but also enables visual assessment of the differences and similarities among different knees. Application of principal component analysis showed not only distinct data clusters corresponding to participating groups, but also an age and degeneration related trajectory progressing from the early adulthood healthy group to the late adulthood healthy group followed by the middle adulthood osteoarthritic group to the late adulthood osteoarthritic group. Furthermore, this trajectory shows increasing areas for each data cluster, with a highly compact cluster for the early adulthood healthy group at one end and a widely spread cluster for the late adulthood osteoarthritic group at the other end. The discoveries formed a strong basis for further development of knee joint acoustic emission as a convenient and non-invasive biomarker for quantitative assessment of joint ageing and degeneration.

LIST OF FIGURES

Figure 1-1	Anatomy of human knee joint (a) bones, ligaments, and cartilages, and (b) muscles and tendons	2
Figure 3-1	AE system	18
Figure 3-2	Electronic angle measurement system	19
Figure 3-3	Block diagram of system connection	20
Figure 3-4	Illustration of the hit definition parameters	21
Figure 3-5	Sensor location and attachment	23
Figure 3-6	Joint angle based AE	24
Figure 3-7	AE waveform example from (a) healthy knee; and (b) OA knee	27
Figure 4-1	Angle signals before and after smoothing	36
Figure 4-2	Durations of individual movements for all knees studied	38
Figure 4-3	Normalised joint angle and angular velocity with AE hits from healthy knee in group H1	39
Figure 4-4	Normalised joint angle and angular velocity with AE hits from OA knee in group OA2	39
Figure 4-5	Cycle-by-cycle variations of joint angle signals	42
Figure 4-6	Cycle-by-cycle variations of instantaneous angular velocities	45
Figure 4-7	Ratios of ascending and descending times	46
Figure 4-8	Ratios of AA and AD times	47
Figure 4-9	Ratios of DA and DD times	48

Figure 4-10	Ratios for peak angular velocities in ascending and descending phases	49
Figure 5-1	Bilateral plots with right versus left knees for each movement phase	53
Figure 5-2	Statistical differences of AE hits between five groups among four movement phases	56
Figure 5-3	Probability distribution of peak amplitudes for OA knees in AA phase	58
Figure 5-4	Cumulative distributions of AE peak amplitude values	60
Figure 5-5	Probability distribution of ASL for OA knees in AA phase	61
Figure 5-6	Cumulative distributions of ASL	63
Figure 5-7	Probability distribution of durations for OA knees in AA phase	64
Figure 5-8	Probability distribution of rise times for OA knees in AA phase	65
Figure 5-9	Probability distribution of fall down times for OA knees in AA phase	65
Figure 5-10	Cumulative distributions of durations	68
Figure 5-11	Cumulative distributions of rise times	69
Figure 5-12	Cumulative distributions of fall down times	70
Figure 5-13	Probability distribution of average frequencies for OA knees in AA phase	72
Figure 5-14	Probability distribution of initial frequencies for OA knees in AA phase	72

Figure 5-15	Probability distribution of reverberation frequencies for OA knees in AA phase	73
Figure 5-16	Cumulative distributions of average frequencies	74
Figure 5-17	Cumulative distributions of initial frequencies	75
Figure 5-18	Cumulative distributions of reverberation frequencies	76
Figure 5-19	Probability distribution of peak frequencies for OA knees in AA phase	78
Figure 5-20	Probability distribution of centre frequencies for OA knees in AA phase	78
Figure 5-21	Cumulative distributions of peak frequencies	80
Figure 5-22	Cumulative distributions of centre frequencies	81
Figure 5-23	Probability distribution of signal strength for OA knees in AA phase	82
Figure 5-24	Probability distribution of absolute energy for OA knees in AA phase	83
Figure 5-25	Cumulative distributions of signal strength	84
Figure 5-26	Cumulative distributions of absolute energy	85
Figure 5-27	Probability distribution of counts for OA knees in AA phase	86
Figure 5-28	Probability distribution of counts to peak for OA knees in AA phase	87
Figure 5-29	Probability distribution of counts down for OA knees in AA phase	87
Figure 5-30	Cumulative distributions of counts	90
Figure 5-31	Cumulative distributions of counts to peak	91

Figure 5-32	Cumulative distributions of counts down	92
Figure 6-1	Scatter plot of peak amplitude and ASL for one healthy and one OA knee	99
Figure 6-2	Display scheme of image based representation of AE feature profile	100
Figure 6-3	Typical AE feature profiles of knee in each group	102
Figure 6-4	PCA of AE feature profiles constructed by peak amplitude and ASL of AE signals (a) all five groups, (b) zoom-in view of H2 and H3 groups, (c) zoom-in view of H1 group	107
Figure 6-5	PCA of AE feature profiles with BMI values (a) all groups, (b) zoom-in view of H2 and H3 groups, and (c) zoom-in view of H1 group	109
Figure 6-6	PCA of AE feature profiles with age and K-L scores for 10 OA knees	111
Figure 6-7	PCA results produced by 13 amplitude intervals and 9 ASL intervals	113
Figure 6-8	PCA results produced by 7 amplitude intervals and 5 ASL intervals	113
Figure 6-9	PCA results produced by 13 amplitude intervals and 5 ASL intervals	114
Figure A.1-1	Reference frequency response of S9204 sensor	129
Figure B-1	AE sensor testing based on pencil lead breaking	132
Figure B-2	Sensor testing response - time domain	133
Figure B-3	Sensor testing response – frequency domain	133
Figure D-1	Calibration curve of electro-goniometers	136

Figure G-1	AE feature profiles of group H1 knees	144
Figure G-2	AE feature profiles of group H2 knees	146
Figure G-3	AE feature profiles of group H3 knees	148
Figure G-4	AE feature profiles of group OA1 knees	150
Figure G-5	AE feature profiles of group OA2 knees	151

LIST OF TABLES

Table 3-1	Age and BMI of each participating group with MA and SD denoting mean age and standard deviation	28
Table 3-2	Age and BMI of healthy and OA sub-groups	29
Table F-1	Number of AE events for 10 individual movements in group H1	140
Table F-2	Number of AE events for 10 individual movements in group H2	141
Table F-3	Number of AE events for 10 individual movements in group H3	142
Table F-4	Number of AE events for 10 individual movements in group OA1	142
Table F-5	Number of AE events for 10 individual movements in group OA2	143

LIST OF ABBREVIATIONS

AA:	Ascending-acceleration
ABMI:	Average bodymass index
ACC:	Average correlation coefficient
ACL:	Anterior cruciate ligament
AD:	Ascending-deceleration
AE:	Acoustic emission
aJ:	AttoJoules
ASL:	Average signal level
AST:	Auto system test
BMI:	Bodymass index
DA:	Descending-acceleration
dB:	Decibel
DD:	Descending-deceleration
DFT:	Discrete Fourier transform
FA:	Factor analysis
HDT:	Hit definition time
HLT:	Hit lockout time
ICA:	Independent component analysis
IQR:	Inter quartile range
K-L:	Kelgren and Lawrence
KOOS:	Knee osteoarthritis outcome score
MA:	Mean age
MRI:	Magnetic resonance imaging
OA:	Osteoarthritis
PAG:	Phonoarthrography
PCA:	Principal component analysis

PC:	Principal components
PDT:	Peak definition time
RA:	Rheumatoidarthritis
RP:	Random projection
SD:	Standard deviation
SVD:	Singular value decomposition
TKR:	Total knee replacement
VAG:	Vibroarthrography

LIST OF SYMBOLS

f_a :	Average frequency of individual AE signal
f_c :	Centre frequency of individual AE signal
f_i :	Initial frequency of individual AE signal
f_r :	Reverberation frequency of individual AE signal
θ_r :	Raw joint angle signal
θ_s :	Smoothed joint angle signals
ω :	Instantaneous angular velocity
ψ :	Movement phases
t_s :	Goniometer sampling interval
t_a :	Total time spent on ascending/acceleration
t_d :	Total time spent on descending/deceleration
i :	The i^{th} sit-stand-sit movement
$\overline{r_a}$:	Average correlation coefficient of joint angle signals
$\overline{r_v}$:	Average correlation coefficient of instantaneous angular velocity signals
c :	Correlation coefficient for individual movement
$\overline{s_t}$:	Average symmetric ratios for the time spent on ascending/acceleration to descending/deceleration
$\overline{s_v}$:	Average symmetric ratios for the peak instantaneous angular velocity in ascending to descending
q :	Quantity of AE events
$\overline{q_\psi}$:	Average quantity of AE events in phase ψ
$p(w)$:	Probability distribution of the AE feature vector
H :	AE feature based profile
\mathbf{F} :	Input data matrix for principal component analysis

\mathbf{F}_M :	Mean-corrected matrix of \mathbf{F}
\mathbf{C} :	Covariance matrix
\mathbf{V}_{PC}^T :	Principal components
\mathbf{K} :	Principal component score
σ_K^2 :	Variance in each dimension of PC space
σ_t^2 :	Total variance

CONTENTS

ABSTRACT	<i>I</i>
LIST OF FIGURES	<i>II</i>
LIST OF TABLES	<i>VII</i>
LIST OF ABBREVIATIONS	<i>VIII</i>
LIST OF SYMBOLS	<i>X</i>
1 INTRODUCTION	<i>1</i>
1.1 BACKGROUND AND MOTIVATION OF THE RESEARCH.....	<i>1</i>
1.2 AIMS AND OBJECTIVES OF THE RESEARCH.....	<i>5</i>
1.3 THESIS ORGANISATION	<i>5</i>
1.4 CONTRIBUTIONS.....	<i>6</i>
2 LITERATURE REVIEW	<i>8</i>
2.1 INTRODUCTION.....	<i>8</i>
2.2 APPLICATIONS OF VIBRATION MEASUREMENT.....	<i>8</i>
2.2.1 Vibration measurement for condition monitoring.....	<i>8</i>
2.2.2 Vibration measurement for biomedical assessment	<i>9</i>
2.3 APPLICATIONS OF ACOUSTIC EMISSION MEASUREMENT.....	<i>11</i>
2.3.1 Acoustic emission measurements for condition monitoring	<i>11</i>
2.3.2 Acoustic emission measurements for biomedical assessment	<i>12</i>
2.4 STUDIES OF KNEE JOINT FLEXION-EXTENSION	<i>13</i>
2.4.1 Studies of knee joint movement based on swinging.....	<i>13</i>
2.4.2 Studies of knee joint movement based on sit-stand-sit.....	<i>14</i>
2.5 SUMMARY.....	<i>15</i>
3 DATA ACQUISITION	<i>17</i>
3.1 INTRODUCTION.....	<i>17</i>

3.2	<i>DATA ACQUISITION SYSTEM</i>	17
	3.2.1 <i>AE system</i>	17
	3.2.2 <i>Angle measurement system</i>	18
	3.2.3 <i>System setup and AE hit definition</i>	19
3.3	<i>DATA ACQUISITION PROTOCOL AND ANGLE BASED AE</i>	22
3.4	<i>STUDY PARTICIPANTS AND DATA COLLECTED</i>	27
3.5	<i>DATA SELECTION</i>	30
3.6	<i>CONCLUDING REMARKS</i>	32
4	<i>ANALYSIS OF JOINT ANGLE SIGNALS</i>	34
	4.1 <i>INTRODUCTION</i>	34
	4.2 <i>MOVEMENT ISOLATION</i>	34
	4.3 <i>ANALYSIS OF JOINT ANGLE SIGNALS</i>	40
	4.3.1 <i>Cycle-by-cycle variations of joint angle signals</i>	41
	4.3.2 <i>Movement symmetry</i>	46
	4.4 <i>CONCLUDING REMARKS</i>	50
5	<i>STATISTICAL EVALUATION OF AE SIGNALS IN FOUR PHASES</i>	52
	5.1 <i>INTRODUCTION</i>	52
	5.2 <i>BASIC STATISTICS IN FOUR MOVEMENT PHASES</i>	52
	5.3 <i>STATISTICAL EVALUATION OF AMPLITUDE BASED FEATURES</i>	57
	5.3.1 <i>Statistical evaluation of peak amplitude</i>	57
	5.3.2 <i>Statistical evaluation of ASL</i>	61
	5.4 <i>STATISTICAL EVALUATION OF TIME BASED FEATURES</i>	64
	5.5 <i>STATISTICAL EVALUATION OF FREQUENCY BASED FEATURES</i>	71
	5.5.1 <i>Statistical evaluation of average, initiation, and reverberation</i> <i>frequencies</i>	71
	5.5.2 <i>Statistical evaluation of peak and centre frequencies</i>	77
	5.6 <i>STATISTICAL EVALUATION OF AE ENERGY BASED FEATURES</i>	82
	5.7 <i>STATISTICAL EVALUATION OF COUNT BASED FEATURES</i>	86
	5.8 <i>CONCLUDING REMARKS</i>	93

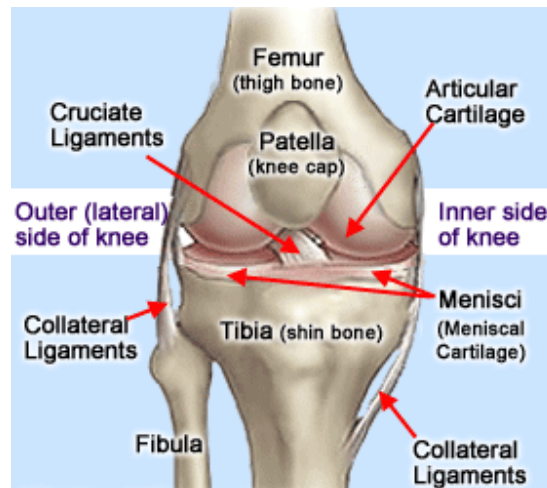
6	MULTIVARIATE FEATURE VISUALISATION AND ANALYSIS.....	95
6.1	INTRODUCTION.....	95
6.2	OVERVIEW OF MULTIVARIATE ANALYSIS.....	96
6.3	MULTIVARIATE BASED AE FEATURE ANALYSIS.....	98
6.3.1	<i>Feature based profiles of knee joint acoustic emission</i>	<i>98</i>
6.3.2	<i>Visualisation of knee joint acoustic emission.....</i>	<i>100</i>
6.4	BIOMARKER IDENTIFICATION BY PRINCIPAL COMPONENT ANALYSIS.....	103
6.4.1	<i>Principal component analysis.....</i>	<i>103</i>
6.4.2	<i>Classification of AE profiles by principal component analysis</i>	<i>105</i>
6.4.3	<i>PCA sensitivity</i>	<i>112</i>
6.5	CONCLUDING REMARKS.....	114
7	CONCLUSIONS AND RECOMMENDATIONS FOR FUTURE WORK.....	116
7.1	CONCLUSIONS.....	116
7.2	FUTURE WORK	117
7.2.1	<i>Discovery of additional biomarker for comprehensive representation of knee joint ageing and degeneration</i>	<i>118</i>
7.2.2	<i>Identification of damage joints.....</i>	<i>118</i>
7.2.3	<i>Identification of OA and RA</i>	<i>119</i>
	REFERENCES.....	120
A	SPECIFICATIONS OF ACOUSTIC EMISSION SYSTEM.....	129
A.1	SPECIFICATION OF S9204 SENSOR.....	129
A.2	SPECIFICATION OF 2/4/6 PREAMPLIFIER.....	130
A.3	SPECIFICATION OF PCI-2 BOARD	130
B	AE SENSOR TESTING.....	132
C	SPECIFICATIONS OF GONIOMETER SYSTEM.....	134
C.1	SPECIFICATION OF SG150 ELECTRO-GONIOMETER.....	134
C.2	SPECIFICATION OF K800 DATA ACQUISITION UNIT.....	134

D	GONIOMETER CALIBRATION.....	136
E	GENERAL HEALTH AND WELL-BEING QUESTIONNAIRE.....	138
F	QUANTITY OF AE EVENTS FROM EACH KNEE IN EACH PHASE AND EACH MOVEMENT CYCLE.....	140
G	AE FEATURE PROFILES FOR ALL KNEES STUDIED.....	144
H	PUBLICATION LIST.....	153

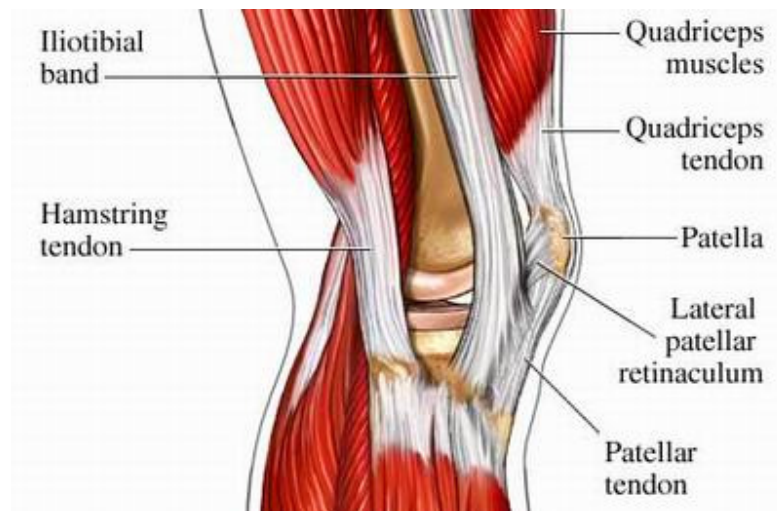
CHAPTER 1 INTRODUCTION

1.1 BACKGROUND AND MOTIVATION OF THE RESEARCH

The human knee joint is one of the most complex synovial joints located between the femur and tibia and capable of withstanding several times body weight [1]. It is one of the largest joints in the human body consists of the most complex musculoskeletal structures (Figure 1-1), and the knee joint movements involving interaction among various anatomical parts (bones, cartilages, muscles, tendons, and ligaments) [2]. The human knee joint has been studied extensively. Typical changes in knees caused by the ageing process mainly consist of the changes of the synovial fluid, ligaments and joint capsules, joint receptors, as well as articular cartilages [3]. For old people, the quantity and quality of synovial fluid are reduced. The joint capsules and ligaments are stiffer due to the increase in the formation of crosslinks in collagen fibres and the loss of elastic fibres. The changes of joint capsules and ligaments in turn influence the quality of information received by the joint receptors. The ageing also causes deteriorations of the articular cartilages, which include reducing water content, chondroitin sulphate quality and content of glycosaminoglycans, quality and content of proteoglycans, articular cartilage thickness, synovial fluid perfusion, as well as increasing articular surface roughness and resistance to gliding. All these changes will have the possibility to result the knee to osteoarthritis (OA) at the late stage [4].



(a)



(b)

Figure 1-1 Anatomy of human knee joint (a) bones, cartilages and ligaments, and (b) muscles and tendons (modified from: http://www.bigkneepain.com/knee_anatomy.html)

Knee OA (also known as degenerative arthritis or degenerative joint disease) is a major type of knee disease that leads to the main cause of disability and morbidity worldwide [4-5]. Its prevalence is predicted to increase as result of ageing populations [6-7]. The primary symptoms include joint pain and stiffness, and the pathologies consist of focal damage and degeneration of articular cartilages, abnormal remodelling and attrition of sub-articular

bones, osteophytes, ligament laxity, weakening of periarticular muscles, and the changes of synovial fluid and inflammation [4]. The current treatments include lifestyle modification, physiotherapy, medications for OA at the early stage, and total knee replacement (TKR) for OA at the advanced stage [5]. However, all treatments aim to relieve the symptoms suffered by patients, and none of the medications available are able to reform the disordered joint structure consistently [8]. As there is currently no cure for OA, early detection of joint degeneration becomes essential.

Currently, a variety of visual imaging techniques such as X-rays [9], ultrasonography, and magnetic resonance imaging (MRI) [9-11] have been widely used to diagnose the knee disease, whereby a set of image based results regarding to the internal knee structure is provided for clinicians to assess the condition of a knee joint. X-ray diagnosis divides the severity level of OA into five stages based on the narrowing of knee joint space [11]. MRI and ultrasonography assess the severity levels of OA based on the degeneration of articular cartilages [12]. Relatively insensitive and highly observer dependent are the main limitations for the conventional radiography assessment. These limitations have led to increased utilisation of MRI for knee joint assessment, as it is more sensitive, and produces 3D anatomical information for visualisation of the knee joint structures [13]. However, the cost, availability, portability and observer dependence are considered as the common limitations of the MRI examination. Although ultrasonography is more convenient for observing knee joint disorders, like the other two methods, it is also heavily observer dependent [14-15]. Furthermore, all the above mentioned methods are only able to provide a static snapshot of the knee joint in a particular pose, and none of these techniques provide dynamic information related to knee movement for activity based joint integrity assessment. Although gait analysis is able to assess the dynamic knee functions, it lacks sensitivity [16]. Additionally, none of these methods are able to detect OA until it is in the advanced stages.

A normal knee with smooth and well-lubricated cartilage surfaces should move quietly, whereas an unhealthy knee covered by rough and poorly lubricated cartilage surface should move unevenly, producing acoustic signals [3]. Based on this scenario, the previous arthritis assessments use phonoarthrography (PAG) and vibroarthrography (VAG). PAG is based on the auscultation by attaching a microphone on the knee surface to record the

audible sound signals (with frequency range from 20 to 20 kHz) emitted during the knee performing regular movements [17-18]. It was followed by the development of VAG, which uses a miniature accelerometer [19], since it provides better attachment and is more sensitive in the lower frequency range, especially below 1 kHz.

Acoustic emission (AE) is a natural phenomenon of high frequency sound (frequency range > 20 kHz) that can be generated by structures under loading or surface interaction, and it can be detected by attaching a piezo-electric transducer on the surface of the structure [20]. For several decades, AE has been widely applied to condition monitoring to detect the micro-growth of damages inside engineering materials [21]. The knee joint also emits sound signals in the ultrasound range when bones, cartilages, ligaments, and soft tissues move against each other. By drawing parallels between condition monitoring and the dynamic joint integrity assessment, the AE waveforms emitted from the knees were studied [22-23]. The previous work consists of the development of the knee AE measurement system by integrating a traditional AE acquisition system which was widely used for condition monitoring of engineering structures, and an electronic joint angle measurement system which has been applied for recording joint movements for biomechanical studies [24]; the investigations and comparison of the sensor locations and sensor attachment; the development of a repeatable measurement protocol based on consecutive sit-stand-sit movements to create the knee joint AE signals; and the exploratory study of the AE signals (hits) emitted from normal and abnormal knees to investigate the differences between them. Through the studies by dividing the AE signals generated during movements into ascending (from sit-to-stand), and descending (from stand-to-sit) movement phases, significant differences have been found between normal and abnormal knees at two extreme ages and conditions (i.e. young adult healthy and old OA) in terms of the quantity of AE events and a set of AE waveform features (peak amplitude, duration, and peak frequency) [22-23]. However, no work has been performed to investigate the possibility of using AE to monitor ageing and degeneration of the knee joints. As the application of AE to the human knee joint is new, and detailed studies in terms of ageing and degeneration required more participants belonging to various age groups.

Building on the previous research findings with clear differences found from young healthy and old OA participants, it is hypothesised that there should be a trend of AE based profiles related to the knees belonging to various age bands and conditions. If such trend could be established, it will form the basis for identifying degenerative change out with the age-related norms. This would not only enable the possibility of early diagnosis for the knees at risk, but also the efficacy of early treatment programmes to be evaluated.

1.2 AIMS AND OBJECTIVES OF THE RESEARCH

The main aim of this project is to discover AE based biomarkers (signatures) for quantitative assessment of joint ageing and degeneration, thereby enabling early diagnosis and prediction of knee joint structure changes. The term biomarker in this thesis is determined by the pattern that indicates the biological status of particular knee [25].

The specific objectives of the research are:

- *To undertake knee joint data selection and classification to form the appropriate groups with different age bands and conditions for analysis.*
- *To discover the relationships between the goniometer derived joint angle signals and joint conditions related to age and degeneration.*
- *To discover the relationships between the joint angle based AE and joint conditions related to age and degeneration.*
- *To establish an AE based biomarker for visualising and classifying the knee joint conditions related to age and degeneration.*

1.3 THESIS ORGANISATION

The organisation of the remainder of the thesis is as follow:

Chapter 2 gives a brief literature review of the related work.

Chapter 3 presents the data acquisition system, measurement protocol based on the sit-stand-sit movements, AE data collection, as well as data selection and stratification for investigation in this project.

Chapter 4 evaluates the joint angle signals created by the sit-stand-sit movements

Chapter 5 devotes to the statistical evaluation of the AE signals, which include the statistical analysis of the quantity of AE events and the typical AE features, thereby determining the most significant features to represent the AE waveforms acquired.

Chapter 6 presents the development of the biomarker based on the most significant AE features in different movement phases for visualisation and assessment of knee joint conditions.

Chapter 7 summarises the experimental results of the work, emphasises the contributions to knowledge, and describes future work to develop AE further for knee joint assessment.

1.4 CONTRIBUTIONS

The original contributions of the work which are considered to be new are as follows:

- *A four movement phase model identified by the instantaneous angular velocity and the joint angle signals has been established for further assessment of AE and joint angle signals acquired during consecutive and repeated sit-stand-sit movements.*
- *The joint ageing and degeneration related trends were discovered via the quantitative assessment of joint angle signals in terms of variations of joint angle and angular velocities. This was found to be particularly significant in the descending phase.*
- *The age/degeneration related differences were discovered via the quantitative assessment of movement symmetry based on the time spent and peak velocity ratios. This was found to be particularly significant in the DA-DD time ratios and ascending and descending peak velocity ratios.*

- *The joint ageing and degeneration related trends were further supported by the quantitative evidences of the AE events and the AE features. The increase in the number of AE events with certain loss of symmetry corresponds to the increase in age and change of joint condition from healthy and OA [26].*
- *An image based AE feature profile was proposed to give a visual and uniform representation based on peak amplitude and ASL values in four movement phases produced by different knee joints.*
- *An age and degeneration related trajectory was discovered in the low dimension PCA space with the early adulthood healthy and late adulthood OA knees at two extremes. The results showed not only the difference between the age-matched healthy and OA groups [27-28], but also the difference between the knees in different age bands and with different conditions [26, 29].*

The work has led to two conference papers and two journal papers (see Appendix H).

CHAPTER 2 LITERATURE REVIEW

2.1 INTRODUCTION

This chapter reviews the applications of both vibration (sound signals in the audible range), and AE (high frequency ultrasound) for condition monitoring of machinery and biomedical assessment of the human body, as well as the study of knee flexion-extension for functional assessment of human knee joints. The applications of vibration and AE measurements for structural health and biomedical assessments are reviewed in Sections 2.2, and 2.3, respectively. As it is easy to examine the conditions by hearing and screening, it is not unreasonable to apply the vibration sound for coarse classifying normal and abnormal conditions [19]. Compared to traditional vibration signals, AE signals are considered to have the following advantages:

- AE is highly sensitive and offers the possibility to detect the defects and the progression of damage at an early stage than vibration sound, as ultrasound is more related to the microscopic changes [30].
- As high frequency elastic waves, AE is less likely to be affected by background noise and insensitive to structural resonances than the traditional vibration signals [30].

With flexion-extension forming the fundamental action of knee joint movements [2], Section 2.4 reviews the studies of two basic movement protocols which have been used for measuring the knee joint functions over the whole movement range, namely, swinging, and sit-stand-sit, respectively [24]. A summary is given in Section 2.5.

2.2 APPLICATIONS OF VIBRATION MEASUREMENT

2.2.1 Vibration measurement for condition monitoring

The condition of machinery is essential for the operators to make decisions regarding to usage, maintenance, and retirement. Vibrations generated by machinery provide a good signature of the current condition [31]. Vibration signals in the audible frequency range (frequency range < 20 kHz) emitted from machinery can be recorded by using a microphone or tri-axial accelerometer. The reasons for the wide use of vibration for condition monitoring are due to a better understanding of vibration mechanisms in machinery and that the change in vibration signal can easily be attributable to the dynamic characteristics and the fault conditions [19, 32]. In this sub-section, condition monitoring of bearing surface and gears based on audible vibration signals are reviewed, as they have a similar mechanical function as the knee joint (carrying the body mass with movement involving interaction among various internal structures) [2].

Vibration measurement based on the audible vibration signals for monitoring the conditions of rolling element bearings were investigated by [33-35]. The investigations include the evaluation of signals and noise generated by vibration in bearing [33], as well as audible vibration signals related to localised defects (cracks, pits and spalls on the rolling surfaces) and distributed defects (surface irregularities like roughness, waviness, or off-size of the rolling elements) [34-35], which are similar to joint disorders due to bone surface roughness and poor lubrication [4]. Applications of audible vibration signals for monitoring the health condition of gears were investigated by [30, 32, 36-38]. The investigations involve the application to detect the gearbox failure in aviation [36]; the local fault of gears in terms of partial damage of tooth, gear crack, and localised wear [32, 37]; the study on the diagnostic capabilities of natural pitting of the gears [30]; as well as on-line monitoring of the artificially induced gear cracks [38]. Via the statistical, time, frequency, and mixed time-frequency approach [39-41], the audible vibration signals showed the ability to determine the normal and defective bearing and gears. However, no investigation has been performed for condition monitoring of defect progression in bearing and gears based on the audible vibration signals.

2.2.2 Vibration measurement for biomedical assessment

As knees also create audible vibration signals during moving, vibration based measurement methods such as phonoarthrography (PAG) [17-18] and vibroarthrography (VAG) [42-53] have been explored as a non-invasive testing technique for assessing knee joints in the past two decades. A set of signal processing techniques has been developed for dealing with the VAG signals emitted from the knee, which started from the analysis of knee vibration signals acquired during knee swinging using a linear prediction method [42, 52], muscle contraction interference cancellation [43], and VAG source identification [44] based on the evaluations of VAG signals acquired from normal knees, knees subsequently underwent arthroscopy, and cadaver knees. The outcomes demonstrated the potential of the VAG based methodology for diagnosis and treatment of knee pathology before and after joint surgery or drug therapy. Based on the cross analysis of the clinical parameters and the signal variability parameters extracted from the segmented signals, VAG signals were also considered as a useful tool for screening normal and chondromalacia patella in the following study [45].

Afterwards, a comprehensive comparative study was carried out in terms of the parametric representations of VAG signals acquired during knee swinging [46], which took into account the signal parametric features and the clinical features of 51 normal and 38 abnormal knees (include knees with chondromalacia, meniscal tear, tibial chondromalacia, and anterior cruciate ligament injuries), by applying the regression model [53] to classify the dominant features extracted from the segmented VAG signals. The highest accuracy rate of 85.9% was achieved. The same VAG signal database has been extended to analyse the differences between healthy and abnormal knees via full wavelet packet tree decomposition [54] and a local discriminant based algorithm [55], and precise identification of normal and abnormal joints can be achieved from certain nodes of the wavelet packet tree (with the highest accuracy rate of 84.2 %) [48]. In the recent studies, statistical moments [39] were applied to extract additional information from the histograms of VAG signals stored in the same database, and the studies include classification of normal and abnormal VAG patterns by combining a strict 2-surface proximal classifier [56] and genetic algorithm [57]. By dividing the VAG signals into the ascending and descending movement phases based on the time scale, feedforward neural networks [58] showed good performance to determine normal and abnormal VAG signals by using the statistical

moments as well as the adaptive turn counts [59] of VAG signals [50-51]. However, all the investigations mentioned above do not show the degree of healthiness and severity of symptoms, and the movement phase isolation is simply performed by dividing the entire signal duration into two halves.

2.3 APPLICATIONS OF ACOUSTIC EMISSION MEASUREMENT

2.3.1 Acoustic emission measurements for condition monitoring

AE occurs as the high frequency transient elastic waves (frequency range > 20 kHz) generated by the materials under pressure or vibrating [19], and it can be detected by attaching a piezo-electric transducer on the surface of the materials being monitored.

AE has been applied to monitor the conditions in machinery. The previous work includes comparative studies on the diagnostic and prognostic capabilities based on AE, vibration as well as other techniques such as spectrometric analysis [30] for bearing surfaces [60-62] and gears [30, 37-38]. After establishing AE as a complementary diagnostic tool for identification of bearing defects, [60-62] extended the experimental investigation to identify the presence and size of a defect on the loaded bearing, and compared AE and audible vibration signals by varying speed and load conditions. From the results obtained, it was concluded that AE offers early fault diagnosis and better identification capabilities of bearing defects in terms of subtle changes than vibration. Furthermore, based on the comparative study of AE, vibration and spectrometric methods, through the time, frequency, and mixed time-frequency analysis of the signals acquired, AE signals have been shown to be able to indicate various types of progressing local faults in terms of partial damage of tooth, gear crack, and localised wear [32, 37], natural pitting [30], and early diagnosis of natural wear [38] in the gear systems.

Additionally, literature results show that the applications of AE also include health monitoring of aerospace structures [63]; indication of tool wear based on chatter vibration and AE response [64]; condition monitoring of various wear particles during repeated dry

rubbing [65]; structure failure detection and quality evaluation of shotcrete in the reinforced concrete slabs [66]; fatigue growth monitoring in the aluminium alloy [67], as well as damage progression monitoring for composite laminates [68]. By analysing and processing the AE signals using the AE waveform features [69], the time reverse modelling method [70], the mixed time-frequency analysis [41], and the multivariate statistics [53], AE were also found to provide a useful signature and sensitivity to detect subtle changes such as the early stage defects and the progression of damage for the above mentioned materials.

2.3.2 Acoustic emission measurements for biomedical assessment

In biomedical assessment based on AE, several studies presented AE as a useful tool for bone condition assessment [71]. In the previous study, it was applied to examination of micromechanics of bone failure [72]. During the study, cyclic loading was applied to the bone to generate AE, and the result showed that AE is sensitive for monitoring the development of damage on the bone. In the following study, AE was extended to predict bone fracture at an early stage [73], and it was found that crack initiation in human bone was detectable by using AE signals emitted. AE has also been employed as a passive experimental method for assessing the acrylic bone cement failure of the hip joint [74-75]. Through the quantitative assessment of a set of AE waveform features (i.e. magnitude, duration, rise time, etc) [68], fatigue related AE trends corresponding to the duration and rise times were found, with severe fatigue related to longer duration and rise times. For other applications, AE also has been successfully explored as the signature for in vitro monitoring of rabbit anterior cruciate ligament (ACL) damages [76]. From the experiments involving the complete rupture of 16 rabbits' tibia-ACL-femur and the complete failure of 4 ACL specimens, the results based on the ratio of AE waveform peak amplitude and rise time were seen to have certain similarities to the categories of matrix deformation, debonding and fibre fracture used in testing of fibre composite materials (with low peak amplitude and short rise time corresponding to matrix deformation and high peak amplitude and long rise time corresponding to fibre fracture). Additionally, the quantitative assessment of AE data acquired from the adult rat femora supports the hypothesis that

immobilisation-related degradation of bone mechanical properties is associated with increasing brittleness of cortical bone tissues [77].

For AE based human knee joint assessment [22-23, 78], early studies involved the observation and identification of AE signals emitted from the knees with various cartilage lesion and the knees at the disordered stage under typical daily loading (include knee bending, stairs ascending/descending and walking) [78]. In the following studies, the AE based joint measurement has been developed for examining the dynamic integrity of normal and abnormal knee joints. Through the exploratory study to investigate the potential of AE for clinical assessment of knee joints based on consecutive and repeated sit-stand-sit movements, the results demonstrated significant differences between young healthy and elder OA knees [22-23], and provide the basis for further development of AE for assessment of ageing and degeneration of human knee joints reported in this thesis.

2.4 STUDIES OF KNEE JOINT FLEXION-EXTENSION

2.4.1 Studies of knee joint movement based on swinging

Knee joint swinging plays an important role in the assessment of pre-operative and post-operative assessment of the TKR [79-81]. Based on the studies over 145 subjects, it has been found that the effectiveness of TKR can be assessed based on the range of motion of knee flexion-extension [79]. In the followed studies [80], by investigating a group of 284 knee replacement cases, increased risks of post-operative flexion contracture were found from the knees with certain flexion-extension deformity. Based on the studies over 5,622 knees after surgery [81], it was confirmed that the range of knee flexion-extension can be a useful marker for post-operative functional assessment of the knees.

Knee flexion-extension based on swinging has also been applied to assess the age-related knee joint disorder [82-86]. Based on the studies of swinging in younger and older normal subjects [82-83], statistical significance in terms of flexion-extension laxity has been found between them with elder subjects related to higher joint laxity in flexion but not in

extension. This finding has led to the following study concentrating on the relationships between certain knee flexion angles and the joint disorders for younger and elder healthy cohorts [86], and significantly higher medial and lateral laxities which results to the changing of knee joint space have been found from older knees when positioning the knees in 10° and 80° flexion. By flexing the knee to 90° and cross analysis with the MRI images of 20 post-operative TKR patients, higher lateral laxity than medial laxity were observed [83]. From the studies of flexion-extension range of motion from 30 elder healthy subjects, no significant differences were found among them [85].

2.4.2 Studies of knee joint movement based on sit-stand-sit

With sit-stand-sit movements involving the kinetic and kinematic variables in trunk-lower limb interaction, they are another important test to determine the functional level of a person [87]. Sit-stand-sit movements have been studied for both healthy and abnormal participants of various ages [88-93].

The studies of normal subjects include the duration and velocity assessments of the sit-stand-sit movement cycles [87]. Based on the investigation of 50 subjects (including young adults, middle aged, and elder normal subjects), and by dividing the sit-stand-sit movement cycles into ascending and descending phases, the average durations showed that the descending movement spent slightly longer time than ascending; the forward lean velocity was significantly higher in ascending than descending; and the recovery velocity was significantly higher in descending than ascending. The sit-stand-sit method was also used to determine the movement characteristics for the healthy bodies [89]. By assessing 34 young and 33 elder healthy participants performing sit-stand-sit movements using self-selected speed, and by including a force measurement system, young adult subjects were found to displace the centre of pressure further forward and through a greater percentage of their initial base of support than older subjects. In the followed study, the motor strategy in terms of the centre of mass of sit-stand-sit movements was investigated [90] based on sit-stand-sit movements performed by 16 young and 35 old healthy subjects via their natural speed.

Compared to the younger healthy subjects, it was found that the elder healthy subjects tend to flex the trunk more in order to bring the centre of mass closer to the based of support at higher speed, thereby compensating the stability when lifting off from the chair.

The comparison of sit-stand-sit movements performed by the healthy and abnormal subjects was also made [91-93]. By including the force plate to acquire the ground reaction force, and taking into account the influence of hand force to the ground reaction force location of the sit-stand-sit movement performed by a total of 51 subjects (17 young, 23 elderly healthy, and 11 elderly impaired), a trend was discovered that impaired elder subjects placed the reaction force the most anterior, elder subjects place it intermediately, and young subjects place the least anterior [91]. The kinematic and kinetic characteristics of the healthy and cerebral palsy children were investigated in the followed study [88]. By taking into account 27 healthy and 21 symptomatic subjects, the kinematic evaluation showed slowness of motion, increased anterior tilting and hip flexion in the abnormal group compared with the normal group, and the major kinetic finding showed that the maximum knee extensor moment was decreased in the cerebral palsy children group. The kinetic, kinematic, and temporal parameters were also assessed for 13 healthy and 7 hemiplegic adults [93] performing sit-to-stand movements. With the sit-to-stand movements partitioned into three phases (i.e. initialisation with the trunk begin to lean forward, seat-off at the first point with body changing from sitting to standing position, and stabilisation at the fully stand position), it was confirmed that the duration of the seat-off for the abnormal adults was around twice as long as for healthy adults, the values of kinematic parameters for the abnormal group were greater than the normal group, and the kinetic parameters showed high asymmetry in the abnormal group with high values observed in the hemiplegic side.

2.5 SUMMARY

In this chapter, the applications of audible and ultrasound acoustic signals, as well as the studies of the knee joint movements in terms of flexion-extension were reviewed. By

evaluating audible vibration signals emitted from the gears and bearings, as well as the human knee joints, there is ample evidence that audible vibration signals could be a useful signature for detecting the defects of materials and the disorders of human joints. As AE signals are more related to the microscopic changes, and more robust against the background noise than the audible signals, it has been applied for assessing subtle changes and the progression of damage. In terms of joint movements, swinging and sit-stand-sit have been used for functional assessment with age and pathology related differences found.

From the literature with AE showing a capability to detect subtle changes in condition monitoring and the progression of damage for both biomedical and machinery assessments; and sit-stand-sit movements showing a capability to reveal differences related to age and degeneration, and from the exploratory study of knee AE signals from sit-stand-sit movements with the results showing significant differences between young healthy and older OA knees, it is reasonable to expect knee AE signals from sit-stand-sit movements to form a biomarker of knee age and condition. If such biomarker can be discovered, it will enable the monitoring of progression of damage, as well as the early evaluation of the knee joints at risk.

CHAPTER 3 DATA ACQUISITION

3.1 INTRODUCTION

This chapter introduces the data acquisition system used to record AE and joint angle signals, the joint movement based data acquisition protocol, the joint angle based AE, as well as the data collected and the signals used for study. The traditional AE and the electronic angle measurement systems, as well as the integration of the two systems and the AE hit definition are introduced in Section 3.2. Section 3.3 is devoted to the movement based data acquisition protocol and the joint angle based AE signals acquired. The data collected and the signal selection criterion are described in Section 3.4 and Section 3.5, respectively. Concluding remarks are given in section 3.6.

3.2 DATA ACQUISITION SYSTEM

The data acquisition system includes a traditional AE system which is frequently used for monitoring engineering structural integrity and an electronic angle measurement system for acquiring joint angle signals. While the former is presented in Sub-section 3.2.1, the latter is presented in Sub-section 3.2.2. The system setup and AE hit definitions are described in Sub-section 3.2.3.

3.2.1 AE system

The AE system (Figure 3-1) is sponsored by the Physical Acoustic Ltd (Cambridge, UK), which consists of two piezo-electric AE transducers (model S9204) to record transient AE signals from two knees, two gain selectable pre-amplifiers (2/4/6 preamplifier) to provide 40 dB gain for each sensor, a PCI-2 data processing board for receiving and pre-processing

the signals acquired, and a PCI expansion card to link the PCI-2 board with the computer [69].

S9204 is a general purpose AE sensor with dimensionalities of 23 mm × 15 mm (diameter × height), which provides an appropriate size to be attached on the knee, and a good sensitivity over a wide frequency bandwidth (50-200 kHz), which is better in terms of investigation when recording new signals from an unknown process (in this case unknown friction inside human knee joints). The details of the sensor specifications are shown in Appendix A. Before data acquisition, the pencil lead breaking approach was applied to test the AE sensor response [94], the details of AE sensor testing can be found in Appendix B.

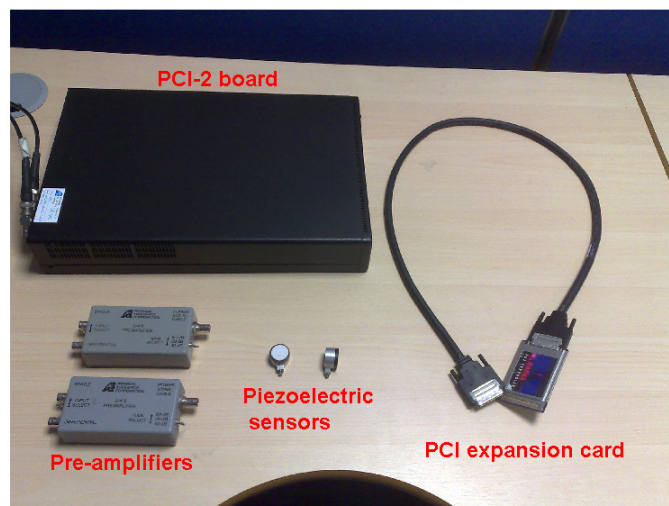


Figure 3-1 AE system

3.2.2 *Angle measurement system*

To link the movement based AE signals with the knee joint angles, an electronic goniometer system which sponsored by Biometrics Ltd (Cwmfelinfach, UK) is integrated to record angular movement from each knee joint (Figure 3-2). It consists of two twin axis goniometers (model SG-150) as well as a goniometer receiver (subject unit) and the

corresponding amplification unit (base unit, model K800) for receiving and pre-processing of joint angle signals [95].

SG-150 is a twin-axis goniometer with a measurement range of $\pm 150^\circ$, which is specially designed for measuring lateral flexion and extension of the knee joints. Detail specifications of the sensors used can be found in Appendix C. Prior to data acquisition, the linear regression approach was used to calibrate the goniometer system [96], and the details of the goniometer calibration process can be found in Appendix D.

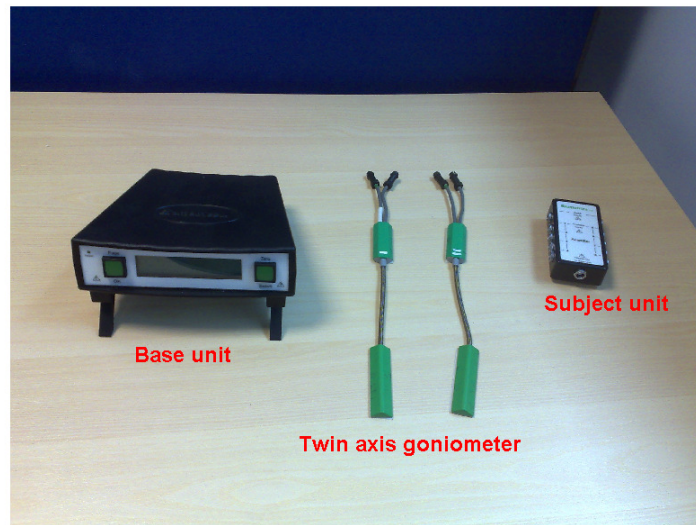


Figure 3-2 Electronic angle measurement system

3.2.3 System setup and AE hit definition

The block diagram of the system setup is shown in Figure 3-3, where the AE sensors and electro-goniometers are connected to the pre-amplifiers and goniometer amplification unit, respectively, before linking both to an AE acquisition board (PCI-2 board). In order to synchronise two systems, the AE sensors are connected to the two receiving channels of the PCI-2 board directly, and the connection between the PCI-2 board and the goniometers are made via a J6 parametric and digital I/O connector [69]. Furthermore, the PCI-2 board is connected with a laptop computer using a PCI expansion card. Based on this connection,

both the electronic angle measurement system and AE system can be triggered by the AEWIn software (AEWin version 3.02, Physical Acoustic Ltd, Cambridge, UK).

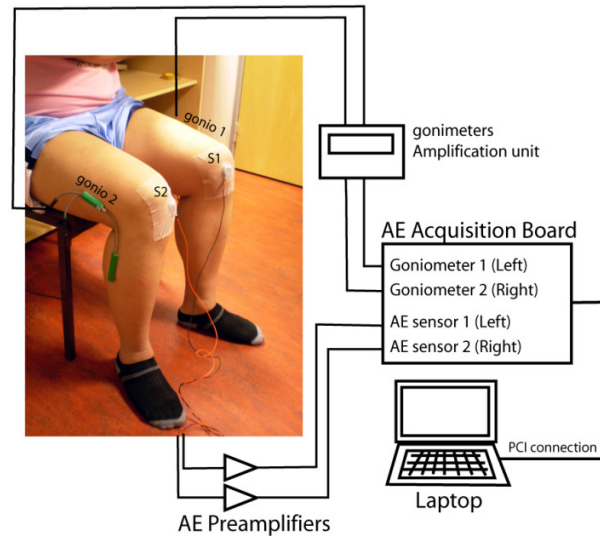


Figure 3-3 Block diagram of system connection

Four hit definition parameters are used to determine an AE transient waveform, namely, threshold, peak definition time (PDT), hit definition time (HDT), and hit lockout time (HLT). A burst signal is recognised as an AE waveform when the burst signal magnitude crosses the threshold. In this project, the threshold is set to 32 dB (39.8107 μ V), thereby minimising the noise signals acquired and ensuring as much appropriate signals acquired as possible, as lower threshold value could cause higher amount of lower-level AE signals acquired by the system, which may include more noise; whereas higher threshold value could result lower amount of AE signals acquired by the system, which may cause certain loss of useful information. The PDT is the retriggerable window used to determine the real peak of an AE hit detected, and it is triggered each time when a new AE maximum has been detected within the duration of PDT. The HDT is the retriggerable window which is used to determine the end of the AE event and store its measured attributes. It is triggered by each threshold crossing from a higher AE magnitude value to a lower AE magnitude value within the duration of HDT. The HLT is used to inhibit the measurement of reflections and late-arriving parts of AE signals, thereby ensuring the data to be acquired at

a faster rate after a hit being detected. HLT is a non-retriggerable window, which is triggered by the last threshold crossing of the AE hit detected. In order to avoid detection of false peak magnitudes, PDT should be set as short as possible but long enough to detect the real AE maximum, whereas HLT and HDT should be at least twice the length of PDT, thereby ensuring that the system is ready for detecting the next hit while the late-arriving part of waveform from the previous hit is locked out, as well as reducing the risk that two separate AE hits will be treated as a single one. As an example shown in Figure 3-4, PDT and HDT are retriggered by the new AE maximum and the new threshold crossing within the window length, respectively, and HLT is triggered to lockout the remaining part and finish the current waveform detection when there is no more maximum detected and threshold-crossing within the length of PDT and HDT. In this particular project, these three parameters are fixed to $PDT = 200 \mu s$, $HDT = 800 \mu s$, and $HLT = 1000 \mu s$, respectively, which is considered as an appropriate setting through the observation of preliminary system tests [23]. In order to minimise the data volume, AE signals are recorded in a non-continuous mode. Each AE event is stored as a waveform digitised at 1MHz sampling

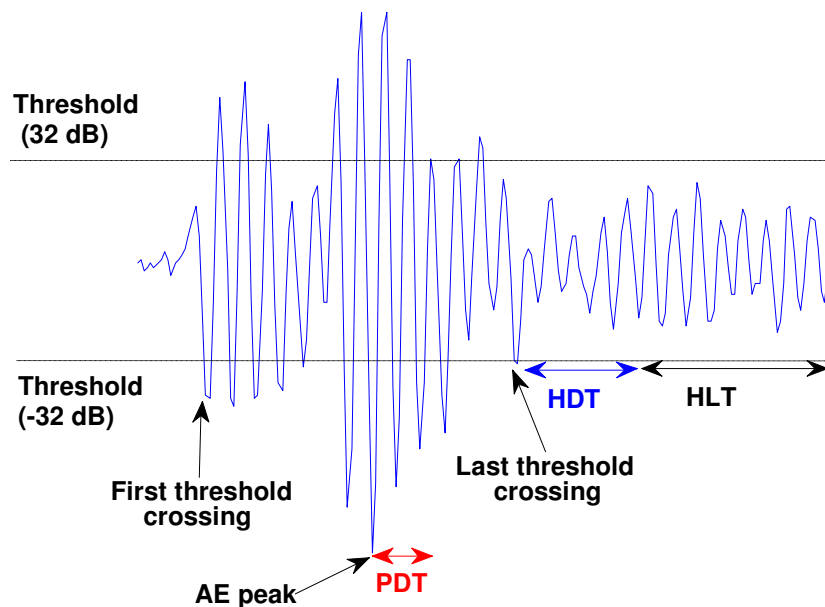


Figure 3-4 Illustration of the hit definition parameters

frequency over a maximum duration of 15 ms which includes a time of 3 ms before threshold crossing.

3.3 DATA ACQUISITION PROTOCOL AND ANGLE BASED AE

The AE events were acquired by attaching the sensor on the location upon medial compartment and below the mid-line of patella. This specific anatomical site has shown to provide good measurement sensitivity [23], because it is closest to the area of contact between surfaces moving against each other in the knee joint, and it offers a relative stable sensor position that is less affected by skin movement. As shown in Figure 3-5, the sensor was attached on the knee through a 130 mm × 130 mm hypoallergenic medical adhesive patch (Tape Specialities, Berkhamsted, UK). In order to make a convenient connection after sensor attachment, a small hole is made in each tape before sticking it on the knee. For sensor attachment, each knee is supported in extension and the adhesive tape is applied in such a way so as to provide the highest possible elastic tension to hold down tightly each AE sensor on the anatomical site. This prevents the AE sensor from sliding during joint movement as joint flexion will create a greater elastic tension to press down further the AE sensor on the anatomical site. To ensure sufficient acoustic coupling between the sensor face and the knee surface with minimum acoustic attenuation [23], the conductive gel was utilised to fill air gaps caused by skin roughness and hairs. To record AE signals consistently, the sensors used for the left and right knees were fixed by the product serial number. The goniometer with a fixed sampling interval of 0.01 second is attached between the lateral side of thigh and shank using double sided medical tape.

For the knee to create AE signals, it is required to move under loading. Based on the previous studies [22-23], the participants were asked to perform 10 consecutive and repeated sit-stand-sit movements at their preferred and comfortable speed through a series of 5 consecutive movements with 30 seconds to 1 minute break between each series. Each sit-stand-sit movement consists of ascending from a 40 cm high chair until reaching a fully erect standing position, and descending back to return to the sitting position. In order to

minimise the influences of movement strategies [87], a chair with backrest and without armrest was used, and all the study participants were required to cross arms in front of their chest when performing the movements. Before starting data acquisition, each participant

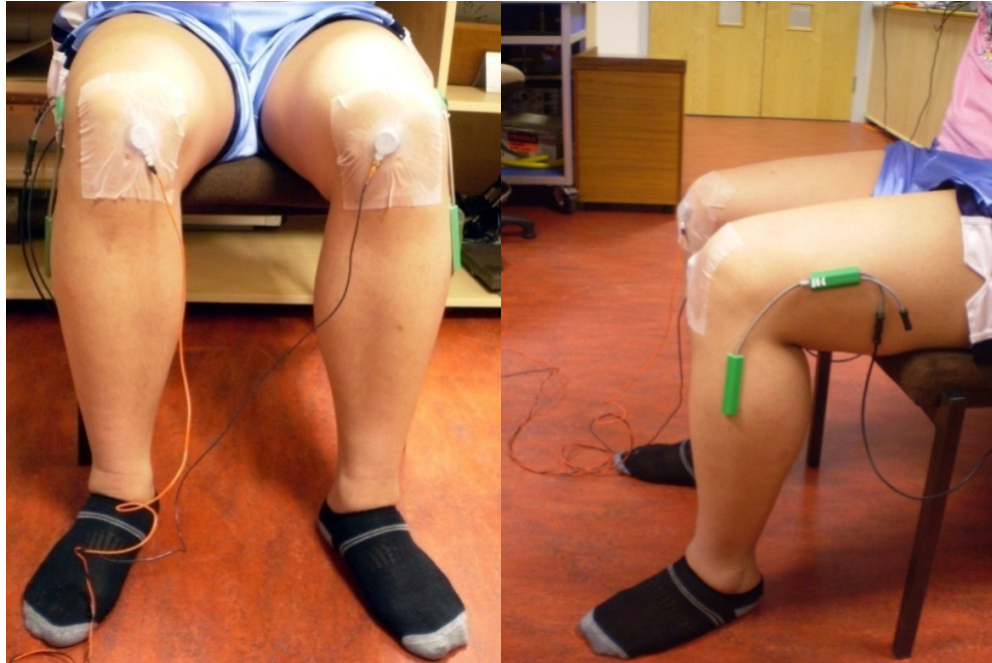


Figure 3-5 Sensor location and attachment

was asked to perform 3 to 5 consecutive movements, in order to become familiar with the movement protocol. The AE signals created by this familiarisation activity were not taken into account.

An example of joint angle based AE acquired by the system from a participant for a set of five consecutive and repeated sit-stand-sit movements is shown in Figure 3-6, there are five cycles in the joint angle signal corresponding to five repeated sit-stand-sit movements. The solid curve represents the joint angle signal, the minimum joint angle in each cycle corresponds to the knee flexion angle in the sitting position and the peak joint angle corresponds to the knee extension angle at the standing position, respectively. There exists a variation in the starting flexion angle among the participants, as it is determined by the participants' leg length which could not be controlled. The red dots superimposed on the angle signal correspond to individual AE events which satisfy the hit definition parameters stated in Sub-section 3.2.3.

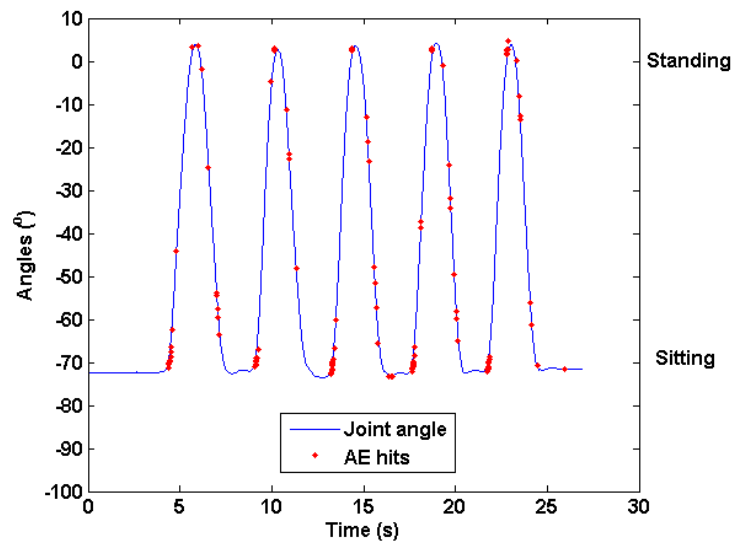


Figure 3-6 Joint angle based AE

Each individual AE event is accompanied by a set of characteristic waveform features [69] that can be grouped as follows:

- Amplitudes:

- Peak amplitude: Peak amplitude value (positive or negative) of individual waveform, measured in unit of dB.
- ASL: Average amplitude of AE signals, measured in unit of dB.
- Times:
 - Duration: Time continuation of the AE event between the first and the last threshold crossing, measured in unit of microseconds (μs).
 - Rise time: Time interval between the first threshold crossing and the AE peak amplitude, measured in unit of μs .
 - Fall times: Time interval between the peak amplitude and the last threshold crossing, measured in unit of μs .
- Energy:
 - Signal strength: Integral of the rectified signal voltage over the duration of AE waveform, measured by picovolt-second (pV-s).
 - Absolute energy: Integral of the squared voltage divided by the reference resistance ($10\text{ k}\Omega$) over the duration of AE event, measured in attoJoules (aJ).
- Signal counts:
 - Counts: Number of AE pulses exceeding the detection threshold.
 - Counts to peak: Number of AE pulses between the first pulse exceeding the threshold and peak amplitude.
 - Counts down: Number of AE pulses between the peak amplitude and the last AE pulse exceeding the detection threshold .
- Frequencies:

In the following, the first two frequency based features are derived from the power spectrum of AE hits calculated using the Discrete Fourier Transform (DFT) [97] and the remaining ones are derived from the relationships between the number of pulses and the time related components in each AE event.

- Peak frequency: Defined as the frequency of peak magnitude in the power spectrum, measures in unit of kilo-Hertz (kHz).
- Centre frequency: Centre frequency over the whole duration, this is determined as:

$$f_c = \frac{\sum_{n=1}^l |a(n)| \times f(n)}{\sum_{n=1}^l |a(n)|} \quad (3-1)$$

where $|a(n)|$ and $f(n)$ are referred to as the corresponding magnitude and frequency of the n^{th} Fourier frequency bin in the total of l frequency bins, respectively. Same as the peak frequency, the centre frequency is also measured in kHz.

- Average frequency: Average frequency over the whole duration, measured in kHz, and it is calculated by

$$f_a = \frac{\text{counts}}{\text{duration}} \quad (3-2)$$

- Initiation frequency: Frequency of the initial waveform before the peak amplitude, also known as the rise time frequency. It is calculated by counts to peak divided by the rise time, and also measured in kHz, as shown in equation (3-3)

$$f_i = \frac{\text{counts to peak}}{\text{rise time}} \quad (3-3)$$

- Reverberation frequency: AE frequency which can be computed by equation 3-4, measured in kHz

$$f_r = \frac{\text{counts down}}{\text{fall time}} \quad (3-4)$$

As an example, Figure 3-7 illustrates a typical AE waveform from a healthy knee, and a typical AE waveform from an OA knee, accompanied by the AE descriptors corresponding to each waveform.

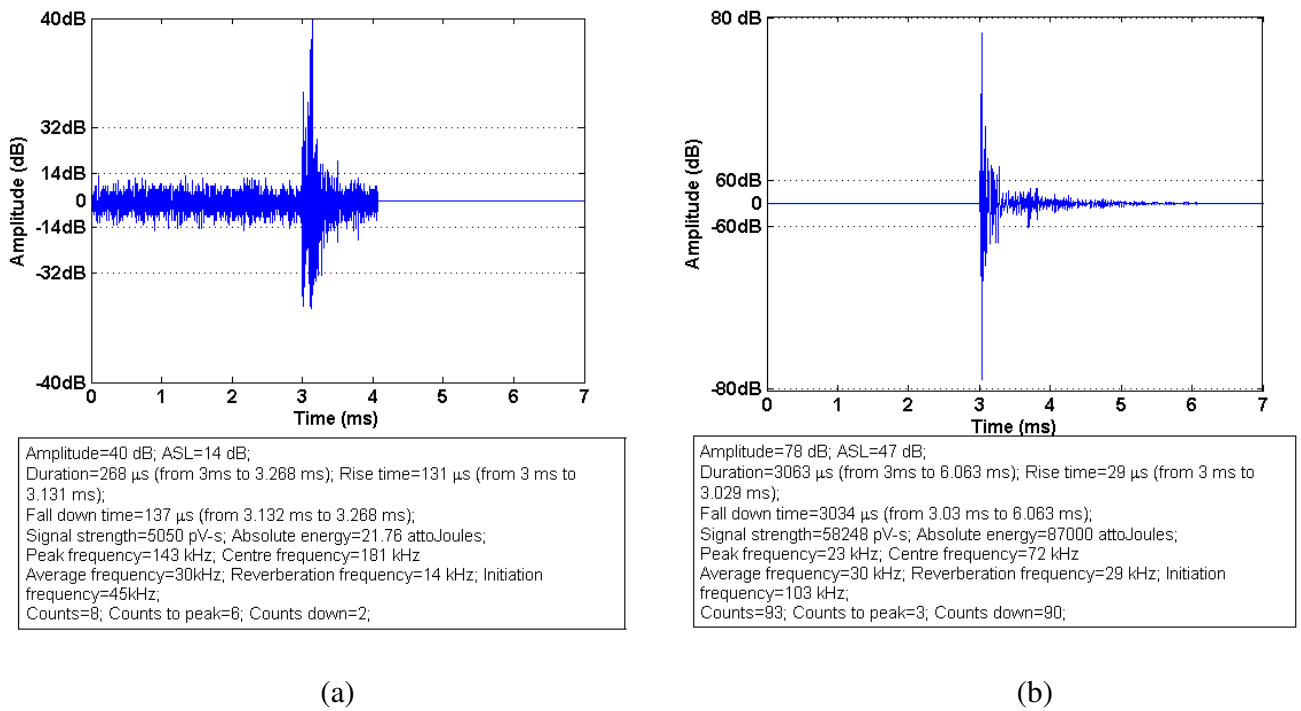


Figure 3-7 AE waveform example from (a) healthy knee; and (b) OA knee

3.4 STUDY PARTICIPANTS AND DATA COLLECTED

As shown in Table 3-1, AE and joint angle signals were collected from 72 participants. It includes 38 healthy subjects, 16 OA subjects, 7 rheumatoid arthritis (RA) subjects, 8 subjects with joint damage, 2 subjects with joint pain and the remaining one subject after

total knee replacement (TKR). The RA group consists of 6 subjects with rheumatoid arthritis and 1 subject with polyarthritis. The damage group includes 2 cartilage damage (two females), 2 ligament and cartilage damage (two males), and 4 joint injury participants (one male and three females). The healthy participants were recruited from the student and staff population at the University of Central Lancashire, and the local population in Preston area. All healthy participants were identified as the participants with knees not receiving any clinical treatments, or not having historic diagnosis as joint disorder by clinicians. The abnormal participants were recruited from among patients referred for physiotherapy to the Blackpool, Fylde & Wyre NHS Foundation Trust, all subjects were clinical-confirmed as joint disorder or symptomatic. The study was approved by the NHS local research ethics committee.

Joint condition	Number of subjects	MA ± SD (years)	ABMI ± SD (kg/m²)
Healthy	38	56.26±21.12	25.84± 3.55
OA	16	63.94 ± 9.53	29.53±3.83
RA	7	59± 12.78	33.25±1.50
Damage joints	8	48.63±15.64	29.13±3.14
Joint pain	2	78 ± 1.41	29 ± 5.66
TKR	1	85	32
Total	72		

Table 3-1 Age and BMI of each participating group with MA and SD denoting mean age and standard deviation

The body mass index (BMI) of each participant was derived from the general health and well-being questionnaire based on the participant's weight and body height, represented by the ratio of body weight and height squared in unit of kg/m². The BMI statistics for 6 main groups are also shown in Table 3-2, two healthy participants (aged 73 and 77 years), and three RA participants (aged 38, 69, 44 years) were excluded due to either body mass or

height missing. As the average BMI (ABMI) values of 6 main groups shown in the table, it is seen that the healthy subjects' ABMI value is slightly higher than the lower bound of the overweight level (ranged from 25 to 29.9 kg/m²). For the subjects with OA, joint damage, joint pain, the ABMI values are close to the upper bound of the overweight level. For RA participants, it is seen to reach the obesity level, with values varying between 30 and 34.9 kg/m².

Additionally, the healthy subjects can be further divided into three sub-groups, and the OA subjects can be further divided into two sub-groups based on their ages, the statistics of these sub-groups are shown in Table 3-2. From the ABMI values of the healthy and OA sub-groups shown in Table 3-2, most of healthy subjects aged from 20 to 40 years are seen to be in the normal weight condition (normal BMI is expected to vary from 18.5 to 24.9 kg/m²). Similar ABMI values are also observed from participants aged from 41 to 60 years and aged over 61 years in the healthy sub-groups, with the ABMI values for these two groups slightly higher than the lower bound of the overweight level. The ABMI values for the two OA sub-groups show that most of the subjects with knee OA are overweight, with

Joint condition	Number of subjects	MA ±SD (years)	ABMI ± SD (kg/m²)
Healthy sub-group aged 20 - 40 years	10	27.70 ± 3.67	24.90 ± 3.67
Healthy sub-group aged 41 - 60 years	10	51.20 ± 5.80	26.60 ± 3.13
Healthy sub-group aged above 61 years	18	74.78 ± 8.61	26.39 ± 3.63
OA sub-group aged 50 - 60 years	6	55 ± 1.90	28.50 ± 3.02
OA sub-group aged above 61 years	10	70.80 ± 6.43	29.60 ± 3.72

Table 3-2 Age and BMI of healthy and OA sub-groups

the maximum ABMI value from the eldest OA sub-group.

In terms of clinical data collection, healthy and OA subjects were required to answer a knee injury and osteoarthritis outcome scores (KOOS) questionnaire [98], an SF36 questionnaire [99], and a general health and well-being questionnaire (appendix E) that includes the body height, the body mass, and the experienced abnormal symptoms of left and right knees (includes clicking, difficulty in moving, grating, locking, pain, reduced range of movement, stiffness, swelling, and tenderness), thereby clarifying the clinical status of both knees for each study participant. Additionally, for OA group, the Kellgren & Lawrence (K-L) X-ray scores [11] of 10 knees with grades 1-4 corresponding to doubtful, minimal, moderate, and severe stages were also recorded, in order to measure the severities of damage. There are 2 knees with grade 1 (aged 55 and 82 years), 2 knees with grade 2 (aged 52 and 55 years), 3 knees with grade 3 (aged 55, 64 and 67 years), and 3 knees with grade 4 (aged 64, 71 and 73 years). For other abnormal subjects, the joint conditions were measured by the SF36 and the general health and well-being questionnaire.

3.5 DATA SELECTION

With a large number of healthy and OA knees in different age groups, it enables the project to focus on discovery of a potential AE based biomarker for quantitative assessment of knee joint ageing and degeneration. In order to ensure all signals used are collected from the knees under the clear clinical statuses. All selected healthy signals were collected from the knees without either previous treatment or experienced abnormal symptoms assessed by the general health and well-being questionnaire, and all selected OA signals were collected from the knees with radiological confirmation. The family arthritis histories, physical activities, and genders are not considered in this study. The data selected can be summarised as below:

- Group H1 early adulthood healthy knees, with 10 asymptomatic healthy knees selected from 8 healthy participants with ages 22-40 years (MA + SD = 29.42 ± 5.45 years). These 10 asymptomatic healthy knees consist of both knees from 2

healthy participants who had claimed both knees being normal and one knee from another 6 healthy participants who had claimed one knee without abnormal symptoms.

- Group H2 middle adulthood healthy knees, with 11 asymptomatic healthy knees selected from 8 healthy participants with ages 42-58 years (MA + SD = 50.00 ± 5.07 years). These 11 asymptomatic healthy knees consist of both knees from 3 healthy participants who had claimed both knees being normal and one knee from another 5 healthy participants who had claimed one knee without abnormal symptoms.
- Group H3 late adulthood healthy knees, with 13 asymptomatic healthy knees selected from 11 healthy participants with ages over 61 years (MA + SD = 71.27 ± 6.99 years). These asymptomatic healthy knees consist of both knees from two healthy participants who had claimed both knees being normal and one knee from another 9 participants who had claimed one knee without abnormal symptoms.
- Group OA1 middle adulthood OA knees, with 7 OA knees selected from 6 OA participants with ages 50-60 years (MA + SD = 55.00 ± 1.90 years). These OA knees consist of both knees from one OA participant based on radiological confirmation and one knee from another five OA participants based on clinician diagnosis.
- Group OA2 late adulthood OA knees, with 12 knees selected from 8 participants with ages over 61 years (MA + SD = 69.50 ± 6.39 years). These OA knees consist of both knees from four OA participants based on radiological confirmation and one knee from another four OA participants based on clinician diagnosis. Two participants were removed from the study due to data conversion problem.

For the healthy groups, the youngest and the eldest knee ages are 22 and 83 years, respectively. For the OA groups, the youngest and the eldest knee ages are 52 and 82 years, respectively.

3.6 CONCLUDING REMARKS

This chapter has focused on the description of the system used to acquire AE and joint angle signals, the system setup, the movement based data acquisition protocol, the joint angle based AE, as well as the data collected. The data acquisition system consists of the traditional AE system and the electronic angle measurement system, which includes two circular piezo-electric AE transducers, and two twin-axis electro-goniometers along with the corresponding signal receiving, amplification and pre-processing units. The motivation of integrating the angle measurement modality with the AE measurement modality is to allow the occurrence of AE signals to be related to the joint angles. Both AE and electronic goniometer system are firstly connected to the corresponding amplification and pre-processing units, and then synchronised by the same trigger, and both of signals are pre-processed by using the PCI-2 data processing board. An AE event is determined when the transient signals satisfy four hit definition parameters, namely, threshold, PDT, HDT, and HLT, respectively.

The AE events were recorded by attaching piezo-electric transducers and goniometers inferior to the patella and anterior to the medial compartment (nearest location toward the knee weight bearing surface) and lateral side of the leg, respectively. As AE signals are generated when the knee is under pressure, participants were required to make two sets of 5 consecutive and repeated sit-stand-sit movements using the preferred and comfortable speeds to create AE and joint angle signals. All participants were required to fold arms in front of their chest, in order to minimise the influence of movement strategies. The joint angle based AE accompanied by a set of waveform features were recorded using the non-continuous mode.

AE and joint angle signals, as well as the clinical records were collected from 72 subjects, including 38 healthy participants, 16 OA participants, 7 RA participants, 8 participants with joint damage, 2 joint pain participants and 1 OA participant after TKR. The healthy and OA subjects can be further divided into five sub-groups based on their ages. In terms of the ABMI values, the values showed that most of the participants in healthy, OA, damage joints and joint pain groups are overweight, and most of participants in RA and after TKR

group are obese. For the five healthy and OA sub-groups, most of the participants in the early adulthood healthy group are seen to have normal weight, whereas most of the participant in the other four groups are seen to have overweight. The AE signals used to study are captured from 10 group H1 knees, 11 group H2 knees, 13 group H3 knees, 7 group OA1 knees and 12 group OA2 knees. In order to ensure all the signals used to investigate joint ageing and degeneration were under clear clinical statuses, all the healthy signals were selected from the knees without any experienced abnormal symptoms or previous treatments, and the OA signals were all selected from the knees that were radiologically-confirmed. The family arthritis histories, physical activities, and genders were not considered.

CHAPTER 4 ANALYSIS OF JOINT ANGLE SIGNALS

4.1 INTRODUCTION

This chapter presents processing and analysis of joint angle signals. Section 4.2 introduces the pre-processing of joint angle signals. As consecutive and repeated sit-stand-sit movements are performed by all participants, they are isolated based on joint angle and angular velocity into individual cycles with four movement phases proposed for measuring the statistical outcomes. Section 4.3 analyses the joint angle signals in terms of the cycle-by-cycle variation and the symmetry of individual sit-stand-sit movement cycle, represented by the average correlation coefficients and the symmetric ratio, respectively. Concluding remarks are given in Section 4.4.

4.2 MOVEMENT ISOLATION

With sit-stand-sit forming the fundamental action in the movement protocol to create knee AE signals, each sit-stand-sit movement cycle performed by a participant can be considered as performing one individual test that gives a particular AE measurement outcome. With all participants performing consecutive and repeated sit-stand-sit movements, it is not unreasonable to assume some meaningful statistics to be embedded in the multiple measurement outcomes generated by the repeated movement actions [23]. Based on this assumption and the underlying biomechanical strategies of movement, the consecutive and repeated sit-stand-sit movements are separated to individual movement cycles with four movement phases proposed for measuring the statistical outcomes.

The procedures for movement cycle separation can be briefly summarised as below:

- Smooth the raw angle signal using a moving average window, which is derived by [40], thereby removing the short-time fluctuations occurred during knee movement. The definition of the moving average window used to smooth the joint angle signals is given by:

$$\theta_s(t) = \frac{\sum_{r=t-k}^{t+k} \theta_r(t)}{k} \quad (4-1)$$

where k is referred to as the window length, $\theta_r(t)$ denotes the joint angles before smoothing with t as the sample index, and $\theta_s(t)$ is the smoothed joint angle at sample t .

- Calculate the instantaneous angular velocity by using the definition given by:

$$\omega(t) = \frac{d\theta_s}{dt} = \frac{\theta_s(t) - \theta_s(t-1)}{t_s} \quad (4-2)$$

where $\theta_s(t)$ and $\theta_s(t-1)$ are the smoothed joint angles at sample t and $t-1$, respectively, and t_s denotes the sampling interval of the goniometer, which was set to 0.01 seconds for all data acquisition.

- With the instantaneous angular velocity calculated, a velocity threshold of $|\omega(t)| = 0.1 \text{ }^\circ/\text{s}$ was provided to determine the start and stop time of each movement cycle. The knee joint is considered to be in motion when $|\omega(t)| > 0.1 \text{ }^\circ/\text{s}$, and static when $|\omega(t)| \leq 0.1 \text{ }^\circ/\text{s}$, where $|\omega(t)|$ denotes the absolute values of the angular velocity computed by equation (4-2).

Figure 4-1 shows an example of angle signal before smoothing and the smoothed angle signal over 10 movement cycles, with the raw angle signals shown in the left half of the figure, it is seen that before smoothing, there are local fluctuations in the signal, mainly at the start and stop of each sit-stand-sit movement. This will influence the movement cycle isolation, because short time fluctuations will have possibility to drive the local velocity to a high level due to the sampling interval being fixed to as short as 0.01 second. By comparing with the signals shown in the right half of the figure, it is seen that the angle signal can be smoothed using the above mentioned moving average window with a length of 50, which was found to be appropriate for all joint angle signals.

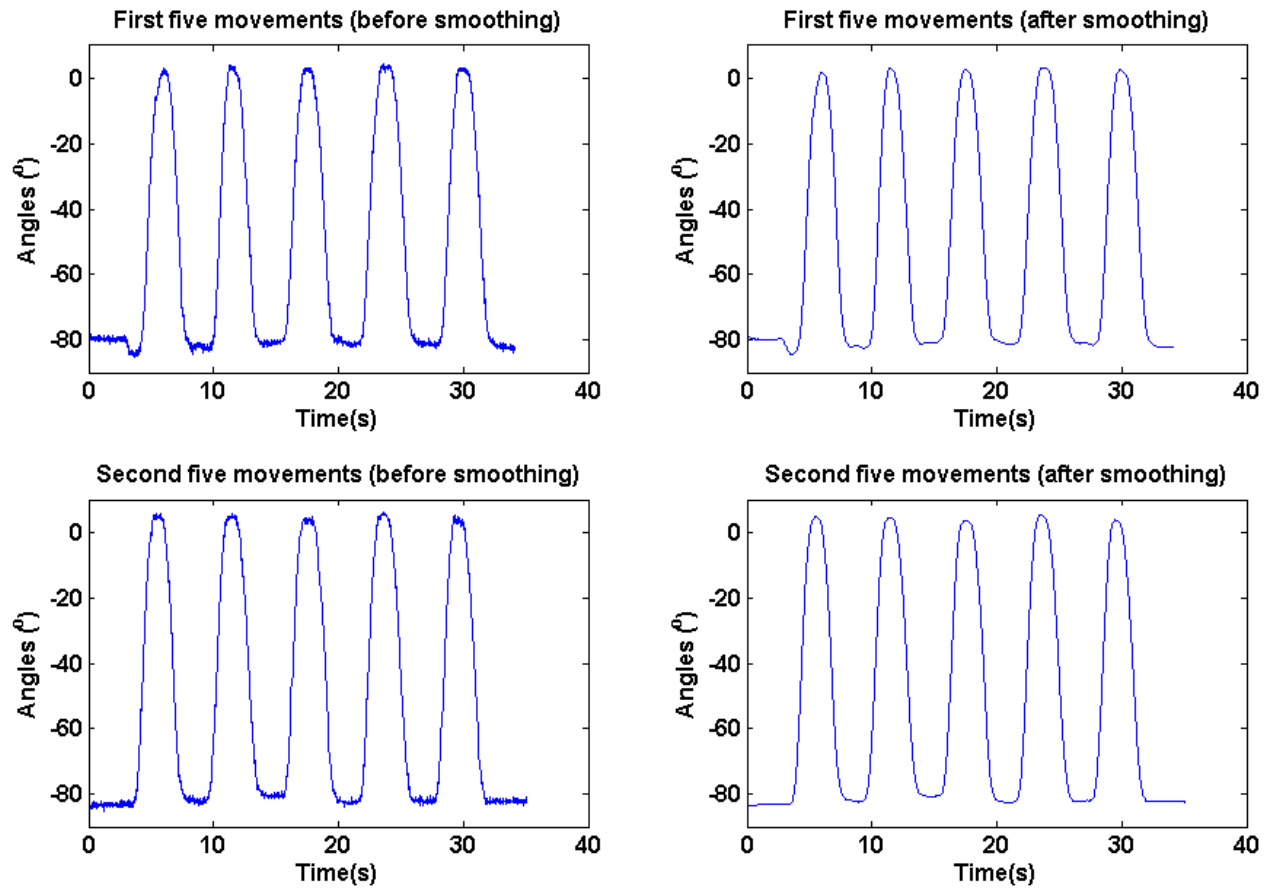


Figure 4-1 Angle signals before and after smoothing

With the knees moved under the preferred and comfortable speed, the variations in the durations of individual movements are analysed. Figure 4-2 shows the statistical differences in individual movement duration for all the knees performing 10 repeated movements, where the dots and whisker represent the average duration and the corresponding SD value over 10 movement cycles. By observing the deviations shown in the figure, it is seen that the consecutive movements performed by most of knees studied can be considered as repeatable, with the SD values less than 1 second for all the knees studied. By using the mean and SD plots of the late adulthood healthy group (H3) as the reference, movement durations of group H1 and H2 knees are shown to be more consistent than two OA groups, with all deviations shorter than 0.5 seconds. Although some movement durations with slightly higher variations start to appear from group H3 knees, they can be considered as repeatable as movement durations with high deviations can be associated mainly with the long average durations (the highest deviation of 0.73 seconds corresponding to the average duration of 4.73 seconds appears in one of OA2 knees).

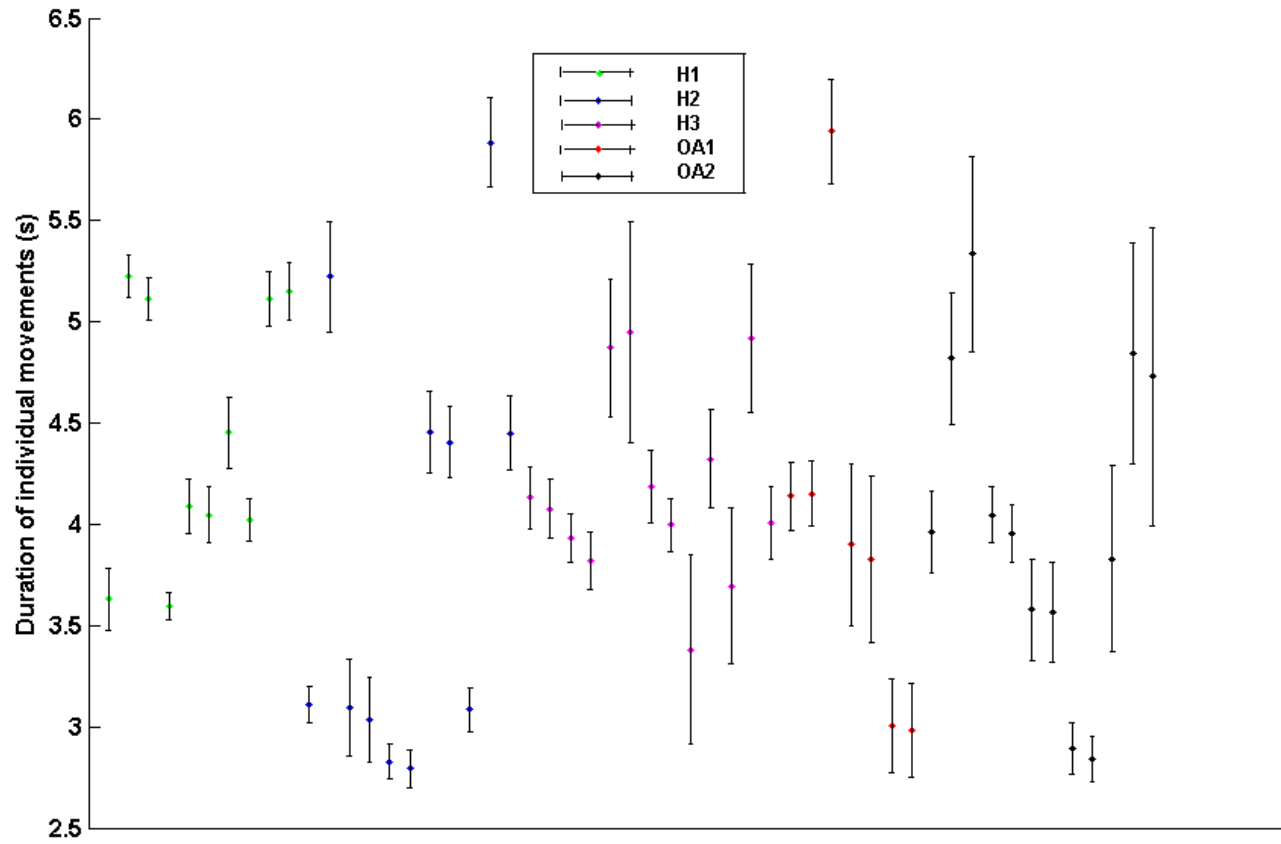


Figure 4-2 Durations of individual movements for all knees studied

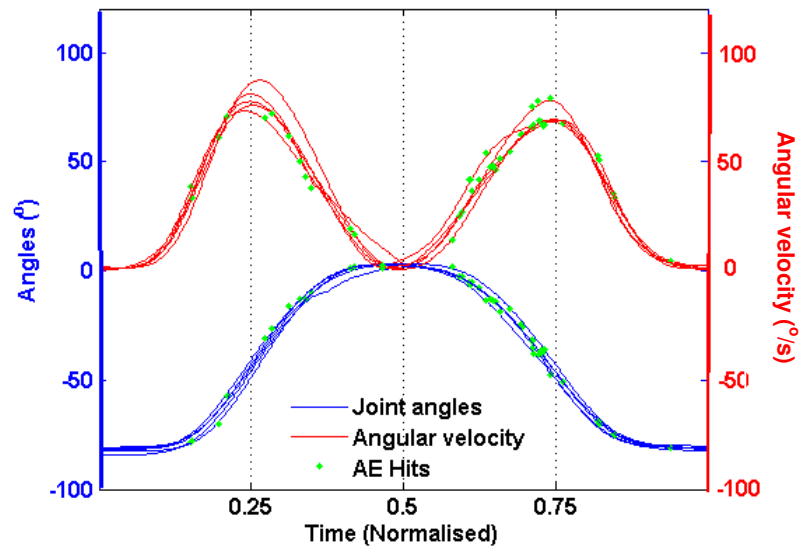


Figure 4-3 Normalised joint angle and angular velocity with AE hits from healthy knee in group H1

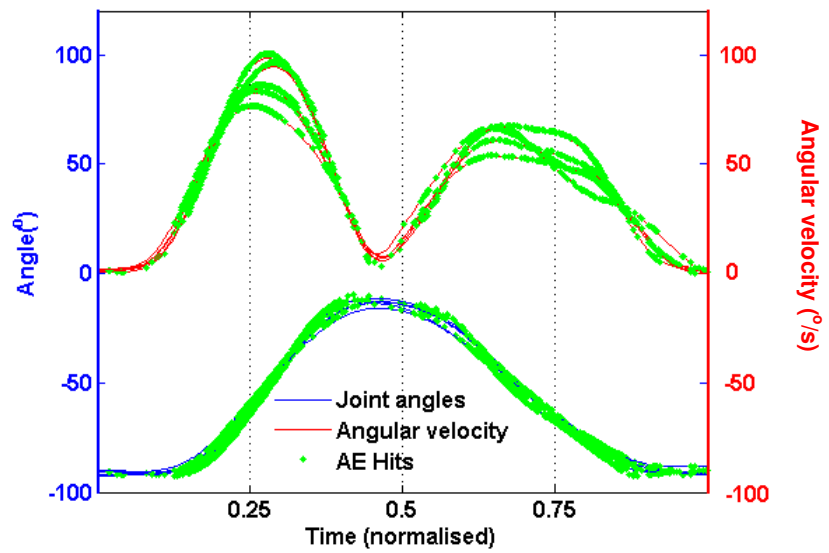


Figure 4-4 Normalised joint angle and angular velocity with AE hits from OA knee in group OA2

By performing movement cycle separation, Figures 4-3 and 4-4 show a set of five cycles of joint angle and angular velocity signals superimposed on each other together with AE hits represented by dots, where the time scale of each movement is normalised by its full duration in order to compare the data from different movements based on a comparable scale. From the angle and angular velocity signals shown in Figures 4-3 and 4-4, it can be seen that each individual sit-stand-sit movement can be divided to the ascending phase (sit-to-stand) and the descending phase (stand-to-sit) by using the occurrence of peak joint angle, and each ascending/descending phase can be further divided into the acceleration phase and the deceleration phase using the maximum velocity values in the ascending/descending phase, thereby forming the following four movement phases:

- The ascending-acceleration (AA) phase from the start of the movement at the sitting position to the occurrence of the peak angular velocity.
- The ascending-deceleration (AD) phase from the peak angular velocity in the ascending phase to the occurrence of the peak angle upon reaching the standing position.
- The descending-acceleration (DA) phase from the occurrence of the peak angle to the occurrence of the peak angular velocity in descending.
- The descending-deceleration (DD) phase from the peak angular velocity to the stop of the movement at the sitting position.

In the previous studies, the individual sit-stand-sit movement cycle has been isolated to ascending-descending phase for movement measurements among various age groups [84], in this thesis, these four phases-model developed are considered to link more closely to the underlying biomechanical strategies of movement including the temporal sequences of segment movement, muscle activity and joint moments.

4.3 ANALYSIS OF JOINT ANGLE SIGNALS

With each individual movement divided into four movement phases, the superimposed joint angle and angular velocity signals from the healthy knee shown in Figure 4-3 are seen to have a lower cycle-by-cycle variation than those from the OA knee shown in Figure 4-4.

Moreover, it can be also observed from these two figures that the angular movements of the healthy knee are more symmetrical than the OA knee in terms of the waveform shapes, the time spent in each movement phase, as well as the peak angular velocities. These observations have led to the analysis in this section of cycle-by-cycle variations of joint angle signals (Sub-section 4.3.1), as well as the movement symmetry (Sub-section 4.3.2).

4.3.1 Cycle-by-cycle variations of joint angle signals

Let the smoothed angle signal of individual sit-stand-sit movement cycle be denoted by $A(i)$ with $i = 1, 2, \dots, 10$. Using the middle movement cycle in each set of five consecutive sit-stand-sit movements as the reference, the cycle-by-cycle variations of joint angle signals are assessed by using the average correlation coefficient (ACC) [100] given by:

$$\bar{r}_\alpha = \frac{1}{8} \left(\sum_{i=1,2,4,5} |C(A(i), A(3))| + \sum_{i=6,7,9,10} |C(A(i), A(8))| \right) \quad (4-3)$$

where c is the correlation coefficient given by:

$$C = \frac{l \sum A(m)A(i) - \sum A(m) \sum A(i)}{\sqrt{\{[l \sum A(m)^2 - (\sum A(m))^2][l \sum A(i)^2 - (\sum A(i))^2]\}}} \quad (4-4)$$

where l denotes the number of samples in two angle signals which are required to have the same length, and $A(m)$ denotes the middle movement cycle of the first and the second consecutive sit-stand-sit movement sets. According to the data acquisition protocol described in Section 3.3, the durations of individual movement cycles performed by the same knee are slightly different (Figure 4-2). In order to make the signals over the duration of interest to have the same length, the peak angle of the reference movement is aligned with the peaks of other movements with the extra parts at the beginning and/or end of the longer angle signal excluded in the correlation computation using equation 4-4. The values of ACC vary between 0 and 1, with the values greater than 0.8 and less than 0.5 considered as strong and weak correlated, respectively.

Similarly, let the angular velocity of each sit-stand-sit movement cycle be denoted by $V(i)$ with $i = 1, 2, \dots, 10$. Using the middle movement cycle in each set of five consecutive sit-stand-sit movements as the reference, the average ACC value for the angular velocities is given by:

$$\bar{r}_v = \frac{1}{8} \left(\sum_{i=1,2,4,5} |C(V(i), V(3))| + \sum_{i=6,7,9,10} |C(V(i), V(8))| \right) \quad (4-5)$$

where

$$C = \frac{l \sum V(m)V(i) - \sum V(m) \sum V(i)}{\sqrt{\{[l \sum V(m)^2 - (\sum V(m))^2][l \sum V(i)^2 - (\sum V(i))^2]\}}} \quad (4-6)$$

As the durations of angular velocity signals in two different movement cycles are also slightly different, like the joint angle signal, the peak velocity of the reference movement cycle is aligned to the peak velocity of other movements with the extra parts excluded in correlation computation.

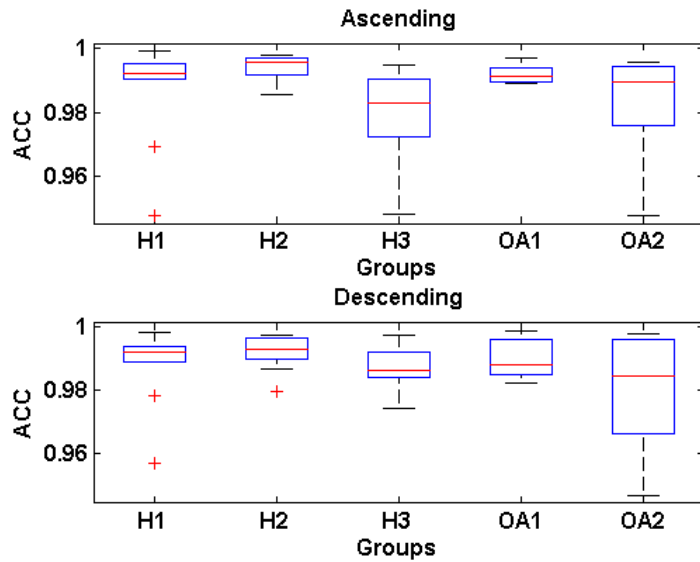


Figure 4-5 Cycle-by-cycle variations of joint angle signals

Figure 4-5 shows the cycle-by-cycle variations of the joint angle signals of all the knees studied in the ascending and descending phases using the box and whisker plot, where the upper and lower bounds of the box represent the upper and lower quartiles (75% and 25% percentiles) of movement durations of each group, respectively; the red line in each box represents the median value (50% percentile); the inter-quartile range (IQR) is defined as the distance between the upper and the lower quartiles; the whiskers at two extremes represent the maximum and minimum values within 1.5 times the IQR; and the red crosses outside the box represent the possible outliers which exceed the $1.5 \times \text{IQR}$ [101].

By observing the ACC values of the five groups shown in Figure 4-5, it can be summarised that:

- Angle signals acquired from individual participants performing the sit-stand-sit movement are shown to have high similarities among different movement cycles, with the maximum ACC for all groups in both ascending and descending movement phases above 0.99.
- From the IQR of the ascending phase, an age related difference is observed, with shorter IQR corresponding to higher movement consistency observed in the early and middle adulthood groups (H1, H2, and OA1), and longer IQR corresponding to lower movement consistency observed in the late adulthood groups (H3 and OA2).
- From the IQR of the descending phase, there is a noticeable age and degeneration related trend. As shown in the bottom of Figure 4-5, the IQR is seen to increase from H1 to OA2, with the maximum inconsistency observed in group OA2.

According to the cycle-by-cycle variations of the instantaneous angular velocity in the four movement phases shown in Figure 4-6, it can be seen that:

- The angular velocities also show strong correlations among different movement cycles in the four movement phases, with the lower quartiles of all the ACC values above 0.95.

- From the IQR in the DA phase, there is a difference between healthy groups and OA groups, with higher angular velocity deviation observed in the three healthy groups and more consistent angular velocity observed in the two OA groups.
- From the IQR in the DD phase, the late adulthood healthy group and the OA groups are seen to have higher angular velocity deviation than the early and middle adulthood healthy groups.

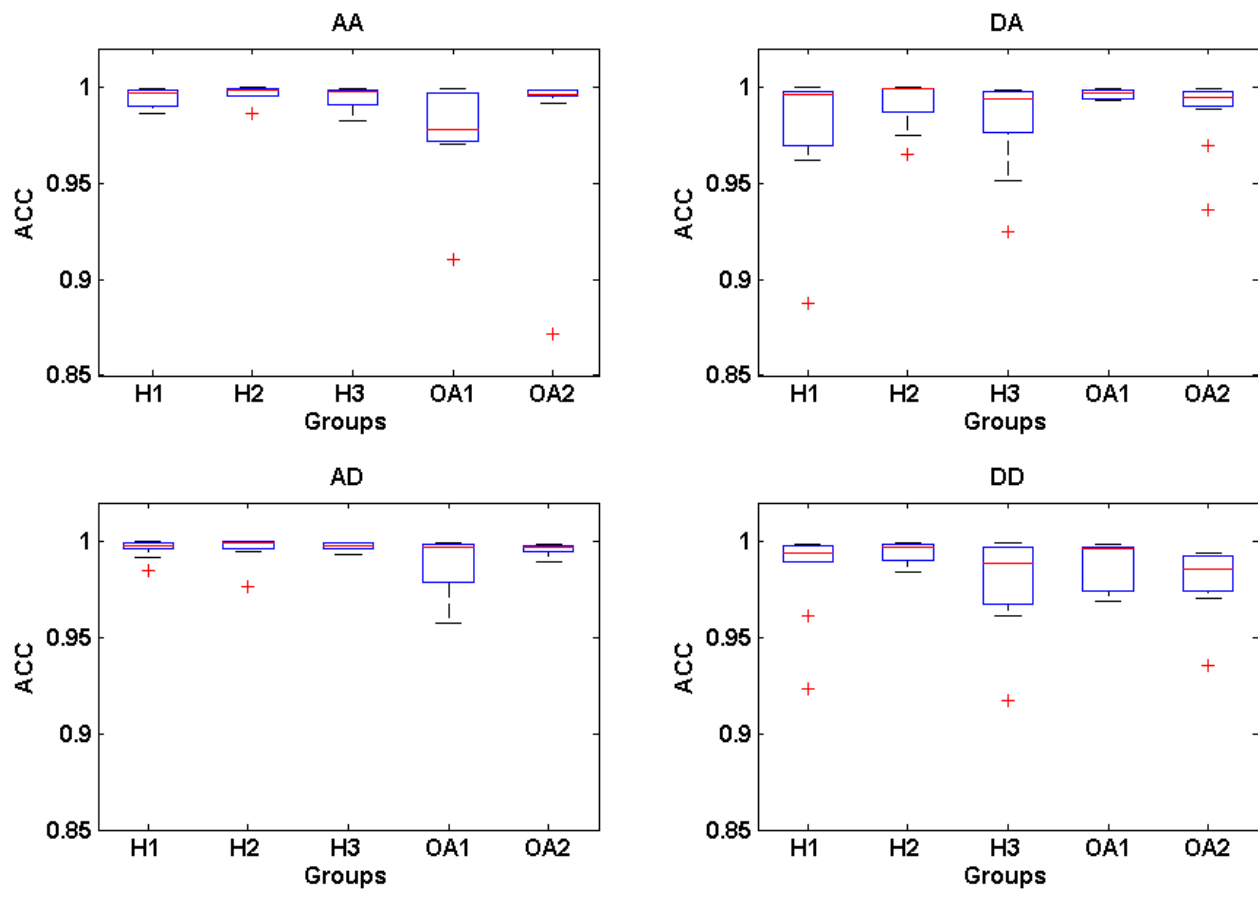


Figure 4-6 Cycle-by-cycle variations of instantaneous angular velocity

4.3.2 Movement symmetry

In order to investigate the movement symmetries when participants performing sit-stand-sit movements using the preferred and comfortable speed, the symmetric ratios of ascending-descending movements and acceleration-deceleration movements within the ascending or descending phase are investigated in this sub-section. The symmetric ratio has been previously applied to study the relationships between the movement symmetry and the agonist/antagonist muscle activities of the elbow movements [102]. The definition of the average symmetric ratio is given by:

$$\bar{s}_t = \frac{1}{10} \left(\frac{t_a}{t_d} \right) \quad (4-7)$$

where, t_a and t_d denote the total time spent on ascending or acceleration, the total time spent on descending or deceleration, respectively.

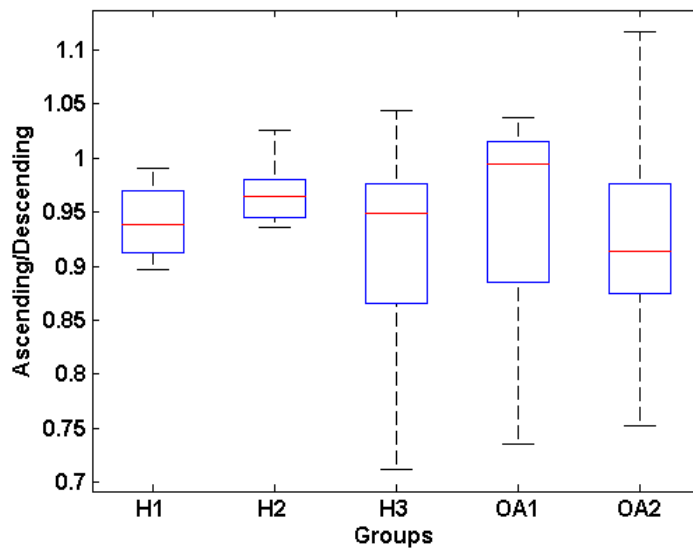


Figure 4-7 Ratios of ascending time to descending time

Figure 4-7 shows the average ratios of the time spent on each ascending movement to the time spent on each descending movement. Based on the results shown in this figure, it is seen that:

- The descending movements take longer time than the ascending movements, which is true for most of the knees studied (48 out of 53 knees shown in the figure), and is in agreement with [87].
- The movements performed by the early and middle adulthood healthy knees (H1 and H2 groups) are seen to be more symmetric and consistent than the other three groups, with all symmetric ratios varied between 0.9 and 1 for H1 knees and between 0.9 and 1.05 for H2 knees, respectively.

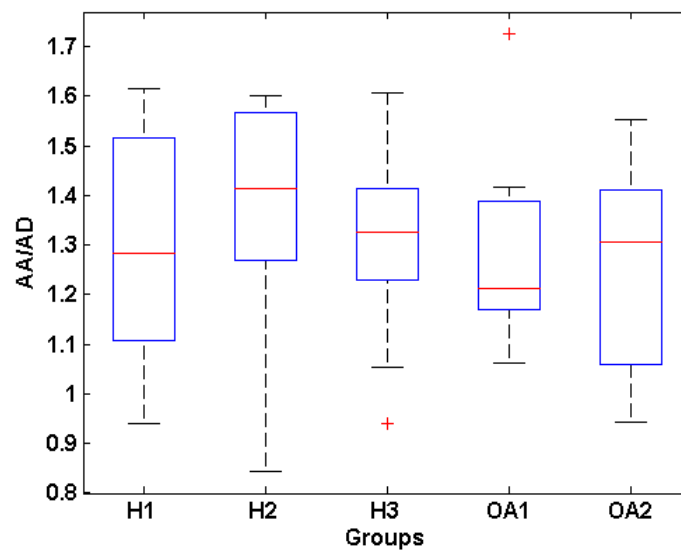


Figure 4-8 Ratios of AA and AD times

Based on the average ratios of the AA to AD times shown in Figure 4-8, it is seen that:

- Most of the knees studied take a longer time to accelerate to the peak velocity than the time to decelerate back to static. Only a few knees are seen to spend similar times on acceleration and deceleration with 3 out of 53 knees shown to have symmetric ratios between 0.9 and 1.1.

Based on the average of the DA to DD time ratios shown in Figure 4-9, it is seen that

- A high percentage of the knees is seen to take more time to decelerate than to accelerate in the descending phase.
- There is an degeneration related difference observed in two age matched groups in terms of IQR, with increasing variations in the middle adulthood groups from H2 to OA1 and the late adulthood groups from H3 to OA2.

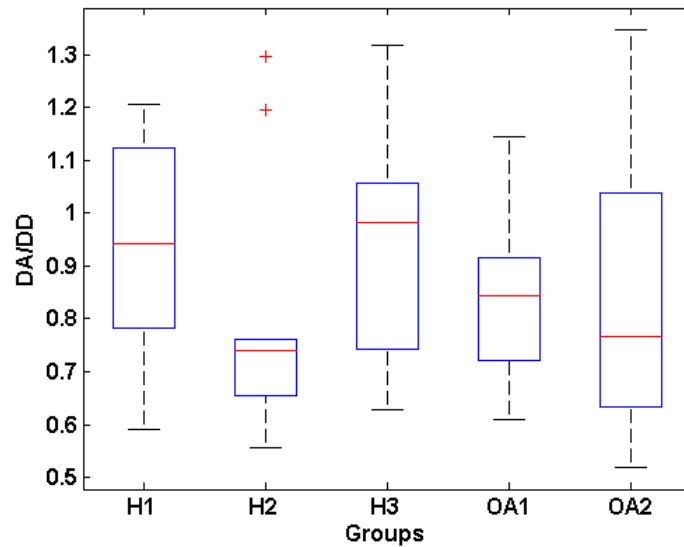


Figure 4-9 Ratios of DA and DD times

Since the sit-stand-sit movement has been divided to four phases based on the instantaneous angular velocity, another obvious symmetric ratio is the peak angular velocity in the ascending to that in the descending phase. The definition of the peak velocity ratio is given by equation 4-8:

$$\bar{s}_v = \frac{1}{N} \left(\frac{\max|\omega(t_a)|}{\max|\omega(t_d)|} \right) \quad (4-8)$$

where $\max|\omega(t_a)|$ and $\max|\omega(t_d)|$ are referred to as the maximum instantaneous angular velocity in each ascending and descending phase, respectively.

As the average ratios of peak angular velocities for the five groups shown in Figure 4-10, it can be summarised that:

- The peak angular velocity in the ascending phase for majority of the knees is generally higher than that in the descending phase.
- The IQR of the early adulthood healthy group shows the highest consistency with the smallest deviation among the five groups observed. This is followed by the middle and late healthy adulthood groups with higher deviation, and the two OA groups with the highest deviation.
- There is also an age related difference, with the early and middle adulthood groups having more similar peak velocities in the ascending and descending phase than the late adulthood groups with higher peak velocity in the ascending phase. This is in agreement with the observation of elder subjects tending to have a higher velocity to lift off the chair as reported in [90] and mentioned in Section 2.4.2.

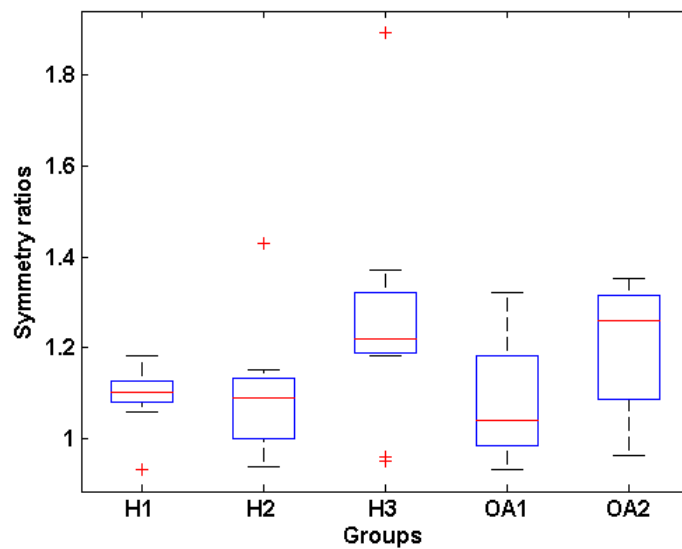


Figure 4-10 Ratios for peak angular velocities in ascending and descending phases

4.4 CONCLUDING REMARKS

This chapter focused on pre-processing and analysis of joint angle signals. It firstly presented the methodology to process the joint angle signal (Section 4.2). A moving average window was applied to the joint angle signals in order to smooth the signal and remove the short time fluctuations. The instantaneous angular speeds within each goniometer sampling interval were calculated and an angular velocity threshold was applied to determine the start and stop of each movement. After the consecutive movements have been separated to individual cycles, the variations of individual movements performed by the same knee were evaluated, and the results showed that the times taken to perform each individual movement for the same knee can be considered as repeatable with relatively small SD. Based on the joint angular signals and the corresponding velocity of them, each movement cycle was divided further into four movement phases for statistical analysis.

By investigating the cycle-by-cycle variations of all knees in the ascending and descending phases (Sub-section 4.3.1), high consistency among different cycles was observed. Additionally, there is a certain age related difference observed in terms of IQR in the ascending phase (with the late adulthood groups having higher IQR), and an ageing and degeneration related trend observed in terms of IQR in the descending phase (with IQR increasing with age from the early adulthood healthy group to the late adulthood healthy group followed by the middle adulthood OA group to the late adulthood OA group). By further investigation of the cycle-by-cycle variations over the four movement phases, highly consistent angular velocities among different cycles were also observed. The degeneration related difference was observed in the DA phase with the healthy groups having higher deviation, and an ageing and degeneration related difference was observed in the DD phase with the late adulthood healthy group and the OA groups having higher deviation, these higher deviations in descending phase could be due to the eccentric muscle contraction [24], while the higher tensions are created during muscle lengthening.

The movement symmetry also showed the age and degeneration related differences (Sub-section 4.3.2). The ascending-descending time ratio reveals a higher movement symmetry

from the early and middle adulthood healthy knees compared with the other three groups. Furthermore, there is a degeneration related difference in the IQR in the DA-DD time ratio by comparing healthy and OA knees in the same age group. Other interesting results from the ascending-descending peak velocity ratio include IQR increases with age and OA, and an age related difference with the late adulthood groups having higher difference between their ascending and descending peak velocities.

CHAPTER 5 STATISTICAL EVALUATION OF AE SIGNALS IN FOUR PHASES

5.1 INTRODUCTION

Following the analysis of joint angle signals in the preceding chapter, the AE signals occurred in the four detailed movement phases are analysed in this chapter. It starts with the basic statistical analysis of the quantity of AE events (Section 5.2). This is followed by the detail analysis on the shapes of distributions and value occurrences of various AE waveform features mentioned in Section 3.3 to investigate further differences in the time and frequency domains among the participating groups. Section 5.3 evaluates the features in the amplitude category, which includes the statistical evaluation of peak amplitude and ASL. The statistical distributions and the value occurrences of time based features are discussed in Section 5.4, which includes the statistical evaluations of duration, rise time, and fall down time. Section 5.5 devotes to the frequency based features, which consists of two frequency features derived from the waveform frequency spectrum, namely, peak frequency and centre frequency, respectively; and three features derived from the time-series waveforms, namely, average frequency, initiation frequency, and reverberation frequency, respectively. The statistical distributions of AE energy based features in terms of signals strength and absolute energy are covered in Section 5.6, and the statistical distributions of AE counts in terms of pulses exceeding the detection threshold (counts, counts to peak, and counts down) are covered in Section 5.7. Concluding remarks are given in Section 5.8.

5.2 BASIC STATISTICS IN FOUR MOVEMENT PHASES

Based on the four movement phase model established, AE signals were firstly analysed according to the quantity of AE events per movement. Although it is considered as a simple

analysis of AE signals, it is seen to form a good statistical observation in terms of gross AE activity from the knee joint during consecutive movements [23].

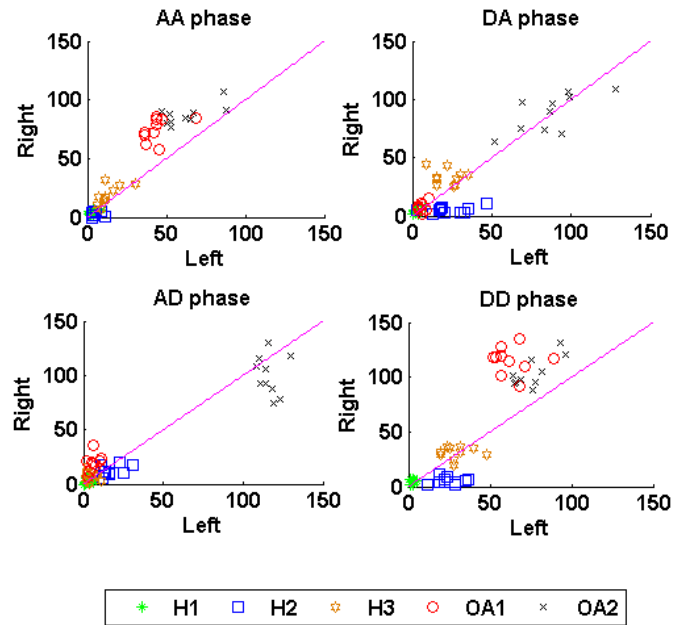


Figure 5-1 Bilateral plots with right versus left knees for each movement phase

Using bilateral plots with left knee versus right knee in each sit-stand-sit cycle, the number of AE hits generated by participants with both knees healthy and OA were compared in each movement phase. As an example, Figure 5-1 shows the bilateral plot for one participant in each group in the four movement phases, where a point near to the diagonal line indicates a symmetrical pair of knees with the number of AE hits from its left knee similar to that from the right knee in a sit-stand-sit cycle. Although the number of participants with both knees selected for the study is small, with consecutive and repeated sit-stand-sit movements performed by the participants generate repeatable results over certain durations, this can be considered as representative of the whole study population according to the ergodic theorem [103]. This enables some general observations to be made. For the early adulthood healthy group (H1), the participants are seen to generate particularly low, repeatable, and symmetrical numbers of AE hits from the left and right knees in all movement phases. With the increase in age, the participants in the middle and

late adulthood healthy groups (H2 and H3) are seen to generate higher but still relatively repeatable numbers of AE hits with a certain loss of symmetry in some movement phases. As the knee condition changed from healthy to OA, the participants in the middle and late adulthood OA groups are seen to generate much higher numbers of AE hits with a wider spread and a certain hit asymmetry in some or all movement phases.

To show the statistical differences between the five groups for all the knees studied, the average AE hits among repeated movements are investigated. Let the $q(i, \psi)$ be the AE hits acquired from the i^{th} movement in phase ψ , the average AE hits acquired from phase ψ can be determined by:

$$\bar{q}_\psi = \frac{1}{10} \sum_{i=1}^{10} q(i, \psi) \quad (5-1)$$

where ψ denotes the AA, AD, DA, DD movement phase, respectively.

The AE hits in each movement cycle for each participant in each movement phase are tabulated in Appendix F and Figure 5-2 shows the average AE hits of the five groups represented by the box and whisker plot [101]. From the figure, it can be summarised that:

- Vast amount of transient AE signals are generated by the knees performing sit-stand-sit movements (up to the maximum of 155.7 hits per movement on average from the late adulthood OA group (OA2) in the DD phase).
- Although there are overlaps between the five groups (with the DD phase showing minimum overlaps), the maximum, median, and minimum average number of AE events are seen to increase in all movement phases based on age and joint conditions, increasing from group H1 to H3 followed by group OA1 to OA2, even with outliers taken into account.
- By using the median value of QA from the early adulthood healthy group as the reference, the maximum increase is seen to occur in the DD phase (around 7 times increase from group H1 to group H3 and 23 times increase from group H1 to group OA2), and the minimum increase is seen to occur in the DA phase (around 4 times

increase from group H1 to group H3 and around 14 times increase from group H1 to group OA2) .

- There is a trend of increasing deviations related to age and OA (as shown by the IQR in the figure), with the number of AE hits generated by the OA groups seen to be more variable than those of the healthy groups.
- The best separation of the five groups based on the number of AE events is seen to occur in the DD phase, with all values within the IQR non-overlapped.

The results are in agreement with the previous work presented in Sections 2.3 and 2.4, and show the potential of using AE for identifying subtle differences in terms of joint age and condition.

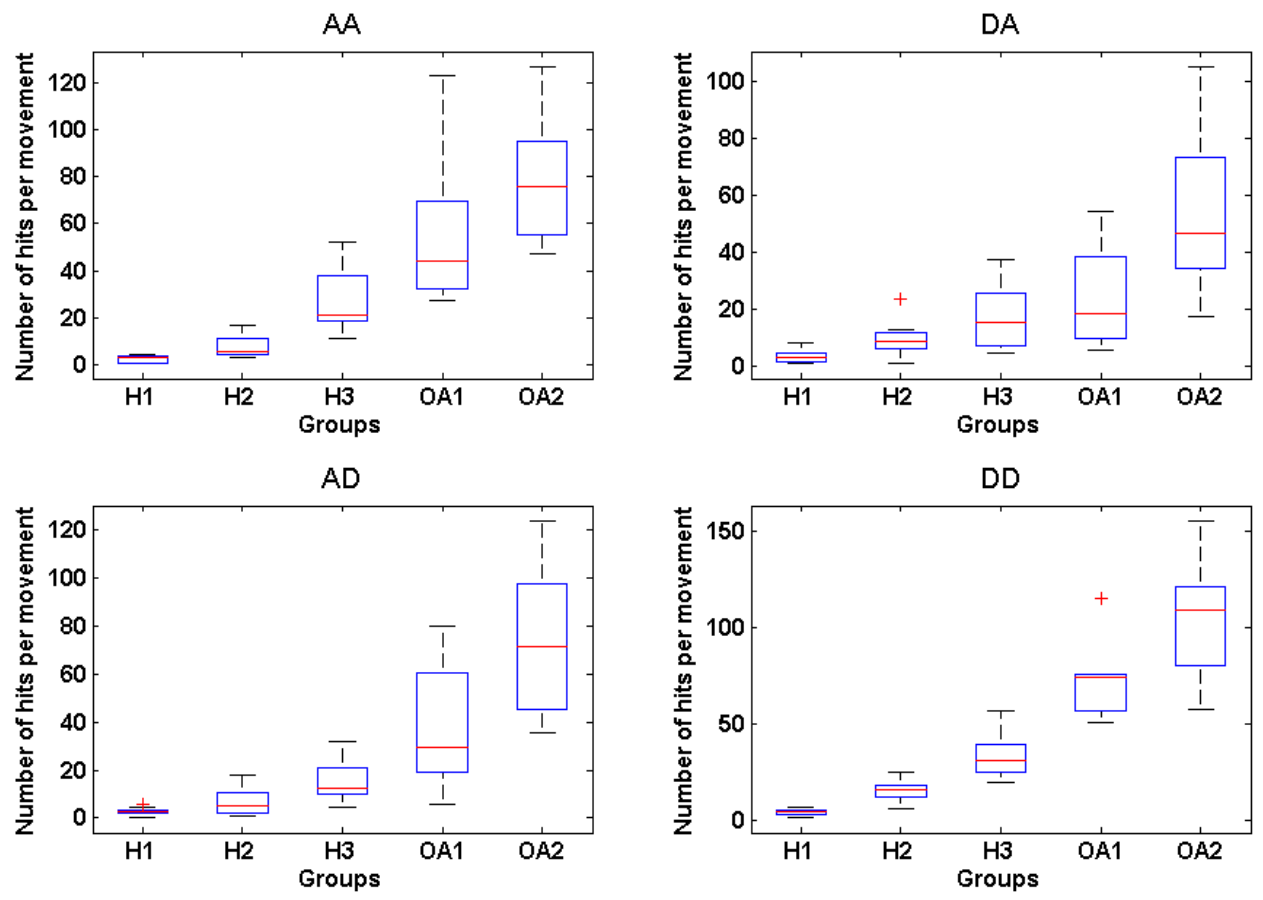


Figure 5-2 Statistical differences of AE hits between five groups among four movement phases

5.3 STATISTICAL EVALUATION OF AMPLITUDE BASED FEATURES

With the basic statistics of AE hits showing the age and degeneration related trends, the following sections are devoted to detailed analysis based on the statistical distributions of various AE waveform features, thereby discovering further differences among the participating groups. Since each individual movement has been further divided into four movement phases using the joint angles and the corresponding instantaneous angular velocity (i.e. AA, AD, DA, and DD), similar to the AE hit analysis in the preceding section, the statistical analysis of waveform features can also be carried out based on these four movement phases. This section focuses on the statistical distribution and value occurrence analysis of AE amplitudes, which is sub-divided into two sub-sections, with Sub-section 5.3.1 for the peak amplitude and Sub-section 5.3.2 for the ASL, respectively.

5.3.1 Statistical evaluation of peak amplitude

Figure 5-3 shows the statistical distribution (or the probability distribution) of the AE peak amplitude values obtained from the OA waveforms in the AA phase, with the horizontal axis denoting the peak amplitude values of all AE events, and the vertical axis denoting the corresponding occurrence probability. All the peak amplitude values shown in the figure are centred by:

$$w(n) = \alpha_n - \alpha_0 \quad (5-2)$$

where α_n and α_0 denote the peak amplitude value of each individual AE hit and the minimum peak amplitude value, respectively. As shown in Figure 5-3, the AE peak amplitude values for OA knees in the AA phase are seen to form an exponential distribution [104], which can be expressed by:

$$p(w) = \lambda e^{-\lambda w} \quad (5-3)$$

where λ and w denote the exponent parameter and AE peak amplitude values from the waveforms, respectively.

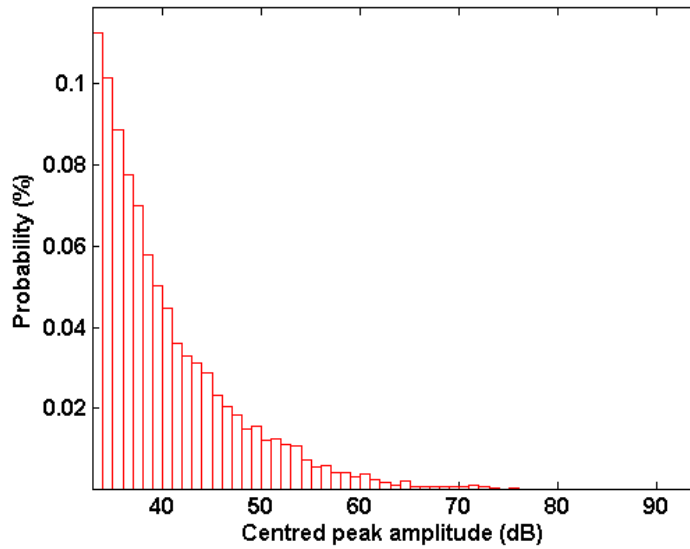


Figure 5-3 Probability distribution of peak amplitudes for OA knees in AA phase

The validity of the underlying exponential distribution over the whole range of values for all groups can be examined more accurately by using the cumulative probability plot of the peak amplitude values, where the horizontal axis denotes the peak amplitude values, and the vertical axis denotes the cumulative appearance probability in an exponential scale. Based on this type of representation, a true exponential distribution of a feature will follow a straight line. Figure 5-4 shows the cumulative appearance of the AE peak amplitude values in percentage (%) with each symbol in the figure denoting a particular group. From the distributions shown in the figure, it can be seen that the curves formed by most of the peak amplitude values are relatively straight implying the exponential distribution as a good model, which is true for both normal and abnormal groups. Although some highest peak amplitude values at the tails of the distributions are seen to deviate from the straight lines, they are actually representing a very low probability of occurrence. While the distributions of the AE peak amplitude values for the five age and symptomatic groups are exponential, their exponents are seen to be different. All participating groups shown in Figure 5-4 are seen to have the same lower bound values of 32 dB in the four movement phases, which corresponds to the threshold set for detection of an AE event. Additionally, a high percentage of overlap in the range of the AE peak amplitude values among the different

participating groups is seen in each movement phase. The best distribution separation is seen in the DD phase with the minimum overlap.

From Figure 5-4, there are significant differences among the five groups in terms of the upper bound peak amplitude values. In the AA movement phase, it is seen that the upper bound peak amplitude values are increased according to age for the three healthy groups, and decreased according to age for the two OA groups, with the maximum peak amplitude values above 90 dB created by group OA1 knees. In the AD movement phase, the maximum peak amplitude values for the healthy groups and OA groups are both increased according to age, with the maximum upper bound peak amplitude value for healthy and OA knees close to 80 and 90 dB seen in group H3 and OA2, respectively. Although similar upper bound peak amplitude values are observed from the late adulthood healthy group (H3) and middle adulthood OA group (OA1) knees in the AD movement phase, there is an absence of peak amplitude values between 60 and 70 dB in the late adulthood healthy group. For the DA movement phase, the difference between the upper bounds of the early adulthood healthy group to late adulthood healthy group is decreased with the maximum upper bound peak amplitude value above 90 dB seen in group H1, which is similar to the upper bound values of two OA groups. However, there are still significant differences in this movement phase, as group H1 knees do not create AE signals with peak amplitude values between 60 and 90 dB and no AE events with peak amplitude value between 70 and 80 dB are seen to be created by group H2 knees. In the DD movement phase, the upper bound peak amplitude values for the healthy groups are seen to be increased from group H1 to H2, and decreased from H2 to H3, with the maximum upper bound value close to 80 dB seen in group H2. Similar upper bound peak amplitude values can be observed in the two OA groups (both above 90 dB) in this movement phase. However, these two groups are still distinguishable as no AE events with peak amplitude values between 80 and 90 dB emitted from group OA2 knees.

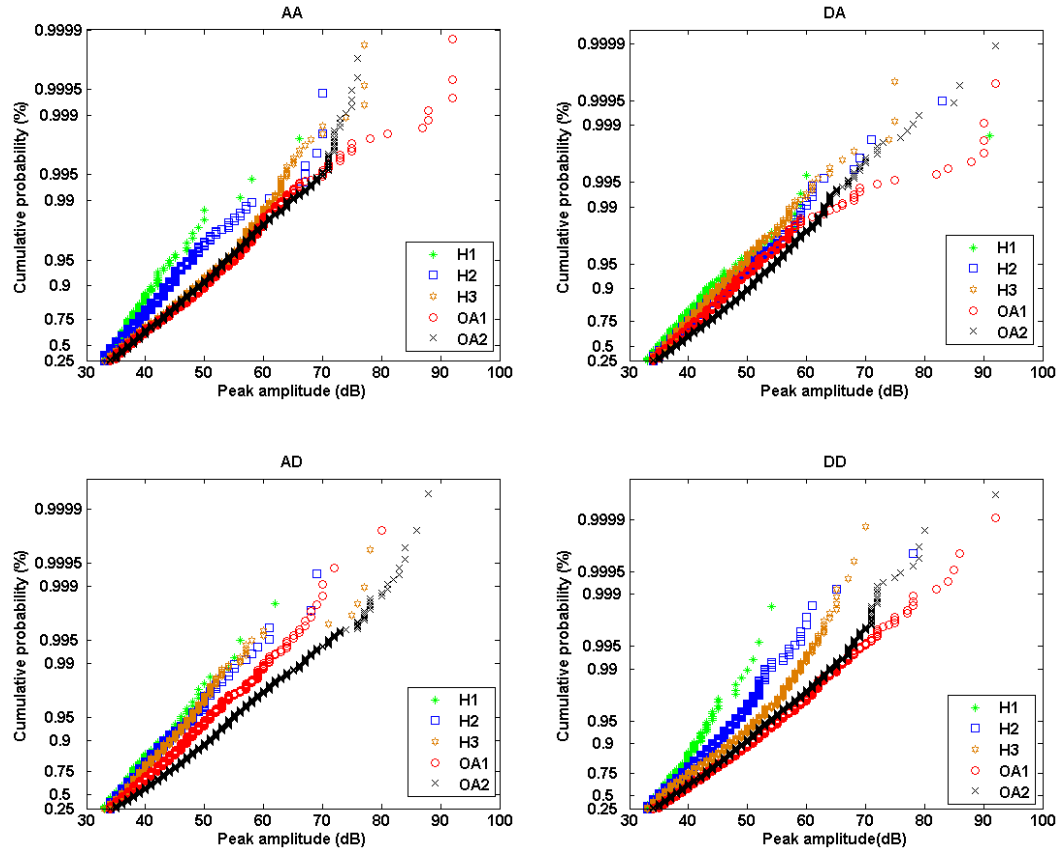


Figure 5-4 Cumulative distributions of AE peak amplitude values

5.3.2 Statistical evaluation of ASL

By replacing the peak amplitude values by the ASL values in equation 5-2, and letting α_0 be the minimum ASL value of 10 dB, the centred ASL probability distribution of OA signals in the AA phase is shown in Figure 5-5. Although it does not fit any particular statistical distribution function, the probability distribution between 0 and 25 dB seems to approach a univariate normal (Gaussian) distribution which can be expressed as:

$$p(w) = \frac{1}{\sigma(2\pi)^{1/2}} e^{\left[\frac{-(w - \mu_w)^2}{2\sigma^2} \right]} \quad (5-4)$$

where w , μ_w and σ , are referred to as the ASL values, and the corresponding mean and SD, respectively.

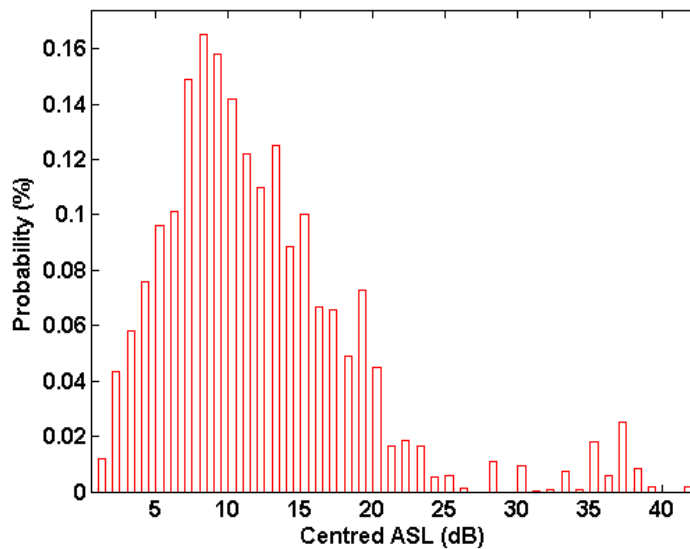


Figure 5-5 Probability distribution of ASL for OA knees in AA phase

Figure 5-6 shows the cumulative distributions of the five age and symptomatic groups in the four movement phases with the cumulative probability expressed using the Gaussian scale. Although the curve shapes produced by different participating groups exhibit some similarities in all four movement phases, they are not straight implying non-Gaussian distributions. The distributions for the five groups show distinctive separation apart from

the OA curves in the AA and DD phases, and the middle and late adulthood healthy groups (H2 and H3) in the DA phase, which show slightly higher overlaps. Furthermore, the early adulthood healthy group (H1) produce ASL with the minimum upper bound values in all movement phases, and the two OA cumulative probability curves are seen to crossover in all phases.

Additionally, significant differences can be observed at the tails of the distributions in each movement phase shown in Figure 5-6. In the AA movement phase, the upper bound values for the three healthy groups and the two OA groups are both increased with age and with around 10 dB difference between them. The upper bound value of group OA1 signals is seen to be 5 dB higher than the upper bound value of group H3 signals. Similar scenarios are observed in the AD and DA movement phases, with the marginal values of at least 5 dB separating the upper bound value of each group. In the DD movement phase, the upper bound values for H2 and H3 knees, and for OA1 and OA2 knees are seen to decrease with age with the maximum upper bound value around 40 dB produced by H2 knees and around 55 dB produced by OA1 knees. Furthermore, the largest difference between the healthy groups and the OA groups in the upper bound values is seen to occur in the DD movement phase.

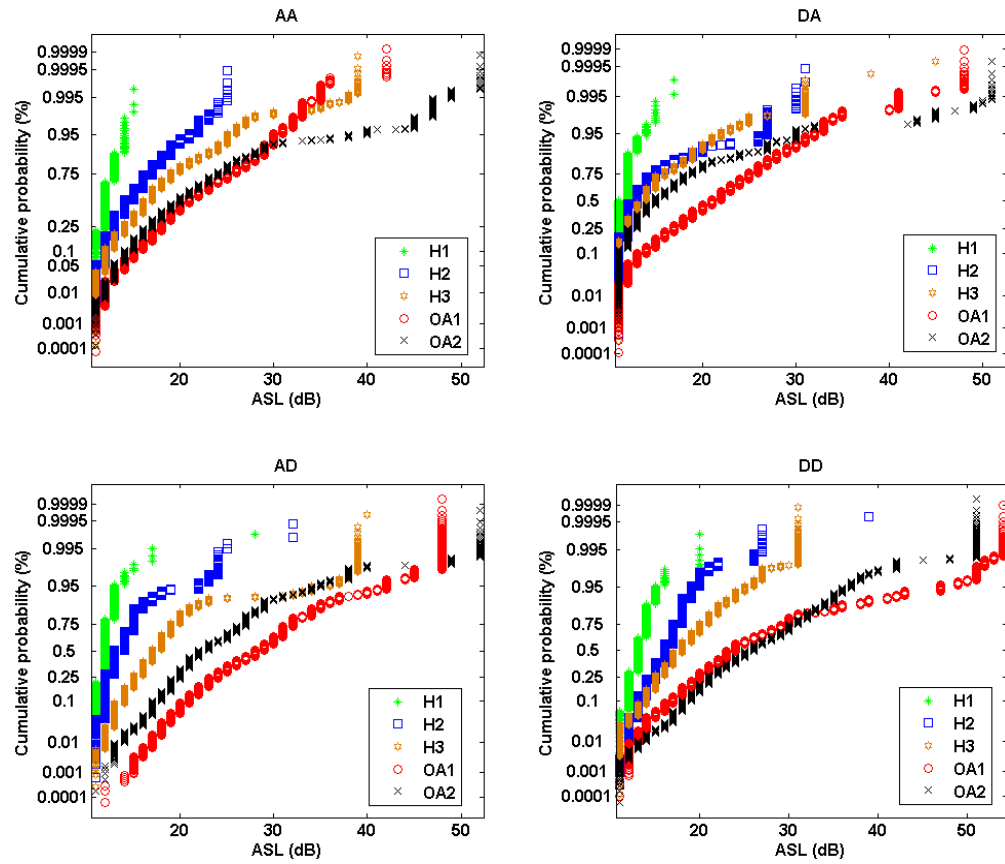


Figure 5-6 Cumulative distributions of ASL

5.4 STATISTICAL EVALUATION OF TIME BASED FEATURES

This section investigates the statistical distributions and value occurrence of the time based features, namely, duration, rise time, and fall time. Like the statistical evaluations of the amplitude features shown in the preceding section, this section firstly evaluates the probability distribution of each time feature from the OA signals in one movement phase, thereby investigating whether or not it follows any particular distribution function. This is followed by the investigation of whether or not each time feature from the signals generated by each group forms the similar distribution in the four movement phases based on the cumulative distributions.

For the AE durations extracted from the OA waveforms in the AA phase, Figure 5-7 shows the probability distribution, where the logarithm scale of durations is used in order to accommodate the wide duration range (from 1 to 10^4 μs).

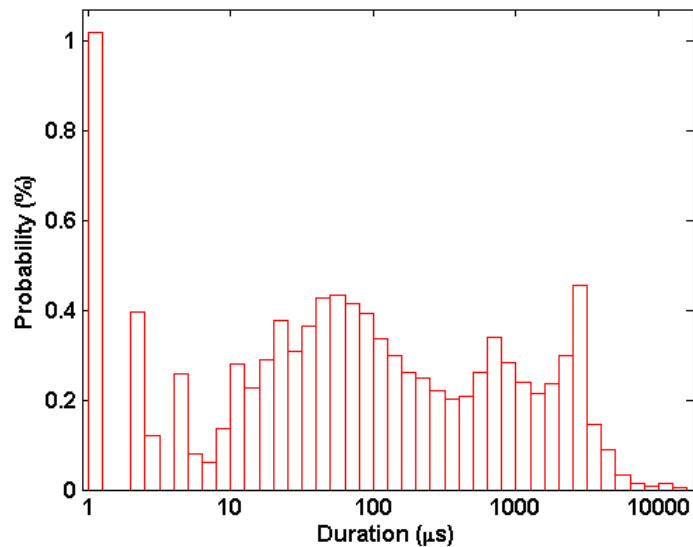


Figure 5-7 Probability distribution of durations for OA knees in AA phase

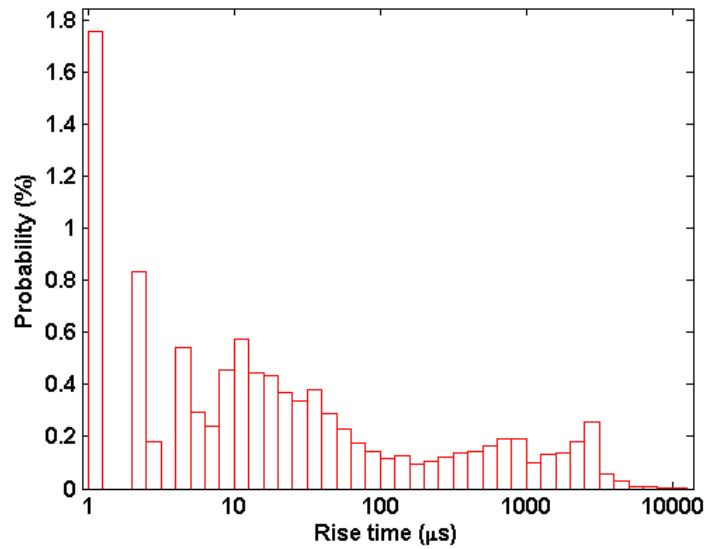


Figure 5-8 Probability distribution of rise times for OA knees in AA movement phase

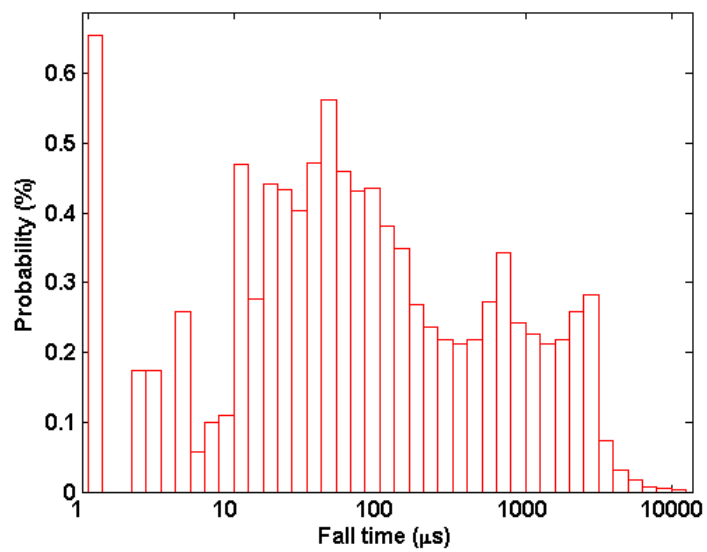


Figure 5-9 Probability distribution of fall times for OA knees in AA phase

Although the probability distribution of the AE durations appears to have multiple peaks, a large part of the distribution in the middle has a Gaussian shape and this leads to the choice of using the Gaussian scale for plotting of its cumulative distribution to investigate the statistical distributions and value occurrence of individual groups.

Figure 5-8 shows the probability distribution function of AE rise times for OA knees in the AA phase, where the logarithm scale is again used to accommodate the wide spread of the rise times. Although multiple peaks are again seen in the probability distribution of the AE rise times, a certain resemblance to a Gaussian shape in the middle section from 10 μ s to 100 μ s leads again to the use of the Gaussian scale for plotting the cumulative distribution to evaluate the statistical distributions and value appearance of the five age and symptomatic groups.

The probability distribution function of the AE fall times based on the logarithm scale is also shown to have multiple peaks (Figure 5-9). Since a large part of the distribution in the middle (with the values between 10 and $10^{2.5}$ μ s) is seen to approximate a Gaussian distribution, the Gaussian scale is again selected for further statistical analysis of the AE fall down time based on the cumulative distribution.

Figure 5-10 shows the cumulative probability of the AE durations, where the five participating groups are seen to produce similar curve shapes in all four movement phases. After a very narrow range of short AE durations at the start, at least 70% of the AE durations are seen to form a relatively straight line, implying a Gaussian distribution. The curves for the five groups are highly overlapped, particularly in the AD, DA, and DD phases. Furthermore, the curves for the late adulthood healthy group are seen to crossover the middle and late adulthood OA group in the DA and DD movement phases to yield the highest upper bound.

Although the distributions of AE durations for different groups are seen to be different, the differences are not as apparent as the amplitude based features. From the occurrence of AE durations among the four movement phases, it is seen that the early and middle adulthood healthy groups produce similar upper bound values around 3×10^3 μ s except in the AA movement phase, where H1 knees produce no waveforms having duration longer than 3×10^3 μ s. For the other three groups, similar upper bound values are observed in all the movement phases, which are around 10^4 μ s.

The cumulative probability plots of AE rise times in the four movement phases are shown in Figure 5-11. After a very narrow range of short rise times at the start, at least 75% of the rise times are seen to form a relatively straight line, implying Gaussian distribution as a

good approximation of the mid range rise time values. Furthermore, a very high percentage of overlaps are again seen to occur among the five curves in all four movement phases. Additionally, the distribution curves for the late adulthood healthy group are seen to follow those for the middle adulthood OA group in all four phases and break away to reach the similar upper bound values of the late adulthood OA group in the last three movement phases.

In terms of the upper bound values of the rise times, group H1 knees are seen to produce the AE waveforms with the shortest rise time values in all of the four movement phases, with the upper bound values shorter than $10^3 \mu\text{s}$ in the AA, AD, and DA movement phases, and shorter than $3 \times 10^3 \mu\text{s}$ in the DD movement phase. However, similar upper bound values can be observed from the H2, H3, OA1, and OA2 groups in the AA phase, with the rise times around $10^4 \mu\text{s}$. In the AD phase, little difference is observed between the upper bound values of group H2 and OA1, as well as group H3 and OA2. In the DA phase, although the distribution curves for the H1 and H2 groups show significant difference at their upper bound values, with the rise times produced by group H2 around 5 times longer than group H1, less difference between the upper bound values of group H3, OA1 and OA2 is observed, with the maximum rise times for these three groups all around $10^4 \mu\text{s}$. In the DD movement phase, the values occurrence also show less discriminations for group H1 and H2, as well as group H3, OA1 and OA2, with the curves of group H1 and H2 highly overlapped, and similar upper bound values ($> 10^4 \mu\text{s}$) observed from another three groups.

For the statistical distributions of fall down times (Figure 5-12), the curves are highly overlapped, and at least 80% of the values for each group are also seen to form the Gaussian distribution with their relative straight curves. In the AA phase, the minimum upper bound is seen to occur in the H1 group (upper bound fall down times $< 3 \times 10^3 \mu\text{s}$), and similar upper bound values are observed in the other four groups, which are around $10^4 \mu\text{s}$. In the AD phase, the curves for group H1 and H2, as well as the curves for the other three groups are highly overlapped, with similar upper bound values. In the DA and DD phases, little differences are observed at the tails of group H1 and H2 distributions, as well as at the tails of OA1 and OA2 distributions, with the maximum fall down time longer than $10^4 \mu\text{s}$ seen in group H3 and OA2 knees in these two phases.

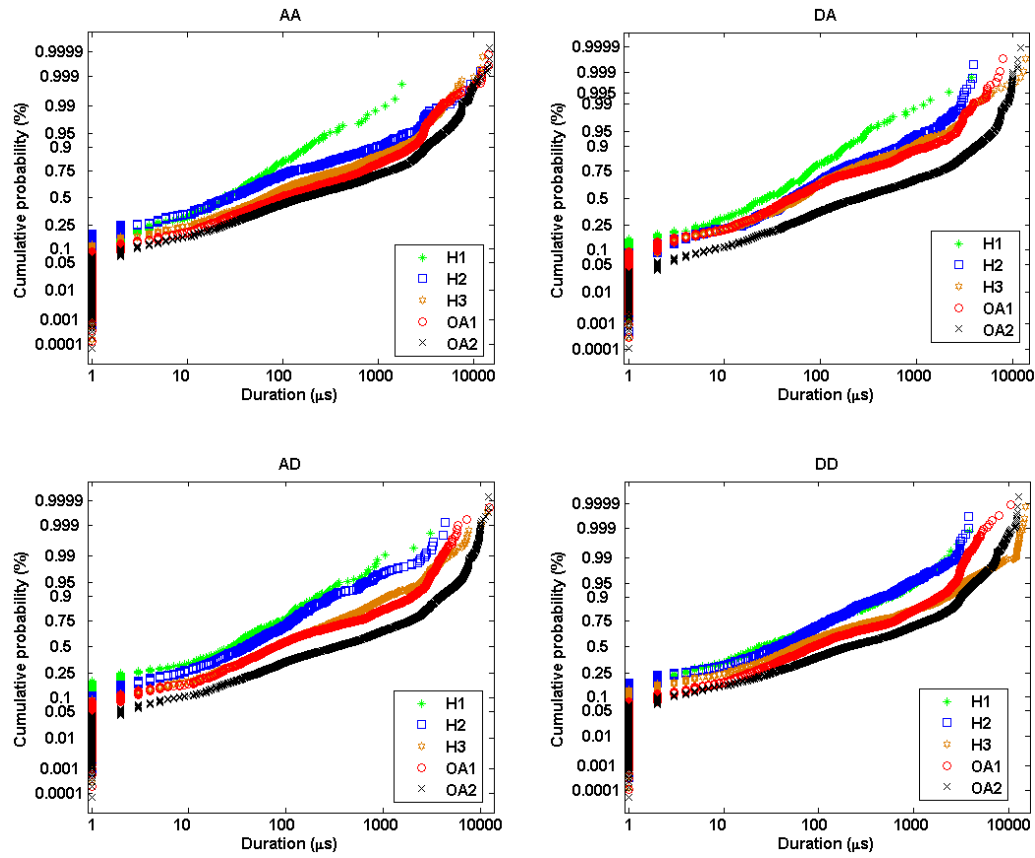


Figure 5-10 Cumulative distributions of durations

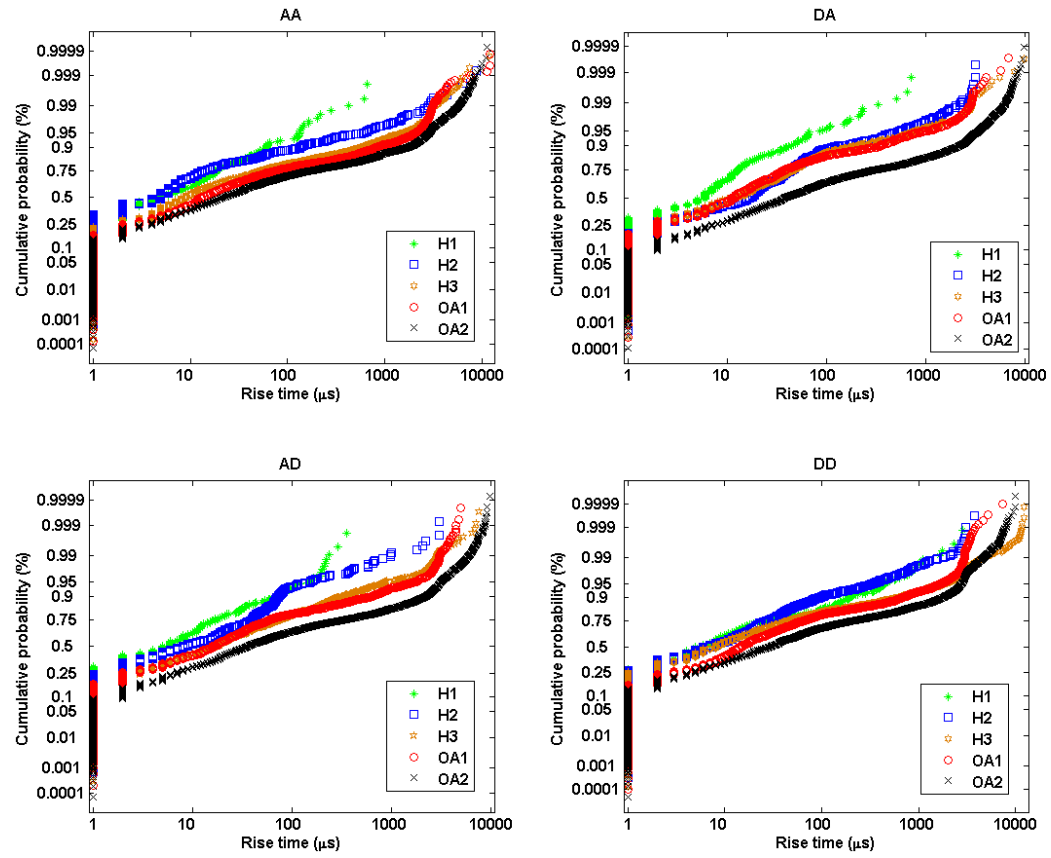


Figure 5-11 Cumulative distributions of rise times

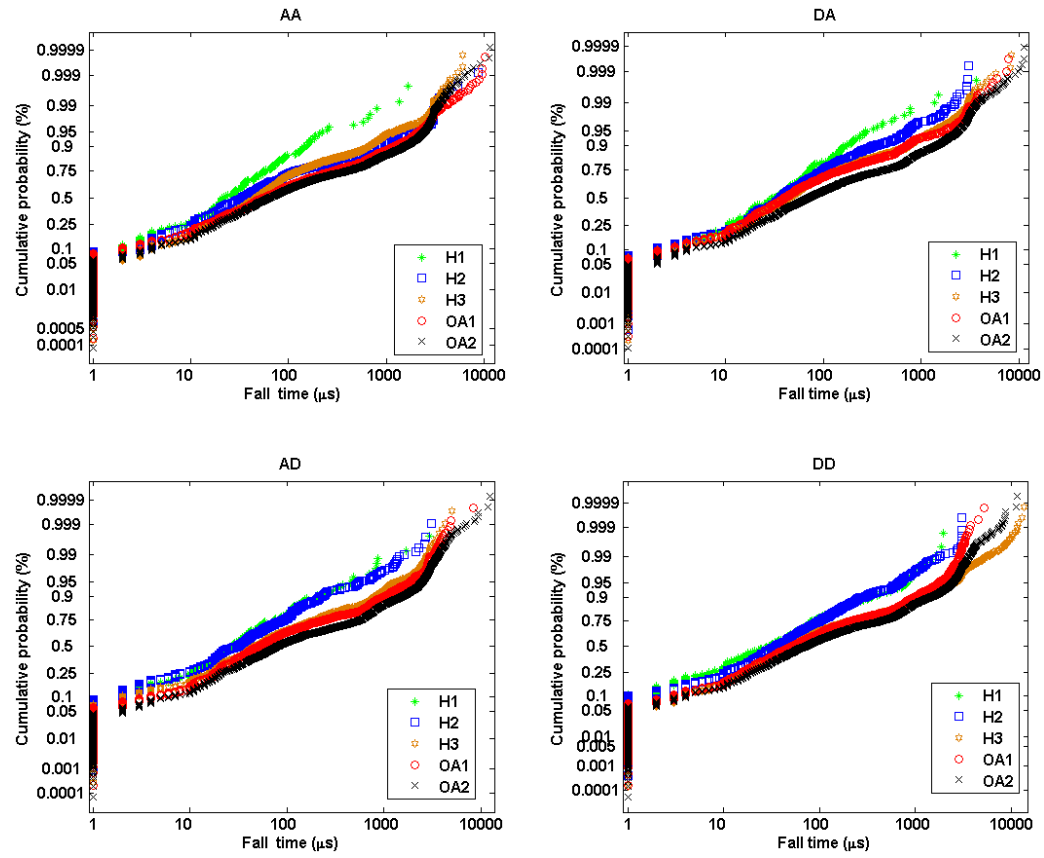


Figure 5-12 Cumulative distributions of fall down times

5.5 STATISTICAL EVALUATION OF FREQUENCY BASED FEATURES

This section focuses on the statistical evaluation of AE frequencies, which includes three frequency features derived from the time domain signals, namely, average frequency, initiation frequency, and reverberation frequency, respectively (Sub-section 5.5.1), as well as two frequency features derived from the waveform frequency spectrums, namely, peak frequency and the centre frequency, respectively (Sub-section 5.5.2).

5.5.1 Statistical evaluation of average, initiation, and reverberation frequencies

Figures 5-13 to 5-15 show the probability distribution functions of the average, initiation, and reverberation frequency of OA AE signals, where the logarithm scale is used to accommodate the spread of the frequency values (from 1 kHz to 1 MHz for these three features). From these figures, it is seen that these three features do not appear to fit any particular statistical distributions. However, there is a certain resemblance to the Gaussian distribution and this leads to the use of the Gaussian scale to represent the cumulative distributions of these three frequency features. For the statistical distributions of average and initiation frequencies, an issue need to be noticed is the high spike at the tail of distribution which represents the highest frequencies, as shown in Figures 5-13 to 5-14, the typical AE signal with such high frequency is the signal that contains 1 pulse exceeded the detection threshold over 1 μ s (sampling interval). As this value is not an artefact, and these two features are not finally selected for classifying AE patterns in the next chapter, it is not necessary exclude them from the study.

From the cumulative distributions of the average frequency values of the five age and OA related groups shown in Figure 5-16, over 80% of the average frequencies are seen to be relatively straight implying the Gaussian distribution apart from the tails of the curves, and high similarities are observed among the cumulative distribution curves in all of the five participating groups in all of the movement phases. Similar comments could be made for the cumulative distributions of the initiation frequency values shown in Figure 5-17.

Although the straight section of the cumulative distributions of the reverberation frequency are longer than those for the average and initiation frequencies, there is no significant difference among the five participating groups in any of the movement phase.

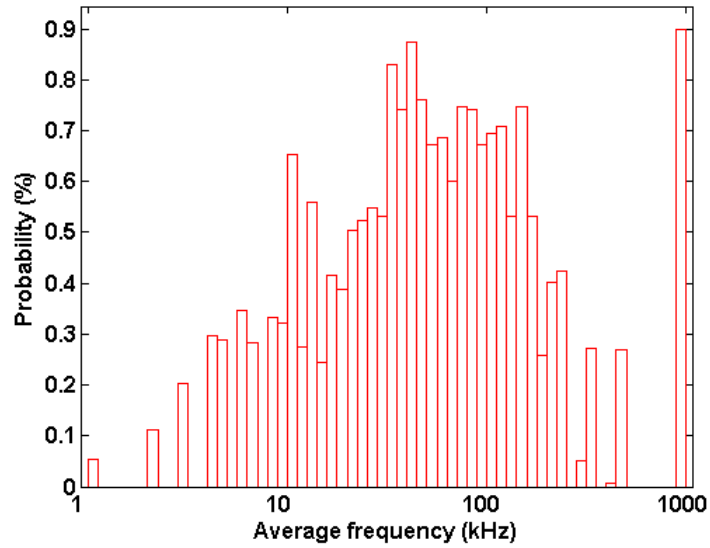


Figure 5-13 Probability distribution of average frequencies for OA knees in AA phase

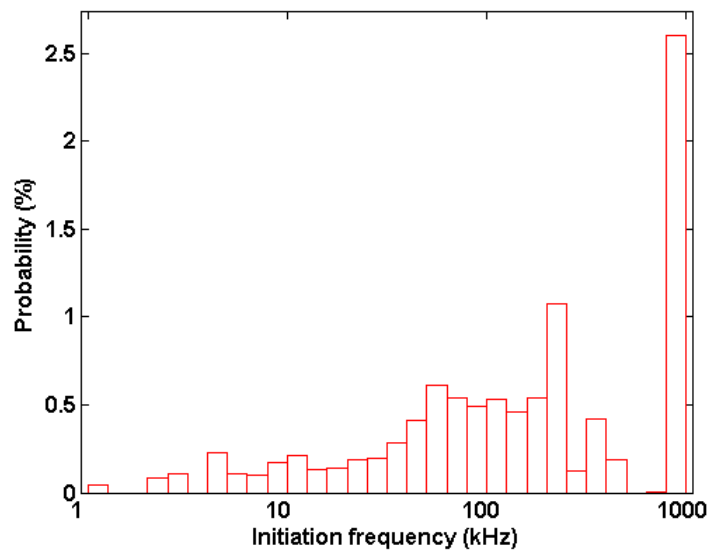


Figure 5-14 Probability distribution of initiation frequencies for OA knee in AA phase

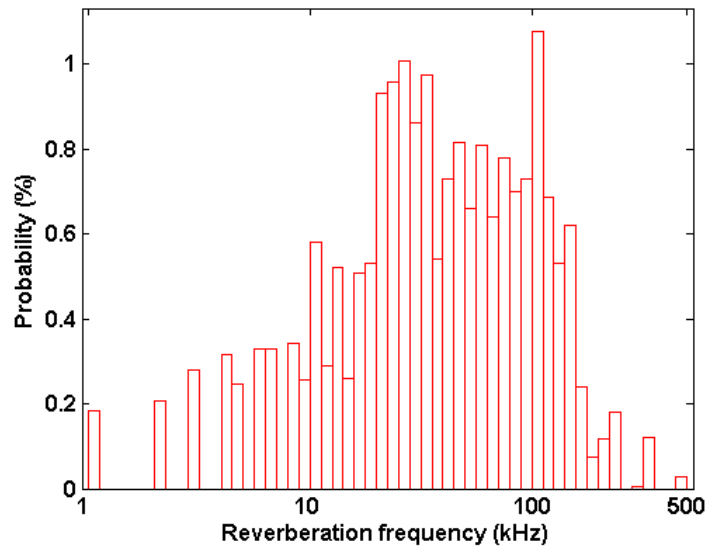


Figure 5-15 Probability distribution of reverberation frequencies for OA knees in AA phase

In terms of the value occurrence of these three frequency based features, as shown by the cumulative plots in Figures 5-16 to 5-18, all groups are seen to have the same upper bound value around 1 MHz in terms of the average and initiation frequencies and around 500 kHz in terms of the reverberation frequencies. Furthermore, all groups are seen to have similar lower bound frequencies in all of the four movement phases, except group H1 knees.

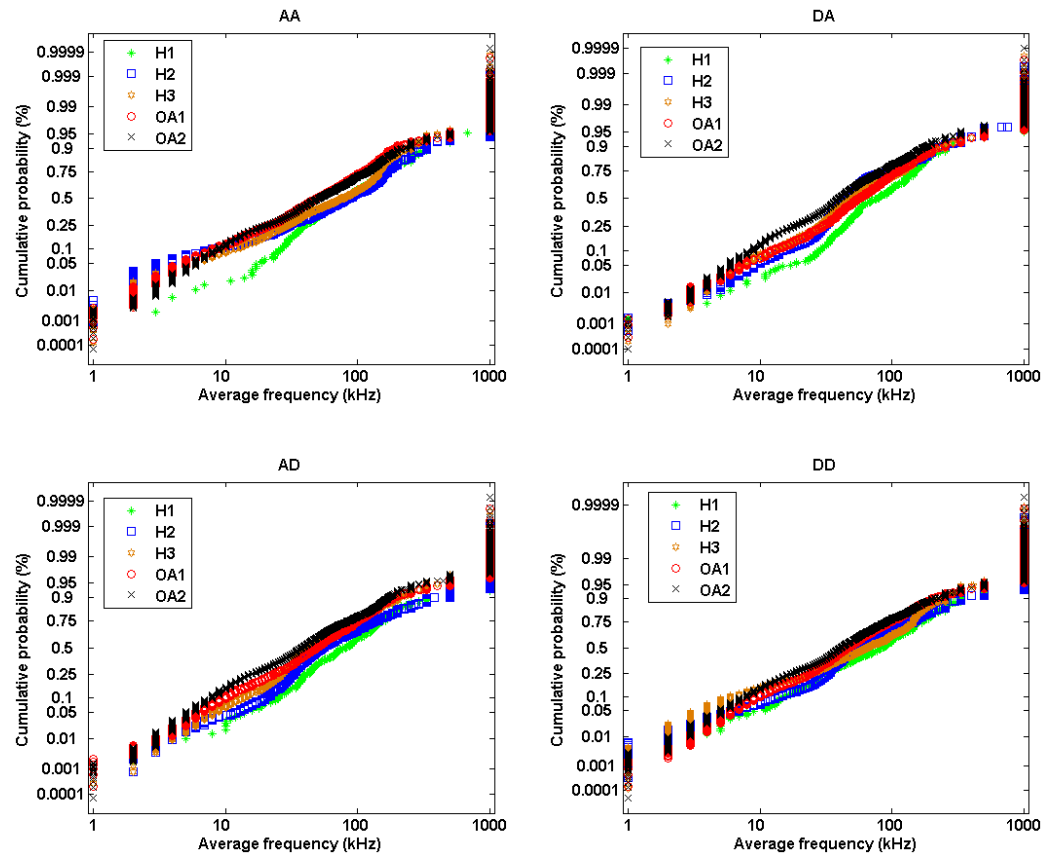


Figure 5-16 Cumulative distributions of average frequencies

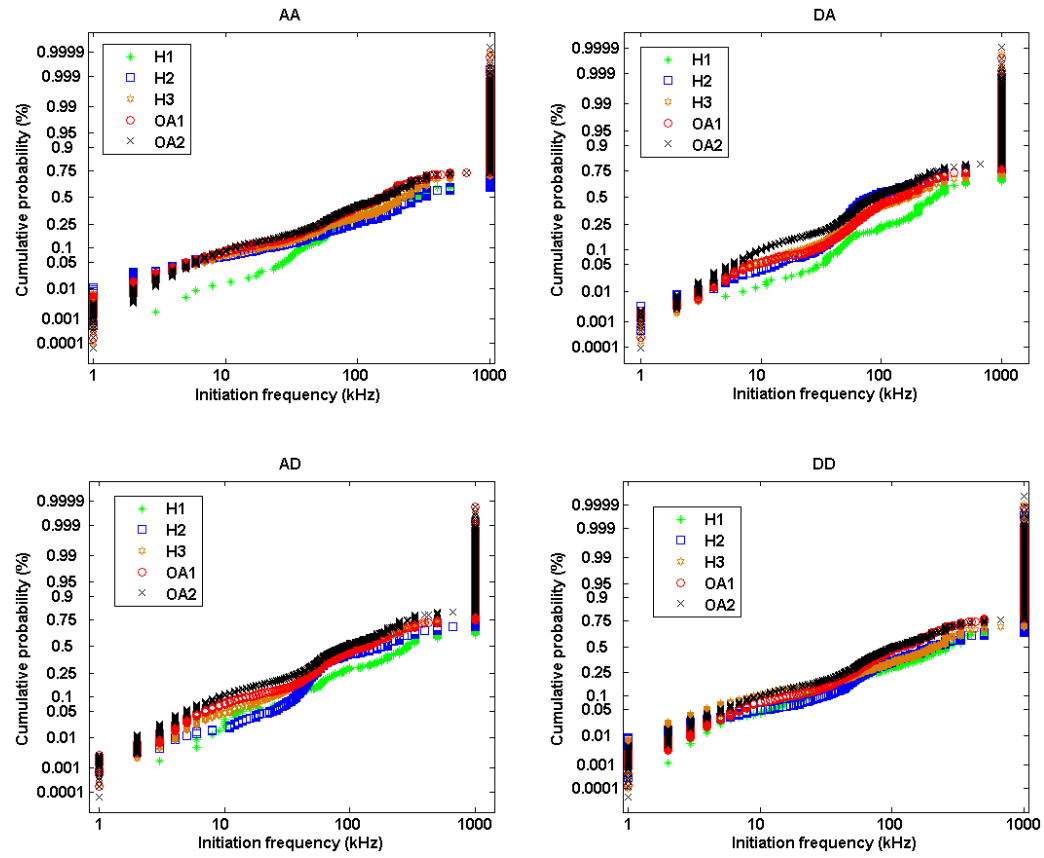


Figure 5-17 Cumulative distributions of initiation frequencies

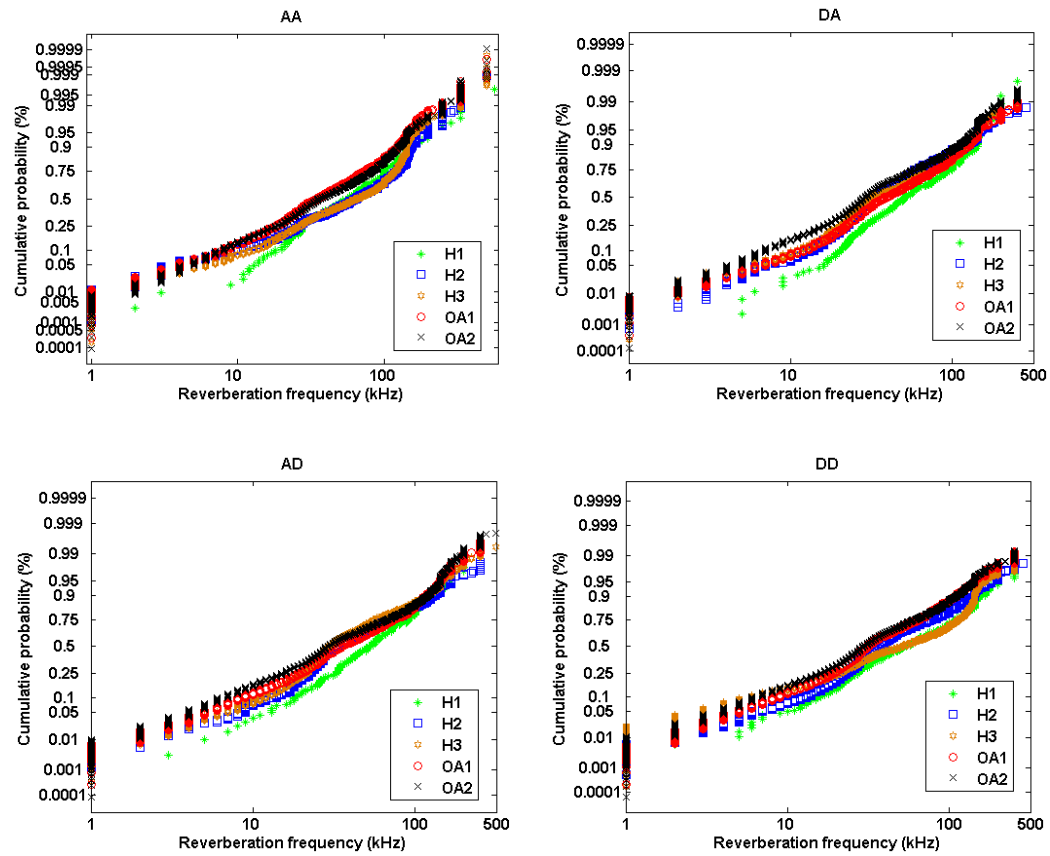


Figure 5-18 Cumulative distributions of reverberation frequencies

5.5.2 Statistical evaluation of peak and centre frequencies

From the probability distribution of the peak frequencies of the AE signals in the AA movement phase from OA knees shown in Figure 5-19, a bi-modal distribution is observed. The values lower than 100 kHz are seen to approach an exponential distribution, and the values above 100 kHz are seen to resemble a Gaussian distribution with two peak probabilities appeared at around 30 (lower band) and 150 kHz (higher band). Figure 5-20 shows the probability distribution of the centre frequencies for the AE waveforms emitted from the OA knees in the AA movement phase, the distribution is seen to fit an asymmetric Gaussian distribution.

In order to assess whether or not the peak frequency of the AE waveforms from the other groups form the similar distribution as the OA group, the statistical distributions of the peak frequencies for the five groups in the four movement phases are investigated. As the bimodal distribution is observed for the OA knees in terms of the peak frequency, and the centre frequency of OA knees is seen to approximately form the Gaussian distribution in the AA movement phase, the Gaussian scale is chosen to represent the cumulative distributions of the peak frequency, in order to make a consistent comparison. From the cumulative distribution of the AE peak frequency values in the four movement phases shown in Figure 5-21, it is seen that the curves generated by the five groups are seen to follow the probability distribution shown in Figure 5-19 with bi-modal occurrence probabilities. Although, the cumulative distributions are seen to be highly overlapped in the lower and higher bands, there is a difference in the relative occurrence probabilities of the peak frequencies in the lower band with respect to the those in the higher band, with highest difference shown in the AA movement phase.

The upper bound peak frequency values for the five groups in the AA, AD and DD movement phases are seen to have less differences, with all peak frequencies above 200 kHz apart from H1 knees in the DD movement phase. In the DA movement phase, there are two upper bound peak frequencies with one for group H1, OA1, and OA2 knees around 150 kHz, and the other one for group H2 and H3 above 200 kHz.

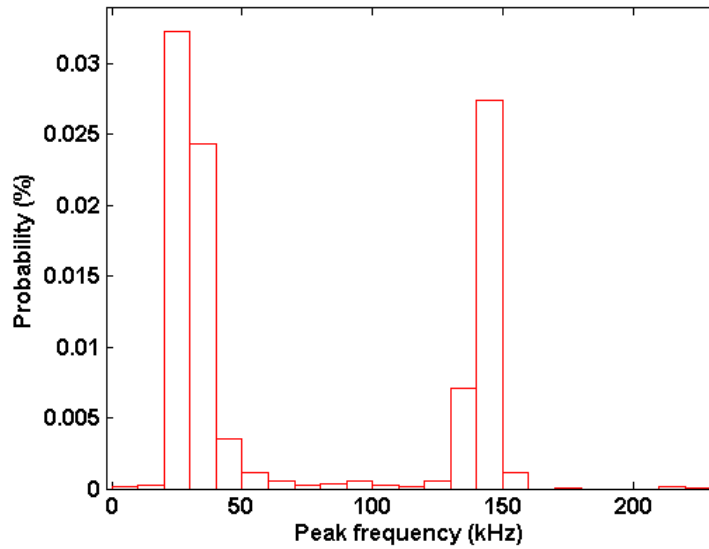


Figure 5-19 Probability distribution of peak frequencies for OA knees in AA phase

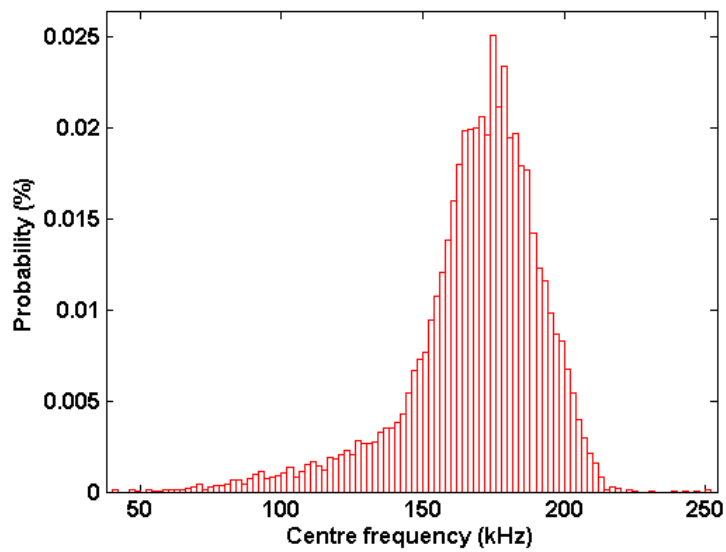


Figure 5-20 Probability distribution of centre frequencies for OA knees in AA phase

From the cumulative distributions of the AE centre frequency values shown in Figure 5-22, they appear to rise exponentially as a result of following the probability distribution shown in Figure 5-20 with the first half of each curve having a lower gradient compared with the second half. Furthermore, the curve for each groups in each phase is seen to rise exponentially at slightly different rates. Although the curves show less overlap in the AA,

AD and DD phases, same value appearances are observed for most of groups in these three phases, with the exception of the early adulthood group seen to have a significant lower bound compared with other groups in the AD phase.

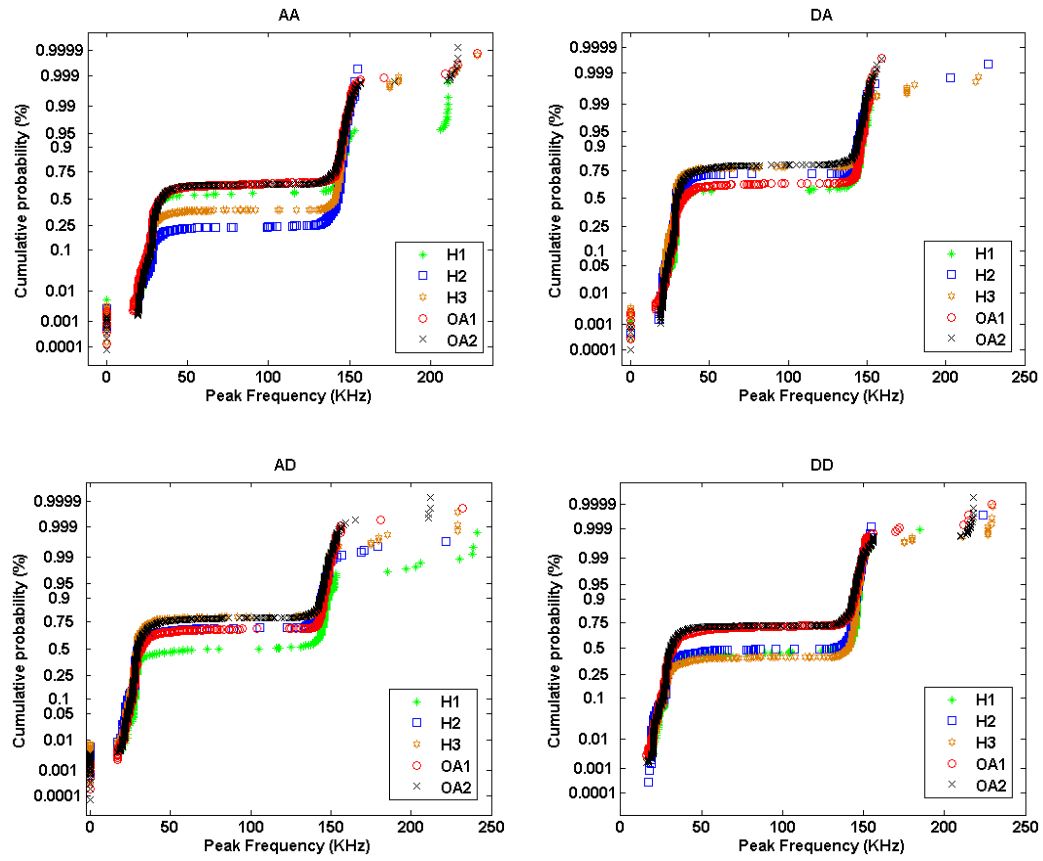


Figure 5-21 Cumulative distributions of peak frequencies

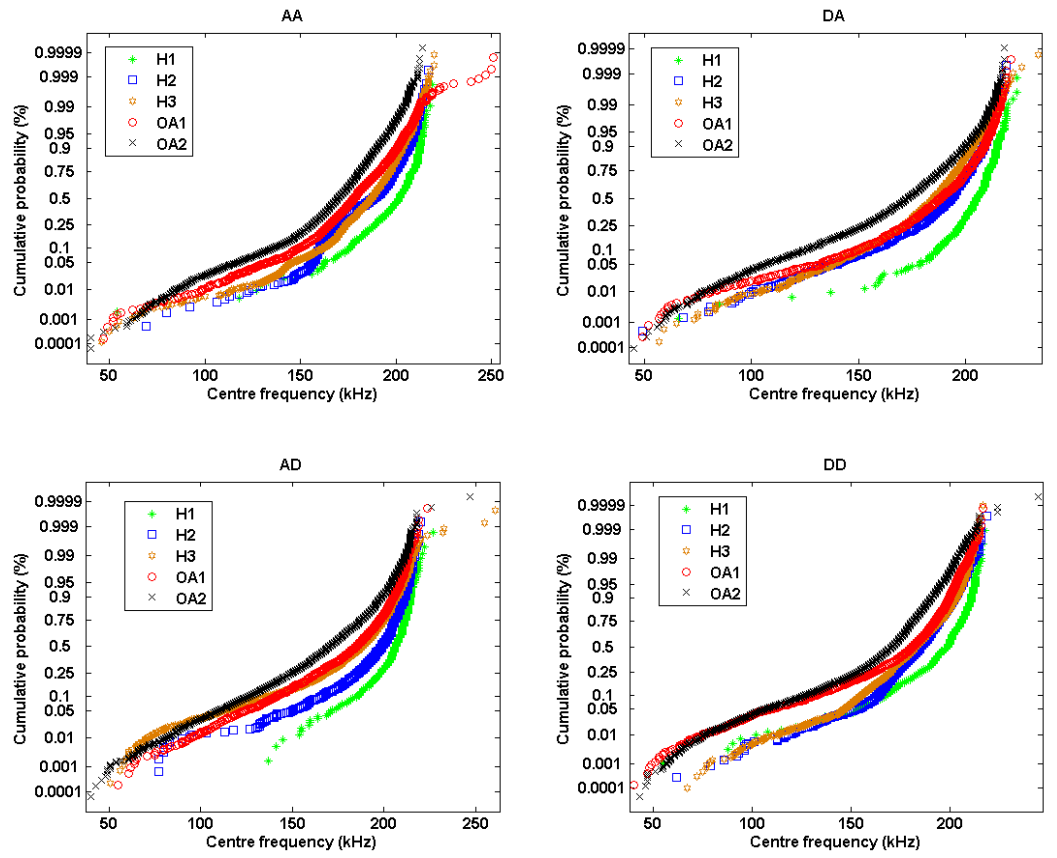


Figure 5-22 Cumulative distributions of centre frequencies

5.6 STATISTICAL EVALUATION OF AE ENERGY BASED FEATURES

This section discusses the statistical distributions and the value occurrence of AE signal strength and absolute energy. Figures 5-23 to 5-24 show the probability distributions for the signal strength and absolute energy of AE waveforms acquired from OA knees in the AA movement phase, where the logarithm scale is used to accommodate the wide spread of values (from 5 to 10^6 pV-sec for signal strength and from 1 to 10^6 aJ for absolute energy). From these two figures, both distributions for the signal strength and absolute energy are seen to be approximately Gaussian with certain asymmetry.

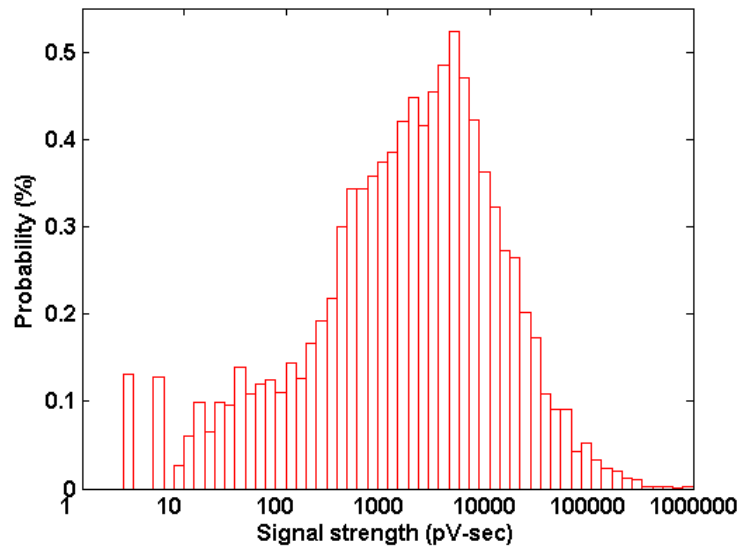


Figure 5-23 Probability distribution of signal strength for OA knees in AA phase

Using the Gaussian scale, the cumulative distributions of the signal strength values are shown in Figure 5-25. Among all four movement phases, at least 95% of the signal strength values are seen to form the straight lines confirming distributions dominated by Gaussian. The distribution curves for the five groups are seen to increase at similar rate from 5 pV-second to 10^6 pV-second, with at least 99% of the signal strength values for the five groups overlapped. Although the upper bound values of the early and middle adulthood healthy groups are seen to increase in the AA, AD, and DA phases, and decreased in the DD phase,

the distributions do not show significant differences among the H3, OA1, and OA2 groups in any one of the movement phases.

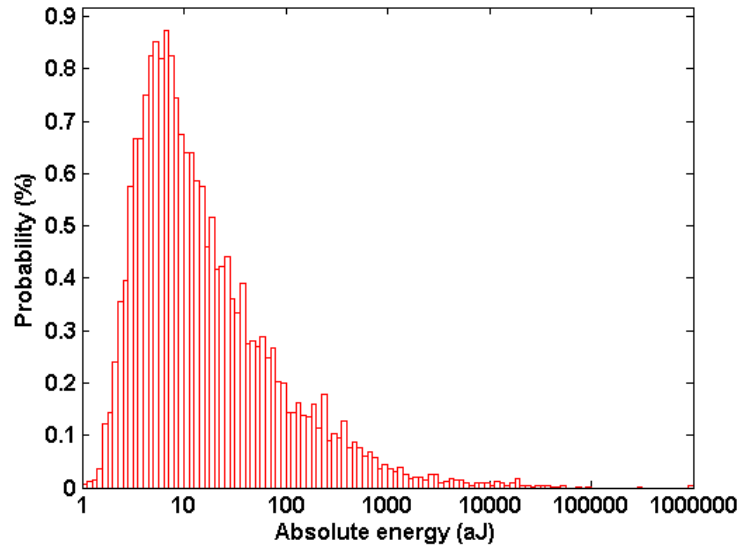


Figure 5-24 Probability distribution of absolute energy for OA knees in AA phase

The cumulative distributions of the absolute energy values for the five age and OA related groups are shown in Figure 5-26, where the curves appear to follow the asymmetric Gaussian probability distribution shown in Figure 5-24 with the first half of each curve having a higher gradient compared with the second half. There are over 90% of the values in the five groups shown to be overlapped. In the AA and AD phases, the upper bound values are seen to increase from group H1 to H3, and similar for the H3, OA1 and OA2 groups. In the DA phase, the upper bound values are seen to increase from the early to the middle adulthood healthy groups, and decrease from the middle to the late adulthood healthy groups with the value range between 10^4 and 3×10^4 aJ absent for the middle adulthood healthy groups. Similar upper bound values around 10^6 aJ are observed in the H2, OA1 and OA2 groups in this phase. In the DD phase, although the upper bound values for group H2 and H3 show some discrepancy compared with the other three groups, it is difficult to spot the differences between the H1, OA1, and OA2 groups, as the curves for these three groups are seen to form a similar trajectory in this phase.

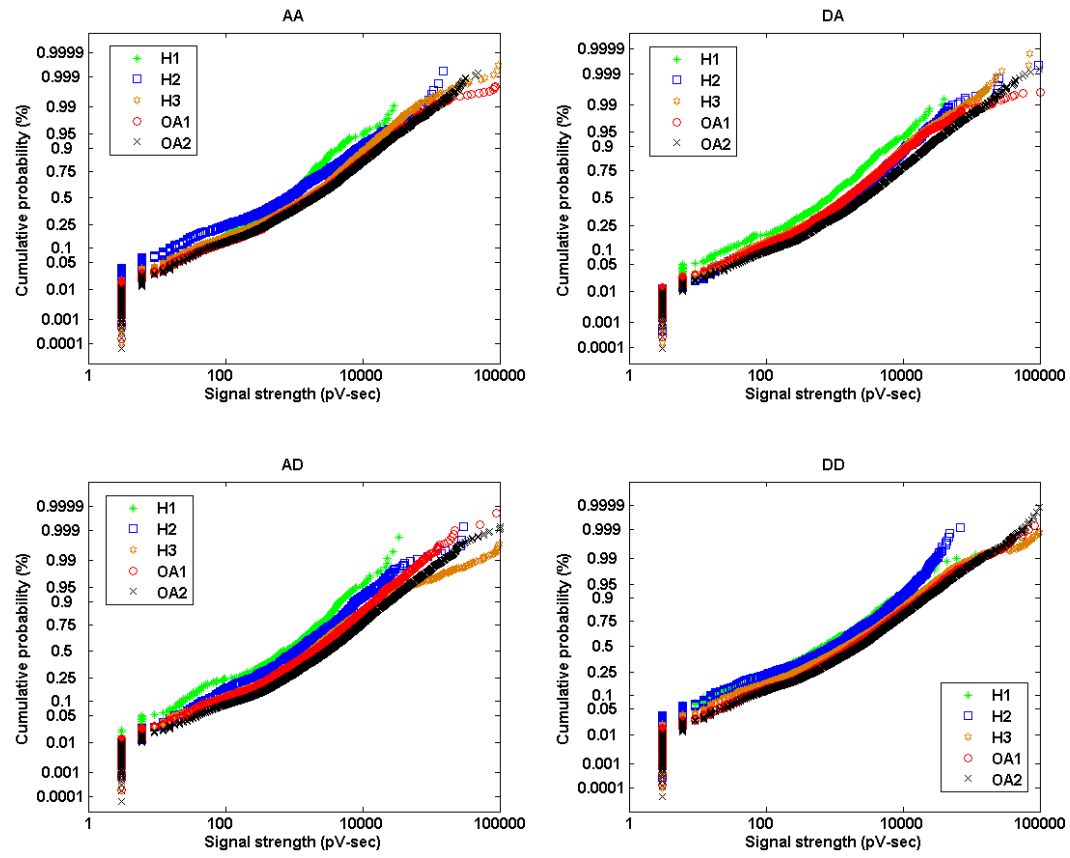


Figure 5-25 Cumulative distributions of signal strength

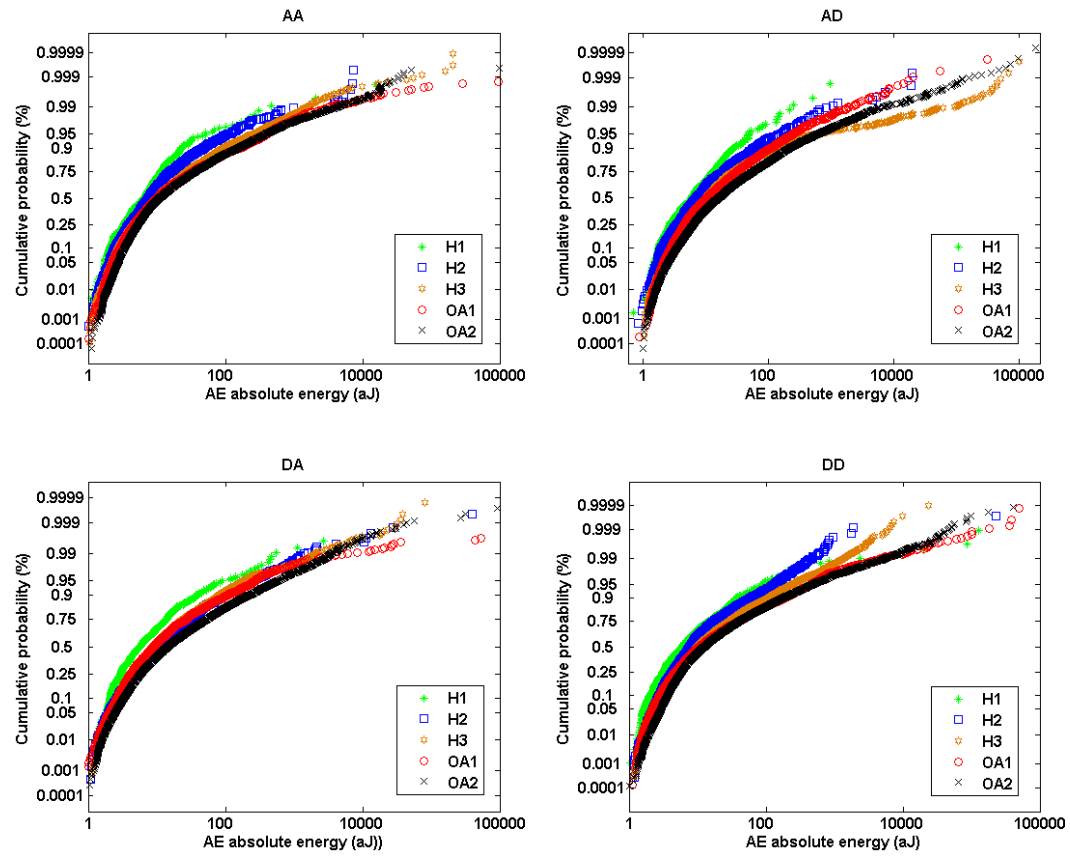


Figure 5-26 Cumulative distributions of absolute energy

5.7 STATISTICAL EVALUATION OF COUNT BASED FEATURES

As the descriptors introduced in Section 3.3, AE counts category includes three features for measuring the number of pulse above the detection threshold, namely, counts, counts to peak, and counts down, respectively. The probability distributions of these three features for OA knees in the AA movement phase are shown in Figures 5-27 to 5-29, where the logarithm scale is applied to accommodate the spread for values (from 1 to 10^3 pulses exceeded the detection threshold for these three features). By observing the statistical distributions of these three features, it is seen that all features follow approximately the exponential distribution, which leads to use the exponential scale to evaluate the statistical distributions and value occurrence for all of the groups over the four movement phase.

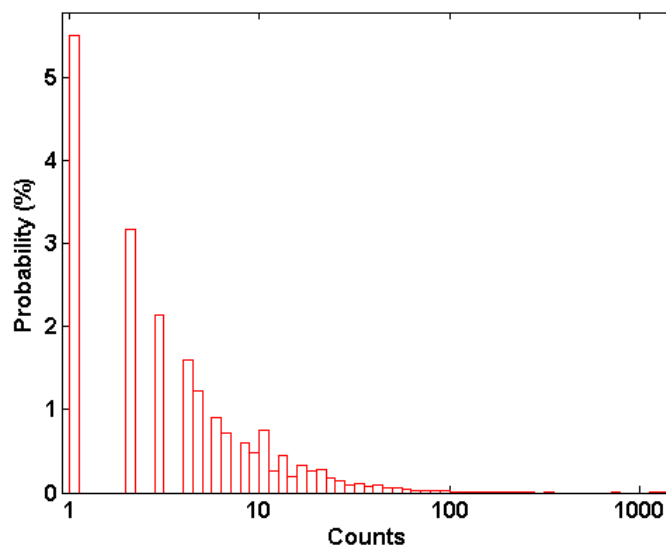


Figure 5-27 Probability distribution of counts for OA knees in AA phase

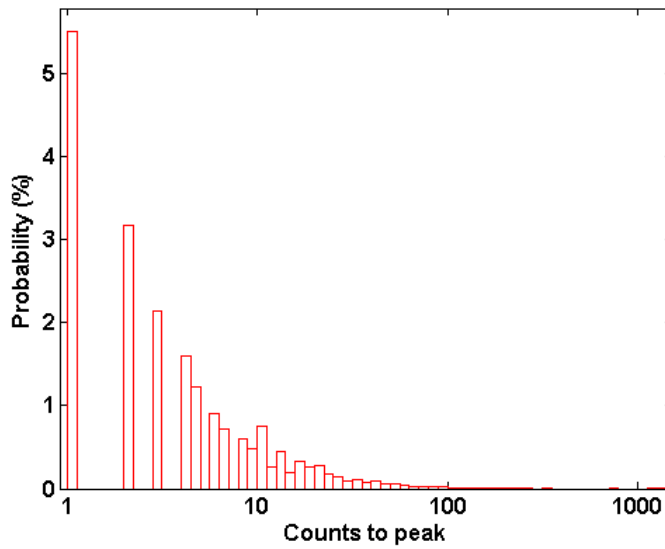


Figure 5-28 Probability distribution of counts to peak for OA knees in AA phase

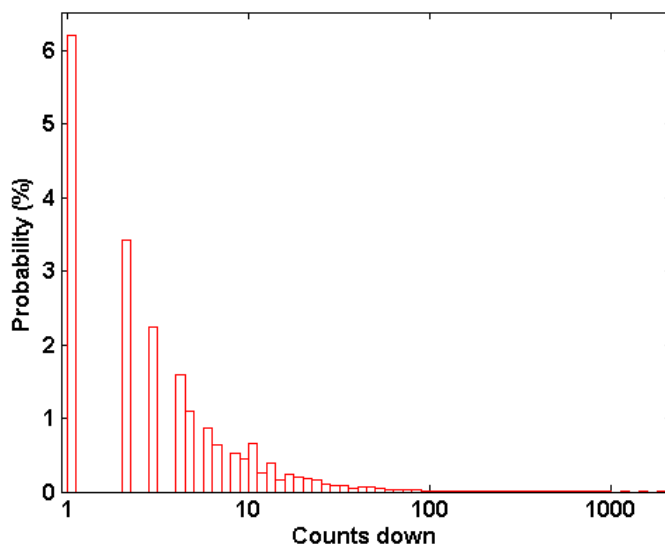


Figure 5-29 Probability distribution of counts down for OA knees in AA phase

From the cumulative distributions of counts among the four movement phases shown in Figure 5-30, it can be seen that although the curves are not exactly the straight lines, at least 95% of the AE counts values are seen to approximately form the exponential distribution. The upper bound values are seen to increase from group H2 to H3, and decrease from group OA1 to OA2 in the AA phase. However, the upper bound values of group H1 and H2,

as well as group H3 and OA1 are seen to be similar. In the AD phase, although the upper bound values are seen to increase from group H1 to H3, and from group OA1 to OA2, over 99.95% of the AE counts for group H3, OA1, and OA2 are seen to distribute within the similar range of values. In the DA phase, the upper bound values increase for both the normal and abnormal groups according to the increasing age bands. However, there is no significant difference in the upper bound values between group H2 and OA1 with round 100 AE pulses exceeded the detection threshold, and between group H3 and OA2 with around 1000 AE pulses exceeded the detection threshold. In the DD phase, although there are distinguishable upper bound values, around 99% of the counts in the five participating groups are seen to form the similar trajectory in this phase.

From the cumulative probability plots shown in Figure 5-31, at least 99% of the AE counts to peak in the AA, AD and DA phases and at least 95% in the DD phase are seen to be relatively straight implying the exponential distribution as a good model. There are high percentages of overlaps, particularly in the AA and DA phases. The curves for the H3, OA1, and OA2 groups in the AA phase, and the H2, H3, and OA1 groups in the DA phase show similarities in terms of the curve exponents. Although the counts to peak values in the DD phase show some differences in terms of the upper bound values, the distributions for the other three movement phases do not show significant difference like the amplitude category features.

Like the above mentioned two features, over 99% of the AE counts down in the AA, AD and DA phases, and over 95% of the values in the DD phase in Figure 5-32 are seen to be relatively straight implying the exponential distribution as a good model for the value distribution of this feature. There are very high percentages of overlaps ($\geq 95\%$), with the curves for group H2, H3, OA1, and OA2 in the AA phase, all groups in the DA phase, as well as group H1, H3, OA1, and OA2 in the DD phase forming very similar trajectories. In the AA phase, the upper bound value of group H1 is similar to H2, and H3 similar to OA1. In the AD phase, similar upper bound values are observed in group H2 and H3, as well as group OA1 and OA2. In the DA phase, the upper bound values for H1 and H2, as well as H3 and OA2 are also similar, with around 100 pulses exceeded the detection threshold observed from the tails of the H1 and H2 distributions, and around 1000 AE pulses exceeded the detection threshold observed from the tails of the OA2 and H3 distributions.

Although the distributions of group H3 and OA2 show significant difference in the DD phase, similar upper bound values are observed from the other groups in this movement phase.

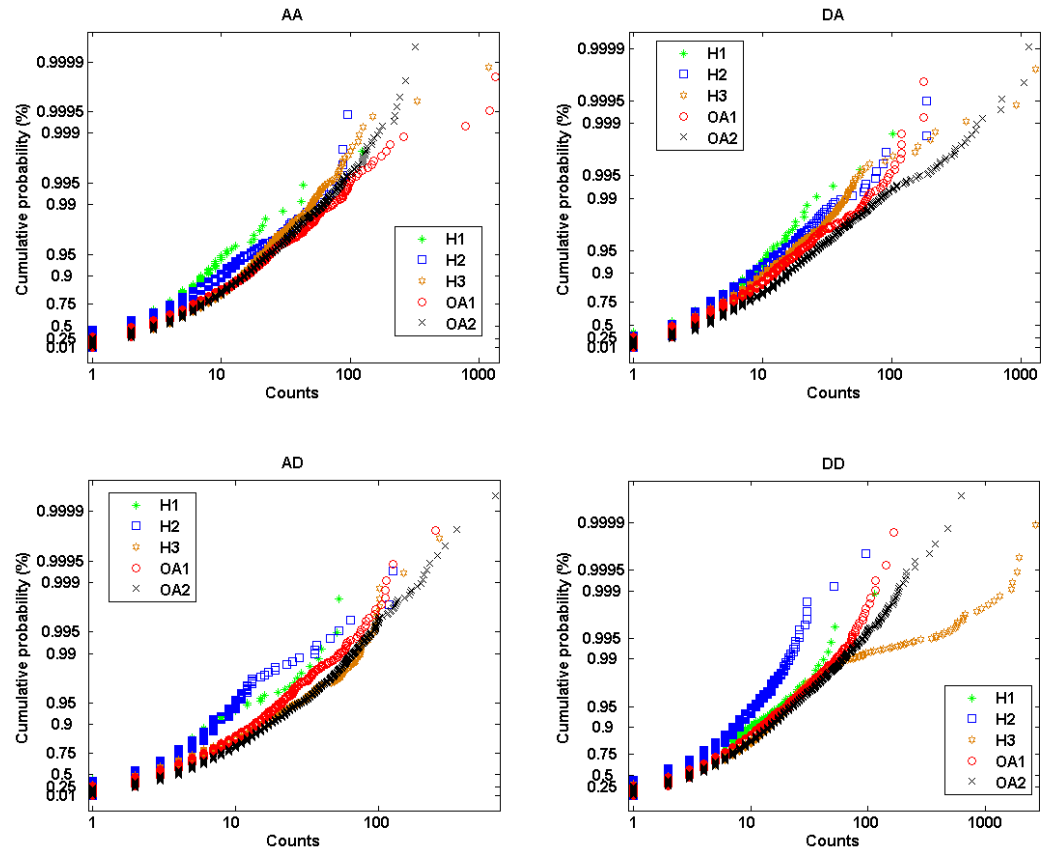


Figure 5-30 Cumulative distributions of counts

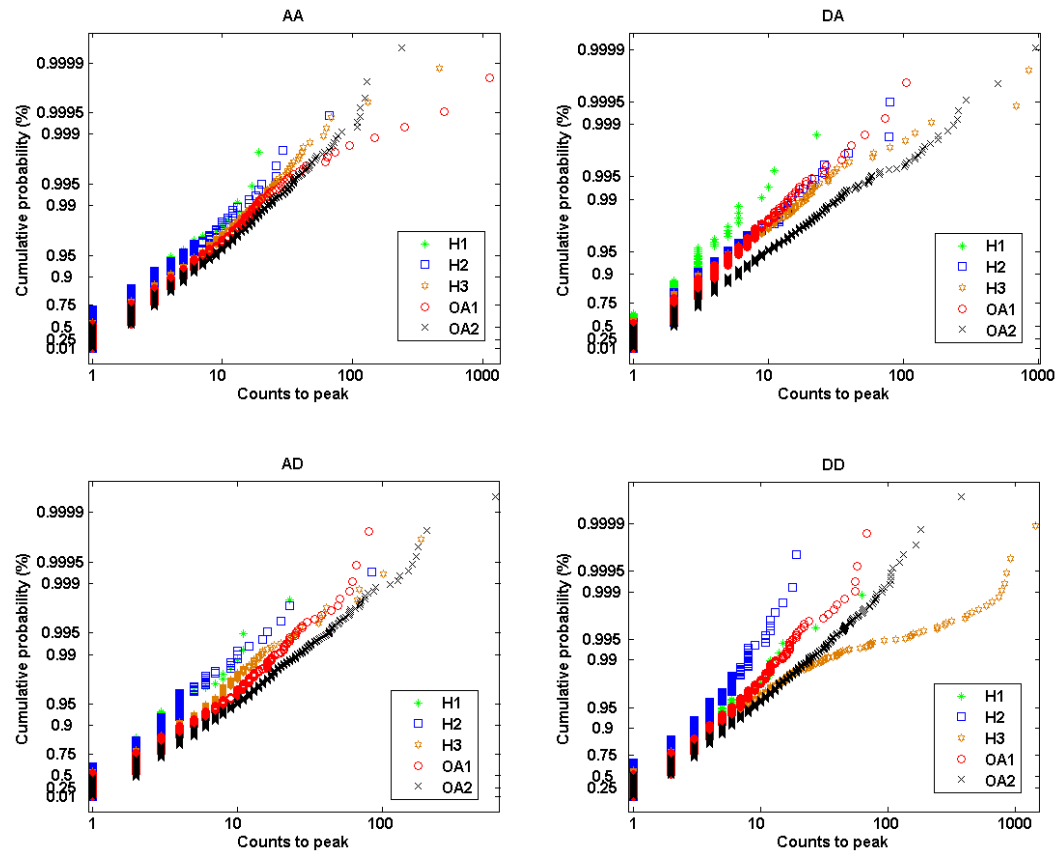


Figure 5-31 Cumulative distributions of counts to peak

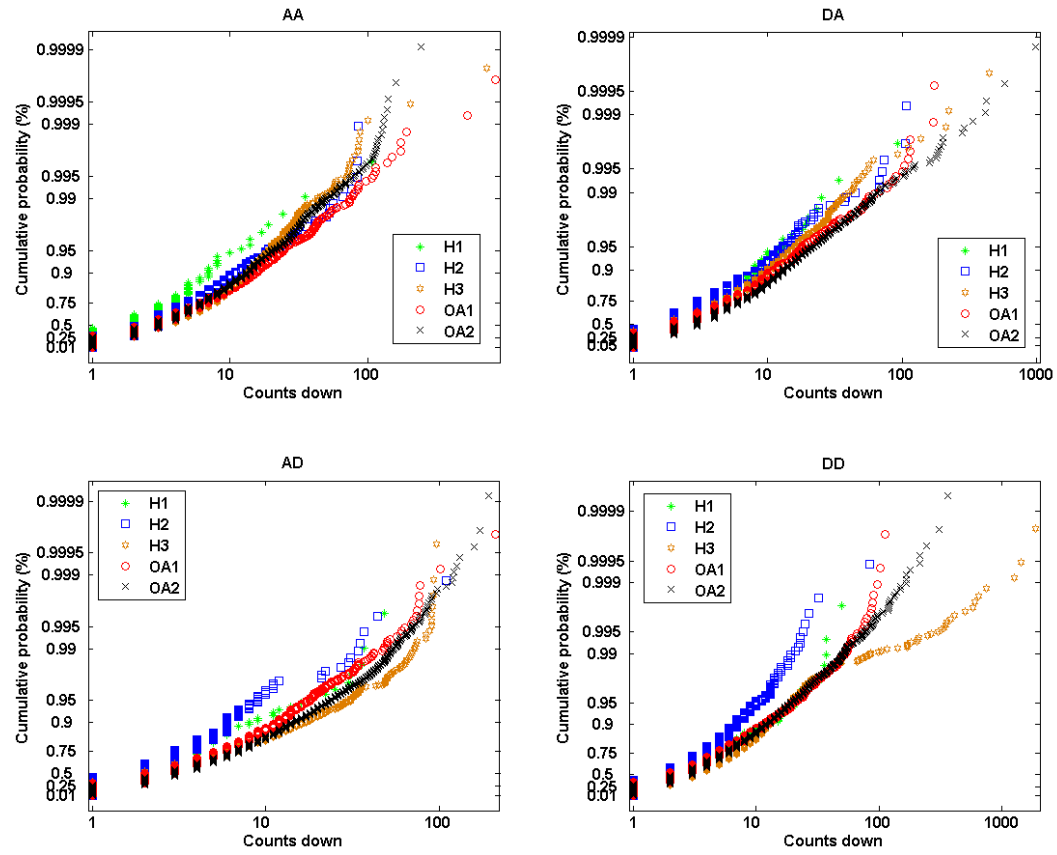


Figure 5-32 Cumulative distributions of counts down

5.8 CONCLUDING REMARKS

This chapter devoted to the statistical evaluation of AE signals. It started with the basic statistics in terms of the quantity of AE events. By investigating the participants with both knees healthy or OA, the number of AE event were found to be low and repeatable with good symmetry in all four movement phases for the early adulthood group, higher and repeatable with certain loss of symmetry for the middle and late adulthood healthy groups, and highest with wider spread and asymmetry for OA knees. The trend of AE events increasing with age was supported by the analysis of the average AE hits per 10 movements. Using the average AE hits of the four movement phases, significant statistical differences and trends between the five age and OA groups in terms of maximum, median, minimum and deviation of the average AE hits were discovered, with the maximum and minimum increments seen to occur in the DA and DD phases, respectively, and with a trend of increasing deviations related to age and symptoms observed in all four movement phases. Moreover, the best separation was observed in the DD phase, with the values within the IQR non-overlapped. These observations form a basic statistical basis for the use of knee AE for quantitative assessment of joint ageing and degeneration.

Via the probability distribution of each AE waveform feature generated by OA knees in the AA phase, the cumulative distributions of each AE waveform feature generated by all the participating groups in each movement phase were analysed. The statistical distributions of the peak amplitude and the features based on counts are seen to follow the exponential distribution. The statistical distribution of the peak frequency feature is seen to be bi-modal, with the peak frequencies lower than 100 kHz seen to resemble exponential, and the values above 100 kHz seen to resemble Gaussian. For other AE waveform features with the exception of ASL, the statistical distributions were seen to either contain a significant part of Gaussian distribution or appear to follow an asymmetric Gaussian distribution.

Compared with the statistical distributions produced by the amplitude based features, the distributions of the other AE features show smaller differences among the five participating groups. In particular, the statistical distributions produced by the time based features show

very high percentage of overlaps with only some movement phases showing noticeable differences between group H1 and the other four groups. The statistical distribution produced by the frequency based features derived from the time-series waveforms show even less discrimination with all the curves forming nearly the same trajectory from the lowest to the highest frequencies apart from the curve for group H1 in the AA phase. Although there are some statistical significance between the healthy and OA groups based on the cumulative distribution of the peak frequency values in the AA phase, the differences appear to be in a small frequency range with low probabilities of occurrence. For the cumulative distributions of the centre frequencies, although they produce better separation between the five participating groups, the values are distributed within the same range apart from group H1. The cumulative distribution curves of the signal strength and absolute energy values showed also a very high percentage of overlap with all the curves seen to have nearly the same slope. Finally, the cumulative distributions produced by the count based features showed some discrepancy among the five participating groups, the differences are not as apparent as those produced by the amplitude based features, with higher percentages of curve overlaps and less differences showed at the tail of distribution.

The cumulative distributions of ASL are shown to provide the best discrimination among the five groups, with the lowest percentage of curve overlaps, and the distinctive value separations at the upper bound of the distributions. Another significant statistical factor for discrimination of different groups is found to be the peak amplitude, with significant differences observed based on the value occurrence, particularly in the DD movement phase.

In this chapter, the increase in the number of AE hits from knees is shown to relate statistically to age and knee condition in each movement phase, and this statistical trend is further supported by the statistical correlation with various AE waveform features. With the AE peak amplitude and ASL values shown to provide the most significant statistical differences, the combination of them with the number of AE events makes it possible to identify each age and knee condition class as shown in the next chapter.

CHAPTER 6 MULTIVARIATE FEATURE VISUALISATION AND ANALYSIS

6.1 INTRODUCTION

Based on the statistical evaluations of AE features illustrated in the preceding chapter, peak amplitude and ASL are considered to have the highest statistical significance for the five age and pathology related groups. With none of two knees found to be exactly the same in terms of the quantity of AE events and the waveform characteristics, it is necessary to develop an appropriate statistical model to simplify the assessment and visualisation of knee AE signals. As several variables are included in the analysis of AE signals emitted from the knees (i.e. peak amplitude, ASL and number of AE hits in different movement phases), multivariate based techniques are required.

This chapter starts with a brief review of the common multivariate statistics (Section 6.2). With a large majority of AE events acquired, Section 6.3 introduces a statistical based AE feature profile to simplify the representation of AE signals emitted from the knee, and transform the AE signals emitted from individual knees to a uniform format (Sub-section 6.3.1). An image based display scheme is used to facilitate visual based comparison of individual knee joint AE profiles (Sub-section 6.3.2). Section 6.4 devotes to PCA of AE patterns between five ageing and degeneration groups, with Sub-section 6.4.1 introducing the fundamental of PCA, Sub-section 6.4.2 showing 3D PCA projections of AE profiles for the knees studied with ages and other clinical scores, and Sub-section 6.4.3 investigating the sensitivity of PCA of the AE feature profiles constructed using various value intervals. Concluding remarks are given in Section 6.5.

6.2 OVERVIEW OF MULTIVARIATE ANALYSIS

The generic term of multivariate analysis in statistics describes a collection of procedures which involve the analysis of more than one variable [53]. It focuses on the understanding of the latent relationships from different forms of variables. This sub-section briefly introduces four main multivariate statistic models which have been developed to deal with various scenarios, namely, clustering [53], discriminant analysis [105-106], regression analysis [107], and multivariate based dimension reduction techniques [108], respectively.

Clustering [53] is a kind of technique that is able to assign a set of observations into subsets based on certain distance measurements, so that the observations belonging to the same group are formed based on the same criterion in some sense. There are two main types of clustering, namely, hierarchical and non-hierarchical clustering (also known as partitional clustering). The hierarchical clustering creates a tree structure called dendrogram to represent the relationships between variables based on pre-determined linkage criteria, with the root of dendrogram denoting the vector consisting of all the variables, and the branches corresponding to the individual variables. There are two main strategies to achieve the hierarchical clustering, namely, agglomerative approaches, which start at the leaves and eventually merge clusters together, and divisive approaches, which start at the root and eventually spread all the variables into detailed clusters. The non-hierarchical clustering is to divide the data into various partitions or groups based on the multi-dimensional distance measurement techniques (such as Euclidean and Mahalanobis distance, and correlation coefficients) [53], with each partition representing one individual cluster. The results of non-hierarchical clustering can be visualised via the scatter plot [53], a method in which variables can be displayed as a collection of points in the Cartesian coordinate system. Both hierarchical and non-hierarchical techniques are based on iterative processing, and the main difference between these two approaches is the number of groups to be assigned for the data which needs to be determined prior to the non-hierarchical clustering, but not necessary for the hierarchical clustering [53].

Multivariate discriminant analysis also aims to isolate the dependent variables into two or more groups. Unlike the clustering methods with separation decided by distance

measurement, the decision rules for the discriminant analysis are determined by fitting the multivariate distributions (such as multivariate normal and quadratic distributions) [105-106] to the probability density function of the multivariable data, thereby creating the decision boundaries for assigning the patterns.

Multivariate regression analysis [107] is the multivariate statistic model that is used to understand the variation of the dependent variables while single or multiple independent variables are changed. In general, this methodology creates a regression function to estimate the conditional expectation or the location parameter of the conditional distribution of dependent variables when the corresponding independent variable is changed. It is widely used for predicting and forecasting, in order to understand the intercorrelation between dependent and independent variables. Parametric and non-parametric regressions are two major types of the regression analysis methodologies. For the parametric regression, the regression function needs to be estimated prior to running of the regression analysis. For the non-parametric regression, the regression function does not necessary need to be pre-determined, as the regression function can be defined according to the information extracted from the independent variables.

To deal with the high dimensional data set, multivariate based dimension reduction techniques have been developed. The central theme of the techniques is to seek the lower dimension representations of the data with high dimensionality [105]. The common techniques consist of PCA [53, 109], factor analysis (FA) [53], random projection (RP) [110], and independent component analysis (ICA) [111]. All of these techniques result in the new data set which has a lower dimensionality than the original data set via the transformation. PCA seeks to reduce the data dimensionality based on the orthogonal transformations, thereby projecting the data with higher variations onto the lower dimension space in the new coordinate system. FA reduces the data dimensionality by estimating the particular factors that correlated with the original variables. Unlike PCA, which seeks the maximum variation of the multivariate data set, FA represents the compressed data based on the similarities. RP is a simple but powerful dimension reduction technique that finds the lower dimension projection of larger data using the random transform. Compared with the other three approaches (i.e. PCA, FA, and ICA), RP is more

effective in terms of reducing the computational burden by randomly projecting the data onto the new coordinate system. ICA also seeks the projection of the high dimension variables. Unlike PCA, the transformations performed by ICA are not necessarily orthogonal, but as nearly statistically independent as possible.

6.3 MULTIVARIATE BASED AE FEATURE ANALYSIS

6.3.1 Feature based profiles of knee joint acoustic emission

Based on the statistical evaluation discussed in the preceding chapter, the number of AE hits, as well as the peak amplitude and ASL values were shown to exhibit certain age and degeneration related trends. As there are vast amount of AE signals created by each knee performing consecutive and repeated movements, and there is a high percentage of overlap in the feature values extracted from signal waveforms among the five participating groups, direct separation of the knee joints using their waveform features is difficult. As an example, Figure 6-1 shows the scatter plot consisting of the peak amplitude and ASL values extracted from one late adulthood healthy knee in group H3, and one late adulthood OA knee in group OA2, and no clear boundary is seen between these two knees with most of the AE feature patterns overlapped. It is therefore difficult to apply the multivariate techniques directly to classify the knee joint AE, even with only one healthy and one OA knee. It will not be possible for clustering methods to decide the group distance, and discriminant analysis to create the decision boundary. Furthermore, very similar regression function will be derived due to the high pattern similarity between the two groups.

Previously, a feature based representation of knee AE has been introduced to represent the discriminative AE features in two movement phases in a compact and uniform format for visualising and identifying the differences between knees [23]. In this thesis, the representation is modified by using different features and extended to the four movement phases. The representation of the feature based profile is given by:

$$H = \frac{1}{10} \sum_{i=1}^{10} (X_i, \psi) \quad (6-1)$$

where X_i denote the feature class in the i^{th} movement, ψ denotes movement phase (i.e. AA, AD, DA, and DD phases), and H denotes the average number of AE hits of particular feature classes in a particular movement phase over 10 repeated movements.

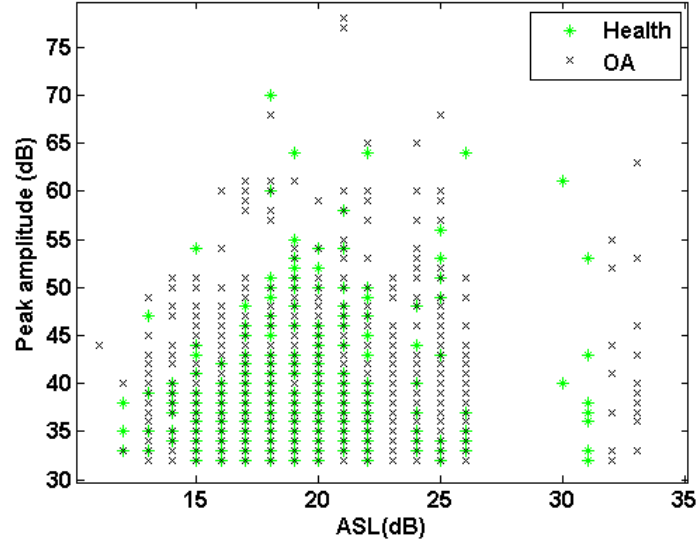


Figure 6-1 Scatter plot of peak amplitude and ASL for one healthy and one OA knee

By using the amplitude and ASL features to create the AE profile for each movement phase, the AE profile in the i^{th} movement can be defined as $X_i(PEAK\ AMPLITUDE_j \cap ASL_m)$. If the value intervals of the peak amplitude and ASL values are defined as:

$$30+10(j-1) \leq PEAK\ AMPLITUDE_j < 30+10j \quad \text{for } j=1,2,\dots,6 \quad (6-2)$$

$$10+5(m-1) \leq ASL_m < 10+5m \quad \text{for } m=1, 2, \dots, 8 \quad (6-3)$$

and the last peak amplitude and ASL intervals are given by $PEAK\ AMPLITUDE_7 > 90$ dB and $ASL_9 > 50$ dB, respectively, then a total of 63 feature classes is created by the combination of amplitude and ASL values for each individual movement phase.

6.3.2 Visualisation of knee joint acoustic emission

To provide a visual display of the AE feature profile, an image based representation is developed with the AE feature profile in each movement phase shown as a 2D colour histogram in each quarter of the image. The representation was firstly introduced by [23] and modified in this thesis for the features and movement phases used. As the display scheme shown in Figure 6-2, the image is partitioned into four quarters corresponding to the AA, AD, DA, and DD movement phases, respectively. AE hits in the ascending phase are allocated in the left half of the image, whereas AE hits in the descending phase are allocated in the right half of the image. The top half and the bottom half are for AE hits during acceleration and deceleration of movements, respectively. In order to gain a symmetrical visualisation effect of the AE profile, the direction of ASL and peak amplitude intervals are oriented outward in an ascending order from the centre of image along the horizontal and vertical axes, respectively.

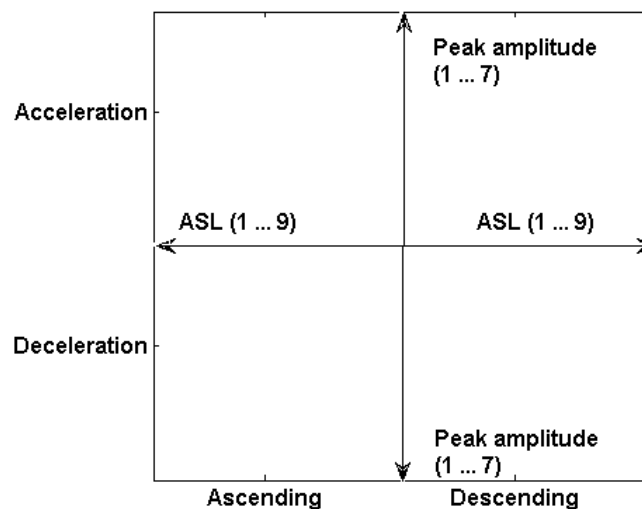


Figure 6-2 Display scheme of image based representation of AE feature profile

Figure 6-3 shows the typical examples of the knee joint AE profiles for the five groups (the image based representation of all AE feature profiles are shown in Appendix G). From the early adulthood healthy knee profiles, it should be apparent that the knees in this group

generate AE signals with the low peak amplitude and ASL values, and with the average number of AE events per movement less than 6 for each feature class. More types of AE feature classes with higher occurrence start to appear in the middle adulthood healthy knee profile as shown in its AE profiles with colours extending in both horizontal and vertical directions. While the average number of AE events per movement for a particular waveform feature class in the ascending phase can be as high as 10, it can be as high as 16 in the descending phase. From the AE profiles of the late adulthood healthy knee, AE signals with medium peak amplitude and medium ASL values start to appear, and the average number of lower level AE signal (i.e. with low amplitude and ASL values) can be up to a maximum of 25 in the AA movement phase.

Comparing the OA1 middle adulthood profiles with the three healthy profiles shown in the same figure (Figure 6-3 and Appendix G), larger number of AE hits with a wider range of peak amplitude and ASL values are generated, with the values spreading along both horizontal and vertical directions in all of the four movement phases. In addition, there are a few AE events with high peak amplitudes, and medium ASL values in the OA1 profiles, which were not generated in the healthy profiles. Comparing the OA2 profiles with the OA1 profiles, even higher number of AE events with the wider range of peak amplitude and ASL values are generated, with the maximum number of average AE events more than 30 hits found in OA2 group. Furthermore, there is an absence of AE events with minimum ASL in the deceleration phase in some of OA knees profiles.

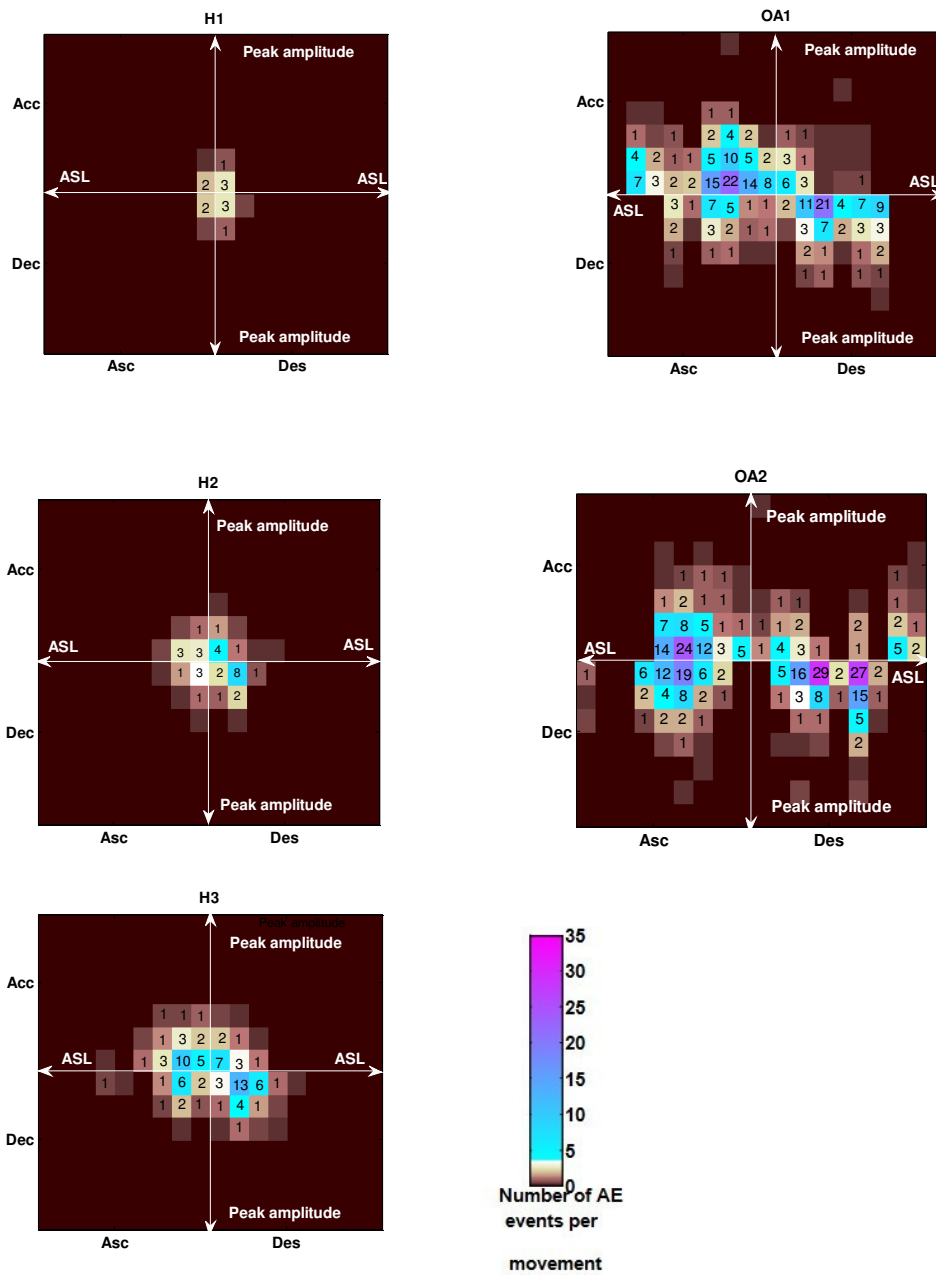


Figure 6-3 Typical AE feature profiles of a knee in each group

6.4 BIOMARKER IDENTIFICATION BY PRINCIPAL COMPONENT ANALYSIS

Using the AE feature profiles based on the four-phase model discussed in the preceding section, the AE signals emitted from the individual knees were transformed into a uniform format, and the differences between individual knees can be visualised by using the image based representation. However, as the AE profiles are still expressed with high dimensionalities (4×63 dimensions for each knee), dimension reduction is necessary in order to give a more quantitative assessment AE score for each knee.

The purpose of reducing the dimensionalities of AE profiles is to maximise the variations between the five ageing and degeneration related groups in the lower dimensional space. The multivariate based dimension reduction techniques were reviewed in Section 6.2. For FA, since it aims to seek the internal correlations among the multivariate dataset, it is not suitable for the purpose of study in this thesis; for RP, since it compresses the high dimension data based on the random transformation by saving the computational time, it may not result the new dataset with the maximum variation in the lower dimensional space; and for ICA, since it seeks the independence of the variables, it is not suitable for the purpose of study. With PCA [109] reducing the dimensionalities by maximising the variability of the multi-dimension dataset in the lower dimension space, it is selected to discover the hidden AE patterns in the five participating groups.

6.4.1 Principal component analysis

As the multivariate based techniques mentioned in the preceding section, the central theme of PCA is to reduce the dimensionality of the multiple variables dataset, thereby retaining as much variations as possible in the first few dimensions of the new dataset. The transformation of the original dataset to the new coordinate system can be done by projecting the original dataset into a new space formed by the principal components (PC), the representation (projection) of the original dataset in the new space can be represented by the PC scores. Let matrix \mathbf{F} with $x \times y$ dimensions be the input data matrix of the PCA,

where x corresponds to the number of data sets and y the number of variables, the computation of the PC and the corresponding scores can be achieved by using two approaches, namely, singular value decomposition (SVD), and spectral decomposition, respectively.

In the first step of both approach, matrix \mathbf{F} is mean-corrected to give \mathbf{F}_M , and this is achieved by subtracting each variable in the matrix to the corresponding column mean, thereby ensuring all variables in the matrix receiving the same weight.

In the SVD approach, \mathbf{F}_M can be expressed as a triple multiplication as:

$$\mathbf{F}_M = \mathbf{U}\mathbf{S}\mathbf{V}^T \quad (6-4)$$

where, \mathbf{V}^T is a $y \times y$ square and orthogonal matrix consisting of the eigenvectors of matrix \mathbf{F}_M in each column, \mathbf{S} is a $y \times y$ diagonal matrix with the main diagonal containing the corresponding square roots of eigenvalues of matrix \mathbf{F}_M [53], and \mathbf{U} is a $x \times y$ matrix decomposed by SVD.

By selecting a small number of eigenvectors associated with highest eigenvalues (i.e. PC) and denoting it as \mathbf{V}_{PC}^T with a dimension of $y \times s$, and with $s \ll y$, the whole set of \mathbf{F}_M can be projected on a different basis formed by a small set of orthogonal and ordered PC axes with the first few PC axes capturing most of variation (i.e PC scores). For the visualisation purpose, three eigenvectors corresponding to the three highest eigenvalues are used with the dimension of \mathbf{V}_{PC}^T set to $y \times 3$, and the PC scores can be calculated by:

$$\mathbf{K} = \mathbf{F}_M \mathbf{V}_{PC}^T \quad (6-5)$$

Another way to implement PCA is based on the spectral decomposition, which is achieved by applying the SVD to the covariance matrix of \mathbf{F} . If the covariance matrix of \mathbf{F} is defined by:

$$\mathbf{C} = \frac{1}{x-1} (\mathbf{F} - \boldsymbol{\mu}_F)^T (\mathbf{F} - \boldsymbol{\mu}_F) \quad (6-6)$$

where, $\boldsymbol{\mu}_F$ is the column mean of \mathbf{F} , the SVD of the covariance matrix can be expressed as:

$$\mathbf{C} = \mathbf{P}\mathbf{D}\mathbf{P}^T \quad (6-7)$$

where, \mathbf{P} is a $y \times y$ square and orthogonal matrix with each column consisting of the eigenvector of \mathbf{C} , and \mathbf{D} is the $y \times y$ diagonal matrix whose main diagonal consists of the corresponding eigenvalues of \mathbf{P} . By selecting again the PC based on the first three highest eigenvalues in \mathbf{D} to form \mathbf{V}_{PC}^T and applying equation 6-5 will produce the same PC scores.

The information capture by each PC correspond to the variance of each column of \mathbf{K} which can be calculated by:

$$\sigma_K^2 = \frac{1}{x} \sum_{i=1}^x (K(i) - \mu_K)^2 \quad (6-8)$$

where $K(i)$ denotes the PC score for the i^{th} row of \mathbf{K} , and μ_K denotes the mean value of the K^{th} column of \mathbf{K} .

The total data variance can be calculated by using either equation 6-9 or equation 6-10:

$$\sigma_t^2 = \text{trace}\left(\frac{\mathbf{S}^2}{x-1}\right) \quad (6-9)$$

$$\sigma_t^2 = \text{trace}(\mathbf{D}) \quad (6-10)$$

Hence, the percentage of the variance captured by each dimension of PC equals the ratio of σ_K^2 and σ_t^2 .

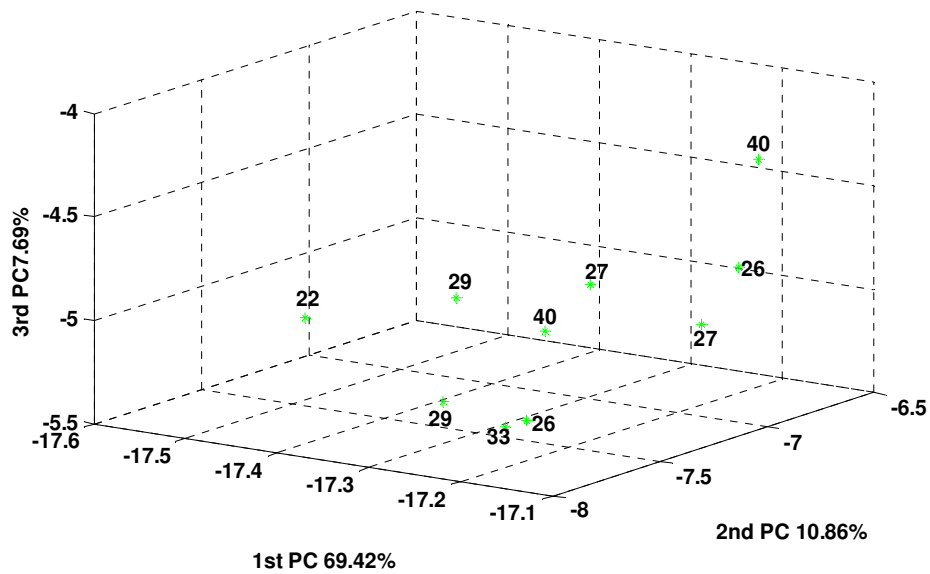
6.4.2 Classification of AE profiles by principal component analysis

For the AE feature profiles constructed by the AE peak amplitude and ASL, PCA is performed to create the visual effects for each individual AE profiles in the lower dimensional space, thereby highlighting the hidden relationships between the AE profiles and the knee joint conditions in the five participating groups.

With the AE features re-formatted to the uniform format by using the image based profile discussed in the preceeding section, let J and M correspond to the total number of peak amplitude and ASL intervals in each movement phase, the image based profile can be converted from its matrix of size $2J \times 2M$ to a row feature vector of length of $4JM$ by row

concatenation. By combining the row feature vectors of all the knees into one data matrix, it results in the data matrix with a size of $\mathbf{F} = 53 \times 4JM$ for the entry of PCA with each row of the matrix consisting of the AE profile of each individual knee.

By applying the SVD approach to find the projections of the mean corrected matrix \mathbf{F}_M in the PC domain, the projection of the AE feature profiles from 53 knees on the PCA space formed by the first three principal components is shown in Figure 6-4. Based on a total of 63 AE feature classes with 7 amplitude and 9 ASL intervals per each movement phase, approximately 87.97% of the total variance in the data is captured. By labelling each projected AE feature profile according to its age and knee condition group, there are five clusters in Figure 6-4 (a) corresponding to the five groups with a trajectory related to knee age and degeneration, progressing from group H1 with the early adulthood healthy knees to group H3 with late adulthood healthy knees, followed by group OA1 with the middle adulthood OA knees to group OA2 with the late adulthood OA knees. Furthermore, this trajectory shows increasing areas for each cluster. It starts from the smallest cluster for the early adulthood healthy knees in group H1 with significant overlapping of the projected AE feature profiles. With the increase in the age, the cluster areas increase with longer distances among the projected AE feature profiles for the middle and late adulthood healthy knees in group H2 and H3. As the knee condition changes from healthy to OA, the cluster areas are seen to spread even further with much longer distances shown among the projected AE feature profiles of the knees in group OA1 compared with those in group H3. At the end of trajectory, group OA2 with the late adulthood OA knees is seen to produce the largest cluster area with the widest spread of the projected AE feature profiles. Additionally, from the zoom-in view of the knees in group H3, there appear to be two potential sub-clusters, with one formed by 6 out of 7 knees with ages over 70 years and the other one formed by 5 out of 6 knees aged 60-70 years.



(c)

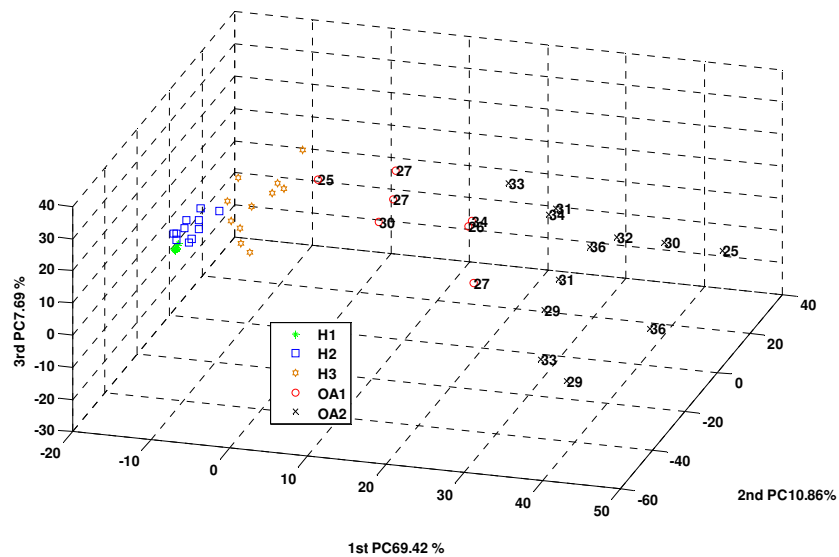
Figure 6-4 PCA of AE feature profiles constructed by amplitude and ASL of AE signals (a) all five groups, (b) zoom-in view of H2 and H3 groups, and (c) zoom-in view of H1 group

As mentioned in Chapter 3, data collection includes BMI, KOOS, SF-36 and K-L X-ray scores, and the relationships between the AE profiles in the first three PC spaces and these clinical scores were investigated. Because the SF-36 scores focus on the assessment of participants' daily life and general health [99], it was not investigated further as it is not knee specific. Although the KOOS scores are concentrated on the knee joint function assessment [98], the assessments are done by the the participants. As the healthy participants with symmptomatic knees and the OA participants with asymmptomatic knees are excluded from the study, KOOS scores are not viewed as a useful clinical scores for the analysis in this thesis, becasue the KOOS scores include a number of non-clinical categories such as quality of life, sports, and daily life.

Figure 6-5 shows the PCA projections of knee joint AE profiles with the BMI values. In Figure 6-5, two knees belonging to group H3 are excluded due to the bodymass and height not recorded (mentioned in Section 3.4). From Figure 6-5(a), it is seen that, although most of group OA2 knees have BMI in the obesity level, and most of OA1 knees have BMI in the overweight level, it does not produce two BMI related clusters for these two groups.

From Figures 6-5 (b) and 6-5 (c) showing the zoom-in views of the three healthy groups, similar results are seen without clear BMI related clusters.

Figure 6-6 shows the PCA projection of 10 OA knee joint AE profiles with X-ray scores (with each knee labelled 'age, [K-L score]'). From Figure 6-6, a certain relationship appears to exist between the AE profile and the X-ray score, since only one participant aged 82 years with K-L score equal to 1 does not match the general trend. Having said that, the result is not conclusive due to a small number of knees available with K-L scores. Nevertheless, it is noteworthy to mention that the K-L scores may not truly reflect the current conditions of the knee studied as they were based on old X-rays and that the K-L scores are rather coarse with observer variability.



(a)

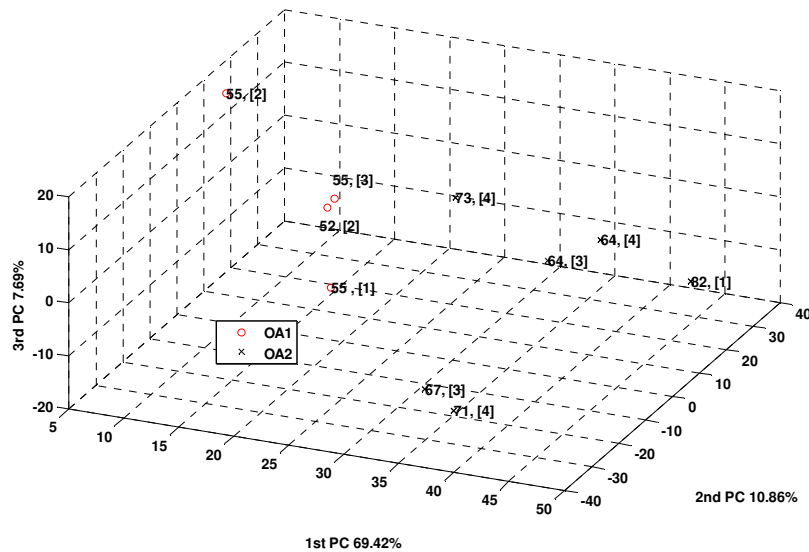


Figure 6-6 PCA of AE feature profiles with age and K-L scores for 10 OA knees

The above results demonstrate the potential of using the projected AE feature profiles in the PCA space as a biomarker for quantitative assessment of knee age and condition. By increasing the number of age groups with a larger number of healthy and OA knees in each age group to establish the reference clusters and trajectory, a knee could be possibly diagnosed based on the position of its projected AE feature profile along the trajectory and the distance of it with respect to the reference cluster or the boundary of the nearest two clusters. The wide spread of the OA clusters observed in the PCA space also suggests the possibility of further group clustering to define sub-domains based on different pathologies. In particular, it has been shown that the projections of the H3 profiles could be divided into two sub-clusters based on age. By including additional AE descriptors to form the AE based profiles, further group isolation may also be achievable for other groups.

Compared with the previous results of AE based knee joint assessment, the AE feature profiles introduced in this chapter enables classification of not only the early adulthood healthy and late adulthood OA knees, but also the knees in different age bands and conditions.

6.4.3 PCA sensitivity

For the statistical AE profiles shown in the preceding sub-sections, an issue can be raised regarding the sensitivity of the AE profile to the change of each feature class, or granularity of the multidimensional AE profile when computing PCA. An investigation was also performed to see the sensitivity of PCA based projection of the AE feature profiles to the change of the value intervals (or granularities) of the AE features. In this sub-section, the AE profile $X_i(PEAK\ AMPLITUDE_j \cap ASL_m)$ for each individual knee is changed by using more or less feature classes based on two other value intervals given by:

$$30+5(j-1) \leq PEAK\ AMPLITUDE_j < 30+5j \quad \text{for } j=1, 2, \dots, 12 \quad (6-11)$$

with the last amplitude class $PEAK\ AMPLITUDE_{13} > 90$ dB,

$$10+10(m-1) \leq ASL_m < 10+10m \quad \text{for } m=1, 2, \dots, 4 \quad (6-12)$$

with the last ASL class $ASL_5 > 50$ dB.

Figures 6-7 to 6-9 show the PCA projections of AE feature profiles of the 53 knees studied with three different granularities. Figure 6-5 shows the 3D PCA projection of AE feature profiles with the possible feature value intervals determined using equations 6-3 and 6-11 (with peak amplitude feature classes increased to 13 and ASL feature classes remained the same). Although the projection shows a slight overlap between group H3 and OA1 knees, the progression for age related degenerations is clear, with the trajectory progressing from group H1 to OA2, and with the wide spreaded knee patterns when the ages growing older. The projections of AE feature profiles shown in Figures 6-6 and 6-7 are obtained using equations 6-2 and 6-12 (with peak amplitude feature classes remained the same and ASL feature classes reduced to 5), as well as equations 6-11 and 6-12 (with peak amplitude feature classes increased to 13 and ASL feature classes reduced to 5), respectively. The projections of these two types of the AE feature profiles also shown to have the trend from the early adulthood healthy knees (H1) to the late adulthood OA knees (OA2) with slightly different group distances. Based on the sensitivity evaluation discussed in this sub-section, it can be concluded that although the PCA results of the AE feature profiles with various

granularities show some discrepancy, they do not change the ageing and degeneration related trajectory and each cluster remains well defined by the projected point in the corresponding group.

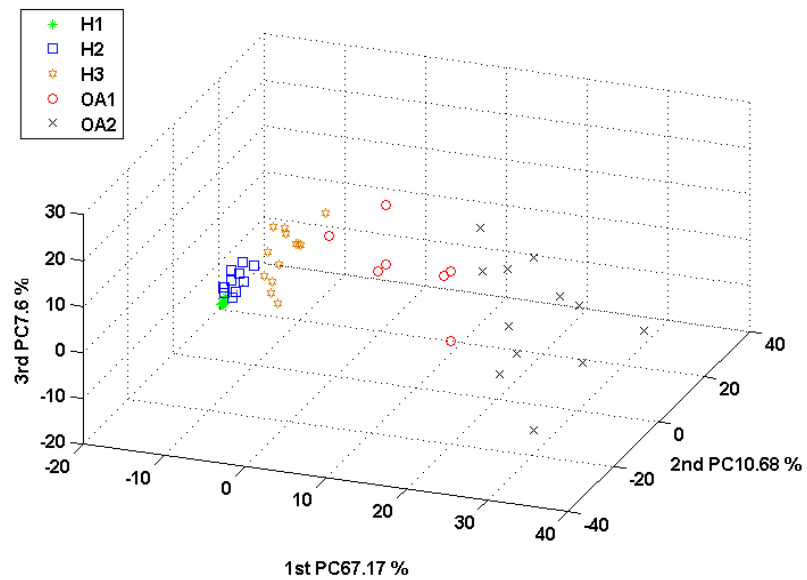


Figure 6-7 PCA results produced by 13 amplitude intervals and 9 ASL intervals

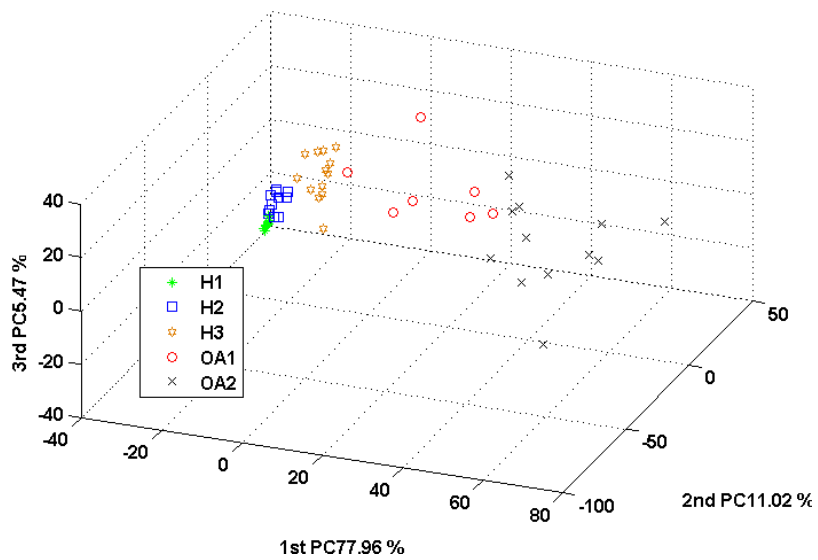


Figure 6-8 PCA results produced by 7 amplitude intervals and 5 ASL intervals

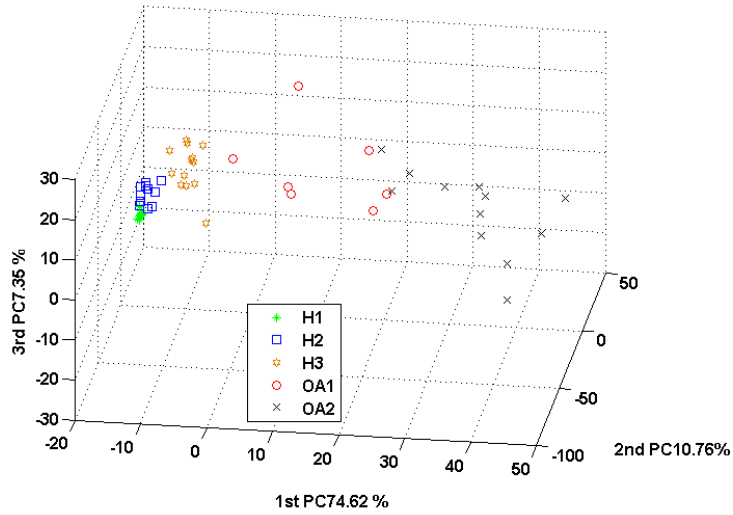


Figure 6-9 PCA results produced by 13 amplitude intervals and 5 ASL intervals

6.5 CONCLUDING REMARKS

This chapter presented the multiple variables based AE feature profile developed as a biomarker for quantitative assessment of knee joint ageing and degeneration. As it is difficult to classify the AE signals emitted from different knees based on the most significant AE features, an AE feature profile based on the statistics of the two AE features in four movement phases over 10 repeated sit-stand-sit cycles was introduced to represent the AE signals in a uniform format, and the 2D image based representation was introduced for visualisation of the AE signals. Based on 7 amplitude and 9 ASL classes in each movement phase, the image based representations showed significant visual differences between the AE signals emitted from different knee conditions, with the number of the feature classes and the number of average hits in each feature class increasing with age and OA.

Although the presentation of the knee joint AE signals was simplified by using the AE profile based on two AE features in four movement phases, it still has a relatively high dimension due to the number of feature classes, and led to the application of PCA to project

the high dimensional feature classes to the low dimension space formed by the first three principal components. Using the projected AE profiles in the low dimension PCA space as the biomarker, an ageing and degeneration related trajectory were observed with five distinctive clusters, where the early and late adulthood healthy knees (group H1 and H3) were seen to occur at two extremes of the healthy groups, and they are followed by the middle and late adulthood OA knees (group OA1 and OA2). Furthermore, the cluster area was seen to increase with the increasing age for the health and OA groups, and the sensitivity of the trajectory and the clusters with respect to the number of feature classes was investigated to show its robustness. The results demonstrated the potential of the AE based biomarker for quantitative assessment of knee joint ageing and condition, and open up the possibility to diagnose the knee joint disorder at the early stage based on the position of the knee profiles in the projected space.

CHAPTER 7 CONCLUSIONS AND RECOMMENDATIONS FOR FUTURE WORK

7.1 CONCLUSIONS

The research described in this thesis deals with discovery of AE based biomarker for quantitative assessments of ageing and degeneration in human knee joints. AE is a type of high frequency ultrasound that is generated from the industrial materials or human body under pressure. Through the literatures reviewed in chapter 2, AE has been discovered as a useful marker for quantitative assessment of damage progression in machinery and human bone, and the knee joint flexion-extension is considered as a useful protocol for joint functional assessment in terms of ageing and degeneration. Along with the exploratory study showing distinctive differences between the young healthy knees and the old OA knees, a solid basis is formed for the research to investigate the potential of AE as a biomarker of more subtle knee joint conditions.

Joint angle based AE signals with corresponding clinical scores were acquired from a total of 72 participants which include healthy, OA, RA, damage joints, and the participants after TKR. With a large number of AE data acquired from the knees belonging to various age ranges, it enables the project to focus on the discovery of ageing and degeneration related AE biomarker for healthy and OA cohorts. In order to ensure all signals used are collected from the knees under the clear clinical statuses, healthy knees without historical abnormal symptoms and OA knees with radiological confirmation were selected.

By dividing each sit-stand-sit movement into four movement phases (AA, AD, DA and DD phases) proposed by the author based on the joint angle and angular velocity signals, quantitative assessments of joint angle and velocity signals based on cycle-by-cycle variations and movement symmetry reveal noticeable statistical differences related to joint age and degeneration, particularly in the descending phase.

Via the quantitative assessment of the basic statistics of AE events in the proposed four movement phases, the number of AE events were found to be low and repeatable with good

symmetry for the early adulthood group, and to increase with certain loss of symmetry and higher variability as the age increases and the knee condition changed from healthy to OA. Significant statistical differences were also found between the five age and OA groups in terms of average AE events per 10 movements, with a trend of an increasing number of average AE events and their deviations related to age and OA in all of the four movement phases. Via the probability distribution analysis of AE waveform features, most of the AE features showed statistical differences between the healthy and OA knees, and the AE peak amplitude value and ASL were showed to provide the most statistical differences between five age and disease groups, particularly at the upper bounds.

A knee AE profile based on two waveform features and four movement phases was developed to reduce the amount of data to a manageable level, and to enable a uniform representation of the AE signals produced by different knee conditions. Using an image based representation to show the AE feature profile, there is a visual trend of increasing peak amplitude and ASL values with the increasing age groups and the change of knee condition from healthy to OA. Application of PCA to the AE feature profiles of all knees yields an age and disease related trajectory with five distinctive clusters of increasing sizes and progressing from the youngest healthy group to the oldest healthy group, then from the youngest OA group to the oldest OA group.

With all the trends from knee AE signal analysis showing a strong correlation with knee age and condition, there is significant prima facie evidence for knee AE as a biomarker for quantitative assessment of joint ageing and degeneration. With the advantages of simplicity and accessibility, a good prospect is viewed to be offered by knee AE as a rapid and non-invasive measurement tool for use in clinic and home settings for objective monitoring of condition change in knee joints.

7.2 FUTURE WORK

The work described in this thesis has shown AE as a potential biomarker for quantitative assessment of joint ageing and degeneration for knees. Based on the research findings

shown in this thesis and the current data collected, the recommendations for potential future work for the project are summarised in the following.

7.2.1 Discovery of additional biomarker for comprehensive representation of knee joint ageing and degeneration

Further analysis can be applied to the signals acquired from the five ageing and degeneration related groups, thereby discovering a more comprehensive biomarker for assessment of knee ageing and degeneration. The four-phase movement model can be extended to more phases to give higher angular sensitivity. For example, the median value of the instantaneous angular velocity in each movement phase could be used as the threshold to divide it into two sub-movement phases (corresponding to low and high speed). This will enable knee joint AE to be analysed at finer joint angle range. The repeatability of AE events is another area to be investigated. The AE signal appearance repeatability can be assessed using the AE descriptors and the detailed joint angle signals (e.g. waveforms described by similar AE features appeared within a similar angular range in different movement cycles can be treated as repeatable). This investigation will enable the use of repeatable, dominant and distinctive AE waveforms as a more comprehensive biomarker for clinicians to monitor ageing and identify the stage of joint degeneration.

7.2.2 Identification of damage joints

As the data collected include a number of joint damage AE signals, it provides an area for further work. By applying the repeatability evaluation techniques explained in Sub-section 7.2.1 to exclude the non-repeatable AE events, and using the AE profiles with more detailed movement phases constructed based on the repeatable, distinctive and dominant AE signals, it is not unreasonable to assume that the AE profiles of damage joints in the PCA projected space will appear between the regions of the late adulthood healthy group and the middle adulthood OA group, as ligament/cartilage damage will have a high

probability to develop to OA eventually [12, 112]. Furthermore, the data selection criteria in this project (described in Section 3.5) excludes healthy knees with abnormal symptoms in the study in order to provide a clear clinical condition. By applying the repeatability and occurrence analysis to these excluded knees, and comparing with the asymptomatic healthy knees, damaged joints, as well as the OA knees, it may be able to discover additional waveform features to build a more sensitive AE profile for clinicians to monitor the knees developing into OA, and predict the subtle joint damages at the early stage.

7.2.3 Identification of OA and RA

Another possible direction based on the current data collected is to investigate the differences between OA and RA knees. These two types of arthritis are considered to be caused by different knee joint changes. While OA is considered to be caused by degeneration or post-injury disorder [3-4], RA is considered to be caused by the autoimmune disorder [113]. If some waveforms can be assumed to be useful to differentiate these two types of arthritis, then the statistical analysis methodology presented in this thesis could be followed. The study can be started with the analysis of AE hits from the OA and RA knees, and followed by the statistical distribution analysis of AE features from the OA and RA knees based on detail movement phases to discover the significant features to differentiate between the OA and RA knees. This will finally lead to construction of the AE profile by using the most significant features and application of the multivariate dimension reduction techniques to show the differences between OA and RA.

REFERENCES

- [1]. **Gray, H.** *Anatomy of the human body*. New York: Bartleby.com, 2000.
- [2]. **Kauffman, T.L., Barr, J.O and Moran, M.L.** *Geriatric rehabilitation manual*. Elsevier, 2007.
- [3]. **Arden, N and Nevitt, M.C.** *Osteoarthritis: epidemiology*. Best Pract Res Clin Rheum, 2006, 20(1): 3-25.
- [4]. **Lane, N.E and Wallace, D.J.** *All about osteoarthritis: the definitive resource for arthritis patients and their families*. Oxford University Press, 2002.
- [5]. **Felson, D.T., Lawrence, R.C., Dieppe, P.A., Hirsch, R and Helmick, C.G.** *Osteoarthritis: The disease and its prevalence and impact*. Ann Intern Med, 2000, 133: 637-9.
- [6]. **Peat, G., McCartney, R and Croft, P.** *Knee pain and osteoarthritis in older adults: a review of community burden and current use of primary health knee care*. Ann Rheum Dis, 2001, 60: 91-97.
- [7]. **Qazi, A.A., Folkesson, J., Pettersen, P.C and Karsdal, M.A.** *Separation of healthy and early osteoarthritis by automatic quantification of cartilage homogeneity*. Osteoarthritis cartilage, 2007, 15: 1199-06.
- [8]. **Cooper, C., Snow, S., McAlindon, T.E., Kellingray, S., Stuart, B., Coggon, D and Dieppe, P.A.** *Risk factors for the incidence and progression of radiographic knee osteoarthritis*. Arthritis Rheum, 2000, 43(5): 995-1000.
- [9]. **Wakefield, R.J., Kong, K.O., Conaghan, P.G., Brown, A.K., O'Connor, P.J and Emery, P.** *The role of ultrasonography and magnetic resonance imaging in early rheumatoid arthritis*. Clin Exp Rheum, 2003, 21 (5 suppl 31): 42-9.
- [10]. **Tehranzadeh, J., Ashikyan, O and Dascalos, J.** *Magnetic resonance imaging in early detection of rheumatoid arthritis*. Semin Musculoskeletal Radiol, 2003, 7: 907-15.
- [11]. **Kellgren, J.H and Lawrence, J.S.** *Radiological assessment of osteoarthritis*. Ann Rheum Dis, 1957, 16, 494-02.
- [12]. **Wang, S.Z., Huang, Y.P., Saarkakkala, S and Zheng, Y.P.** *Quantitative assessment of articular cartilage with morphologic, acoustic and mechanical properties obtained using high-frequency ultrasound*. Ultrasound in Med Biol, 2010, 36(3): 512-27.

- [13]. **Roemer, F.W., Holsbeeck, M.V and Genant, H.K.** *Musculoskeletal ultrasound in rheumatology: a radiologic perspective.* Arthritis Rheum, 2005, 53(4): 491-3.
- [14]. **Naredo, E., Moller, I., Moragues, C., Agustin, J.J.D., Scheel, A.K., Grassi, W., Miguel, E.D., Backhaus, M., Balint, P., Bruyn, G.A.W., Agostino, M.A.D., Filippucci, E., Lagnocco, A., Kane, D., Koski, J.M., Mayordomo, L., Schmidt, W.A., Swen, W.A.A., Szkudlarek, M., Terslev, L., Torp-Pedersen, S., Uson, J., Wakefield, R.J and Werner, C.** *Interobserver reliability in musculoskeletal ultrasonography: results from a "teach the teachers" rheumatologist course.* Ann Rheum Dis, 2006, 65: 14-19.
- [15]. **Gold, G.E.** *Dynamic and functional imaging of the musculoskeletal system.* Semin Musculoskelet Radiol, 2003, 7: 245-8.
- [16]. **Kaufmana, K.R., Hughsea, C., Morreya, B.F., Morreyb, M and An, K-N.** *Gait characteristics of patients with knee osteoarthritis.* J Biomech, 2001, 34: 907-15.
- [17]. **Chu, M.L., Gradisar, I.A., Railey, M.R and Bowling, G.F.** *Detection of knee joint diseases using acoustic emission pattern recognition technique.* J Biomech, 1976, 9: 111-4.
- [18]. **Chu, M., Gradisar, I and Mostardi, R.** *A non-invasive electroacoustical evaluation technique of cartilage damage in pathological knee joints.* Med Biol Eng Comput, 1978, 16: 437-42.
- [19]. **Hemelrijck, D.V., Anastassopoulos, A and Philippidis, T.** *Emerging technologies in NDT.* A.A. Balkema, 2000.
- [20]. **Scrubby, C.B.** *An introduction to acoustic emission.* J Phys E Sci Instrum, 1987, 20: 946-53.
- [21]. **Tandon, N and Mata, S.** *Detection of defects in gears by acoustic emission measurement.* J Acoust Emiss, 1999, 17(1-2): 23-7.
- [22]. **Prior, J., Mascaro, B., Shark, L-K., Stockdale, J., Selfe, J., Bury, R., Cole, P and Goodacre, J.** *Analysis of high frequency acoustic emission signals as a new approach for assessing knee osteoarthritis.* Ann Rheum Dis, 2010, 65, 929-30.
- [23]. **Mascaro, B., Prior, J., Shark, L-K., Selfe, J., Cole, P and Goodacre, J.** *Exploratory study of a non-invasive method based on acoustic emission for assessing the dynamic integrity of knee joints.* Med Eng Phy, 2009, 31, 1013-22.
- [24]. **Richards, J.** *Biomechanics in clinical and research.* ELSEVIER, 2008.
- [25]. [Online] [Cited: 4/8/2011.] <http://en.wikipedia.org/wiki/Biomarker>

- [26]. **Shark, L-K., Chen, H and Goodacre, J.** *Knee acoustic emissions: a potential biomarker for quantitative assessment of joint ageing and degeneration.* Med Eng Phy, 2011, 33: 534-45.
- [27]. **Chen, H., Mascaro, B., Shark, L-K and Goodacre, J.** *Signal analysis and classification of joint movement based acoustic emission from health and osteoarthritis knees.* 1st biosensing technology conference, Bristol, 2009.
- [28]. **Shark, L-K., Chen, H and Goodacre, J.** *Discovering differences in acoustic emission between healthy and osteoarthritic knees using a four-phase model of sit-stand-sit movements.* J Open Med Infor: Special issue on "Intelligent signal and image processing in eHealth", 2010; (4): 116-25.
- [29]. **Shark, L-K., Chen, H and Goodacre, J.** *Knee acoustic emission: a clue to joint ageing and failure.* Rheumatology, 2010, 49: Supl(1), i78-80.
- [30]. **Tan, C.K., Irving, P and Mba, D.** *A comparative experimental study on the diagnostic and prognostic capabilities of acoustic emission, vibration and spectrometric oil analysis for spur gears.* Mech Syst Signal Process, 2007, 21: 208-33.
- [31]. **Barron, R.** *Engineering condition monitoring: Practice, methods and applications.* Longman, 1996.
- [32]. **Baydar, N and Ball, A.** *A comparative study of acoustic and vibration signals in detection of gear failures using wigner-ville distribution.* Mech Syst Signal Process, 2001, 15(6): 1091-1107.
- [33]. **Tandon, N and Choudhury, A.** *A review of vibration and acoustic emission measurement methods for the detection of defects in rolling element bearings.* Trib Int, 1999, 32: 469-80.
- [34]. **Choudhury, A and Tandon, N.** *A theoretical model to predict vibration response of rolling bearings to distributed defects under radial load.* J Vibr Acoust, 1998, 120(1): 214-20.
- [35]. **Kuhnell, B.T and Stecki, J.S.** *Correlation of vibration, wear debris analysis and oil analysis in rolling element bearing condition monitoring.* Maint Manage Int, 1985, 5(2): 105-15.
- [36]. **Gadd, P and Mitchell, P.J.** *Condition monitoring of helicopter gearboxes using automatic vibration analysis techniques.* AGARD CP 369, 1984, 29: 1-10.

- [37]. **Baydar, N and Ball, A.** *Detection of gear failures via vibration and acoustic signals using wavelet transform.* Mech Syst Signal Process, 2003, 17(4): 787-04.
- [38]. **Loutas, T.H., Sotiriades, G., Kalaitzoglou, I and Kostopoulos, V.** *Condition monitoring of a single-stage gearbox with artificially induced gear cracks utilising on-line vibration and acoustic emission measurements.* Appl Acoust, 2009, 70: 1148-59.
- [39]. **Marques de Sa, J.P.** *Applied Statistics using SPSS, STATISTICAL, and MATLAB.* Springer, 2003.
- [40]. **Stanley, W.D., Dougherty, G.R and Dougherty, R.** *Digital signal processing.* Prentice-Hall, 1984.
- [41]. **Qian, S and Chen, D.** *Joint time frequency analysis: methods and applications.* Prentice Hall Inc, 1996.
- [42]. **Tavathia, S., Rangayyan, R.M., Bell, G.D., Ladly, K.O and Zhang, Y.T.** *Analysis of knee vibration signals using linear prediction.* IEEE Trans BioMed Eng, 1992, 39(9): 959-69.
- [43]. **Zhang, Y and Rangayyan, R.M.** *Adaptive cancellation of muscle contraction interference in vibroarthrographic signals.* IEEE Trans BioMed Eng, 1994, 43(1): 15-23.
- [44]. **Shen, Y., Rangayyan, R.M., Bell, G.D., Frank, C.B and Zhang, Y.** *Localisation of knee joint cartilage pathology by multichannel vibroarthrography.* Med Eng Phys, 1995, 17(8): 583-94.
- [45]. **Moussavi, Z.M.K., Rangayyan, R.M., Frank, C.B., Ladly, K.O and Zhang, Y.** *Screening of vibroarthrographic signals via adaptive segmentation and linear prediation modelling.* IEEE Trans BioMed Eng, 1996, 43(1): 15-22.
- [46]. **Rangayyan, R.M., Krishnan, S., Bell, G.D., Frank, C.B and Ladly, K.O.** *Parametric representation and screening of knee joint vibroarthrographic signals.* IEEE Trans BioMed Eng, 1997, 44(11): 1068-74.
- [47]. **Krishnan, S., Rangayyan, R.M., Bell, G.D and Frank, G.B.** *Adaptive time-frequency analysis of knee joint vibroarthrographic signals for non-invasive screening of articular cartilage pathology.* IEEE Trans Biomed Eng, 2000, 47(6): 773-84.
- [48]. **Umopathy, K and Krishnan, S.** *Modified local discriminant bases algorithm and its application in analysis of human knee joint vibration signals.* IEEE Trans BioMed Eng, 2006, 53(3): 517-23.

- [49]. **Mu, T., Nandi, A.K and Rangayyan, R.M.** *Screening of knee-joint vibroarthrographic signals using the strict 2-surface proximal classifier and genetic algorithm.* Comput Biol Med, 2008, 38: 1103-11.
- [50]. **Rangayyan, R.M and Wu, Y.** *Analysis of vibroarthrographic signals with features related to signal variability and radial-basis functions.* Ann BioMed Eng, 2009, 37(1): 156-63.
- [51]. **Rangayyan, R.M and Wu, Y.** *Screening of knee-joint vibroarthrographic signals using probability density functions estimated with Parzen window.* Biomed Signal Process Contr, 2010, 5(1): 23-8.
- [52]. **Makhoul, J.** *Linear prediction: A tutorial review.* Proc IEEE , 1975, 63(4): 561-80.
- [53]. **Sharma, S.** *Applied multivariate techniques.* John Wiley and Sons, Inc, 1996.
- [54]. **Burus, C.S., Gopinath, R.A and Guo, H.** *Introduction to wavelets and wavelet transforms: A primer.* Prentice Hall Inc, 1998.
- [55]. **Satio, N and Coifmann, R.R.** *Local discriminant bases and their applications.* J Math Imaging Vis, 1995, 39(9): 337-58.
- [56]. **Mu, T., Nandi, A.K and Rangayyan, R.M.** *Strict 2-surface proximal classification of knee-joint vibroarthrographic signals.* Proc Ann Int Conf IEEE Eng Medicine Biol Soc, 2007, 4911-4.
- [57]. **Edward, G.D.** *Genetic algorithms in search, optimisation, and machine learning.* Addison-Wiley, 1989.
- [58]. **Bose, N.K.** *Neural network fundamental with graphs, algorithms and applications.* McGray, 1996.
- [59]. **Willison, R.G.** *Analysis of electrical activity in healthy and dystrophic muscle in man.* J Neurol Neurosur Psychiatry, 1964, 27: 386-94.
- [60]. **Choudhury, A and Tandon, N.** *Application of acoustic emission technique for the detection of defects in rolling element bearings.* Trib Int, 2000, 33: 39-45.
- [61]. **Al-Ghamd, A.M and Mba, D.** *A comparative experimental study on the use of acoustic emission and vibration analysis for bearing defect identification and estimation of defect size.* Mech Syst Signal Process, 2006, 20: 1537-71.
- [62]. **Eftekharnjad, B., Carrasco, M.R., Charnley, B and Mba, D.** *The application of spectral kurtosis on acoustic emission and vibrations from a defective bearing.* Mech Syst Signal Process, 2011, 25(1): 266-84.

- [63]. **Finlayson, R.D., Friesel, M., Carlos, M., Cole, P and Lenain, J.C.** *Health monitoring of aerospace structures with acoustic emission and acousto-ultrasonics*. Insight, 2001, 43(3): 155-8.
- [64]. **Chiou, R.Y and Liang, S.Y.** *Analysis of acoustic emission in chatter vibration with tool wear effect in turning*. Int J Mach Tool Manu, 2000, 40: 927-41.
- [65]. **Hase, A, Wada, M and Mishina, H.** *The relationship between acoustic emissions and wear particles for repeated dry rubbing*. Wear, 2008, 265: 831-9.
- [66]. **Watanabe, T., Hosomi, M., Yuno, K and Hashimoto, C.** *Quality evaluation of shotcrete by acoustic emission*. Constr Build Mater, 2010, 24: 2358-62.
- [67]. **Chang, H., Han, E.H., Wang, J.Q and Ke, W.** *Acoustic emission study of fatigue crack closure of physical short and long cracks for aluminum alloy LY12CZ*. Int J Fatigue, 2009, 31:403-7.
- [68]. **Oskouei, A.R., Zucchelli, A., Ahmadi, M and Minak, G.** *An integrated approach based on acoustic emission and mechanical information to evaluate the delamination fracture toughness at mode I in composite laminate*. Mater Design, 2011, 32: 1444-55.
- [69]. *PCI-2 based AE system user's manual*. Physical Acoustic Corporation, 2003.
- [70]. **Fink, M.** *Time-reversed acoustics*. Sci Am, 1999, 281:67-73.
- [71]. **Shrivastava, S and Prakash, R.** *Assessment of bone condition by acoustic emission technique: A review*. J BiMed Sci Eng, 2009, 2: 144-54.
- [72]. **Zioupos, P., Currey, J.D and Sedman, A.J.** *An examination of the micromechanics of failure of bone and antler by acoustic emission tests and laser scanning confocal microscopy*. Med Eng Phy, 1994, 16: 203-12.
- [73]. **Schwalbe, H.J., Bamfaste, G and Franke, R.P.** *Non-destructive and non-invasive observation of friction and wear of human joints and of fracture initiation by acoustic emission*. Proc Inst Mech Eng, 1999, 213: 41-8.
- [74]. **Davies, J.P., Tse, M-K and Harris, H.H.** *Monitoring the integrity of the cemental interface of total joint components in vitro using acoustic emission ultrasound*. J Arthroplasty, 1996, 11(5): 594-601.
- [75]. **Roques, A., Browne, M., Thompson, J., Rowland, C and Taylor, A.** *Investigation of fatigue crack growth in acrylic bone cement using the acoustic emission technique*. Biomaterials, 2004, 25: 769-78.

- [76]. **Azangwe, G., Fraser, K., Mathias, K.J and Siddiqui, A.M.** *In vitro monitoring of rabbit anterior cruciate ligament damage by acoustic emission.* Med Eng Phys, 2000, 22: 279-83.
- [77]. **Trebacz, H and Zdunek, A.** *Three-point bending and acoustic emission study of adult rat femora after immobilisation and free remobilisation.* J BioMed, 2006, 39: 237-45.
- [78]. **Wierzcholski, K.C.H.** *Friction forces for human hip joint lubrication at a naturally permeable cartilage.* s.l. : Int J Appl Mech Eng, 2006; 11(3):, Int J App Mech & Eng, Vols. 11(3): 525-27, pp. 515-27.
- [79]. **Ritter, M.A and Stringer, E.A.** *Predictive range of motion after total knee replacement.* Clin Orthop Relat Res, 1979, 143: 115-9.
- [80]. **Lam, L.O., Swift, S and ShakeSpeare, D.** *Fixed flexion deformity and flexion after knee arthroplasty. What happens in the first 12 months after surgery and can a poor outcome be predicted.* Knee, 2003, 10: 181-5.
- [81]. **Ritter, M.A., Lutgring, J.D and Davis, K.E.** *The role of flexion contracture on outcomes in primary total knee arthroplasty.* J Arthroplasty, 2007, 22(8): 1092-6.
- [82]. **Sharma, L., Lou, C., Felson, D.T., Dunlop, D.D., Kirwan-Mellis, G., Hayes, K.W., Weinrach, D and Buchanan, T.S.** *Laxity in healthy and osteoarthritic knees.* Arthritis Rheum, 1999, 42: 861-70.
- [83]. **Takuhara, Y., Kadoya, Y., Nakagawa, S., Kobayashi, A and Takaoka, K.** *The flexion gap in normal knees. An MRI study.* J Bone Joint Surg Br, 2004, 86:1133-6.
- [84]. **Okazaki, K., Miura, H., Matsuda, S., Takeuchi, N., Mawatari, T., Hashizume, M and Iwamoto, Y.** *Asymmetry of mediolateral laxity of the normal knee.* J Orthop Sci, 2006, 11: 264-6.
- [85]. **Heesterbeek, P.J.C., Verdonschot, N and Wymenga, A.B.** *In vivo knee laxity in flexion and extension: A radio graphic study in 30 older healthy subjects.* Knee, 2008, 15: 45-9.
- [86]. **Stahelin, T., Kessler, O., Pfirrmann, C., Jacob, H.A and Romero, J.** *Fluoroscopically assisted stress radiography for varus-valgus stability assessment in flexion after total knee arthroplasty.* J Arthroplasty, 2003, 18: 513-5.
- [87]. **Jassen, W.G.M., Bussmann, H.B.J and Stam, H.J.** *Determinants of the sit-to-stand movement: a review.* Phys Ther, 2002, 82(9): 866-79.
- [88]. **Kerr, K., White, J., Barr, D and Mollan, R.A.B.** *Analysis of the sit-stand-sit movement cycle in normal subjects.* Clin Biomech, 1997, 12(4): 236-45.

- [89]. **Cavanaugh, J.T., Shinberg, M., Ray, L., Shipp, K.M., Kuchibhatla, M and Schenkman, M.** *Kinematic characterisation of standing reach: comparison of younger vs. older subjects.* Clin Biomech, 1999, 14(4): 271-9.
- [90]. **Papa, E and Cappozzo, A.** *Sit-to-stand motor strategies investigated in able-bodied young and elderly subjects* J Biomech, 2000, 33: 1113-22.
- [91]. **Scheulz, A.B., Alexander, N.B and Ashton-Miller, J.A.** *Biomechanical analysis of rising from a chair.* J Biomech, 1992, 25: 1383-91.
- [92]. **Park, E.S., Park, C., Lee, H.J., Kim, D.Y., Lee, D.S and Cho, S.R.** *The characteristics of sit-to-stand transfer in young children with spastic cerebral palsy based on kinematic and kinetic data.* Gait Posture, 2003, 17: 43-9.
- [93]. **Galli, M., Cimolin, V., Crivellini, M and Campanini, I.** *Quantitative analysis of sit to stand movement: Experimental set-up definition and application to healthy and hemiplegic adults.* Gait Posture, 2008, 28: 80-85.
- [94]. **Nielsen, A.** *Acoustic emission source based on pencil lead breaking.* The Danish Welding institute publication, 1980.
- [95]. *Laboratory amplifier operating manual.* Biometrics Ltd.
- [96]. **Lavagnini, I and Magno, F.** *A statistical overview on univariate calibrate, inverse regression, and detection limits: application to gas chromatography/mass spectrometry technique.* Mas spectrometry reviews, 2007, 26(1):1-18.
- [97]. **Burrus, C.S.** *DFT/FFT and convolution algorithms: theory and implementation.* Wiley, 1985.
- [98]. **Roos, E.M and Soren, T-L.** *Knee injury and osteoarthritis outcome score (KOOS) - validation and comparison to the WOMAC in total knee replacement.* Health Qual Life Outcomes, 2003, 1(17): 1-10.
- [99]. **Connor, J.O.** *User's Manual for the SF-36v2™ Health Survey – Second Edition.* Qual Metric Health Outcomes Solution, 2007.
- [100]. **Larsen, R.J. and Marx, M.L.** *An introduction to mathematical statistics and its application.* Prentice Hall, 2005.
- [101]. **Turkey, J.W.** *Exploratory data analysis.* Addison-Wesley, 1977.
- [102]. **Mirkov, D.M., Milanovic, S., Ilic, D.B and Jaric, S.** *Symmetry of discrete and oscillatory elbow movements: does it depend on torque that the agonist and antagonist muscle can exert.* Motor Control, 2002, 6: 271-81.

- [103]. **Crauel, H., Gundlach, M.** *Stochastic dynamics*. Springer, 1999.
- [104]. **Evans, M., Hastings, N and Pekcock, B.** *Statistical distributions*. John Wiley & sons, Inc, 1993.
- [105]. **Mardia, K.V., Kent, J.T and Bibby, J.M.** *Multivariate analysis*. Academic press, 1995.
- [106]. **Duda, R and Hart, P.E.** *Pattern classification and scene analysis*. John Wiley & Sons Inc, 1973.
- [107]. **Aiken, L.S and West, S.G.** *Multiple regression: testing and interpreting interactions*. Sage Publication, 1991.
- [108]. **Utts and Jessica, M.** *Seeing Through Statistics*. Thomson Brooks/Cole, 2005.
- [109]. **Jolliffe, I.T.** *Principal component analysis*. Springer-Verlag, 1986.
- [110]. **Ritter, H and Kohonen, T.** *Self-organising semantic maps*. *Bilo Cybern*, 1989, 61: 241-54.
- [111]. **Hyvarinen, A., Karhunen, J and Oja, E.** *Independent component analysis*. Wiley, 2001.
- [112]. **Wang, Y., Ding, C., Wluka, A.E., Davis, S., Ebeling, P.R., Jones, G and Cicuttini, F.M.** *Factors affecting progression of knee cartilage defects in normal subjects over 2 years*. *Rheumatology*, 2006, 45: 79-84.
- [113]. [Online] [Cited: 2/1/2011.]
http://www.medicinenet.com/rheumatoid_arthritis/article.htm.

APPENDIX A SPECIFICATIONS OF ACOUSTIC EMISSION SYSTEM

This appendix lists the specifications of the acoustic emission system extracted from the user operating manuals [69].

A.1 SPECIFICATION OF S9204 SENSOR

Dimensionality (diameter × height): 23mm×15mm.

Weight: 17 g.

Peak sensitivity (Ref V/(m/s)): 68.

Operating frequency range: 50-200 kHz.

Resonant frequency: 75 kHz.

Directionality: ±1.5 dB.

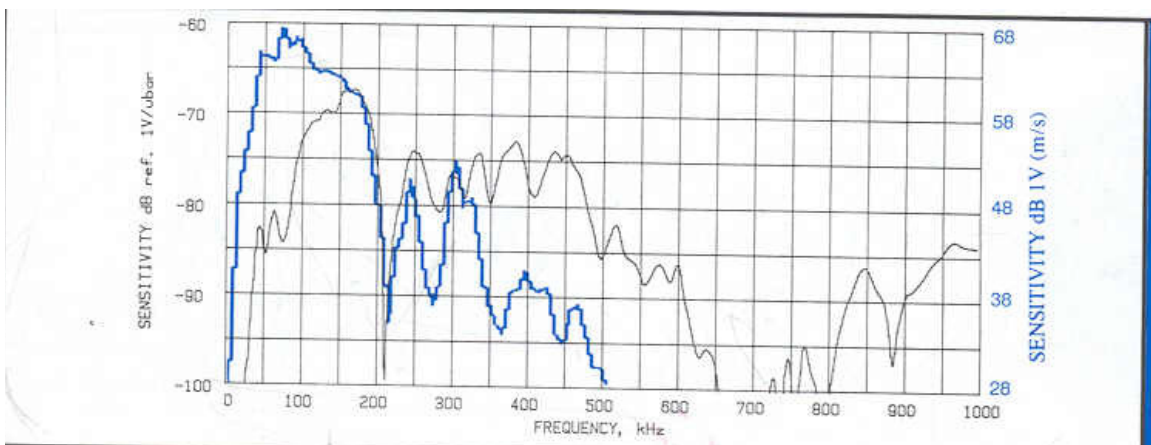


Figure A.1-1: Reference frequency response of S9204 sensor

A.2 SPECIFICATION OF 2/4/6 PREAMPLIFIER

Gain selectable: 20/40/60 dB \pm 0.5% dB.

Input impedance: 10 k Ω /15 pF.

Power required: 18-28 Vdc.

Operating current: 30 mA (With auto sensor test (AST) installed [64]).

28 mA (Without AST installed).

Dynamic range: 15 dB (Utilizing an R15 sensor).

80 dB (50 Ω input).

A.3 SPECIFICATION OF PCI-2 BOARD

Size (LxHxT inch): 13.4x4.8x0.7.

Weight (lbs): 1.1.

Power consumption: 12 Watts.

DC power: +12 volts, 0.6 amps.

-12 volts, 0.05 amps.

+ 5.0 volts, 0.8 amps.

AE inputs: 2 channels.

Input impedance: 50 Ω or 1000 Ω , switch selectable.

Preamp power: 0 or 28 volts, 100 mA current limited.

Sensor testing: AST.

Frequency response: 3kHz – 3MHz (-3dB).

AE signal gain: 0/6 dB, computer selectable.

Filters: 4 high pass 4th order Butterworth filter (3 kHz, 100 kHz, 200 kHz), and 6 low pass 6th order Butterworth filter (100 kHz, 200 kHz, 400 kHz, 1000 kHz, 2000 kHz, 3000 kHz).

Noise:

- 3kHz-3MHz (filters).
- 4 dB (ASL without input).
- 17 dB w/o preamp or sensor (Minimum threshold).

Maximum signal amplitude: 100 dB AE

99 dB ASL.

ADC type: 18 bit 40 MSPS per channel maximum.

Dynamic range: >85 dB.

Sample rate: 100 kS/s, 200 kS/s, 500 kS/s, 1M/sample/sec, 2MSPS, 5MSPS, 10 MSPS, 20 MSPS, 40 MSPS.

Digital I/O: 8 digital inputs/outputs (0-3.3 volt, 5v tolerant, TTL level compatible).

APPENDIX B AE SENSOR TESTING

Prior to data acquisition, the piezoelectric transducers were tested by using the pencil lead breaking method. Pencil lead breaking is a standard methodology that can be used to simulate the source of AE signals [94]. The testing setup of the method is shown in Figure B-1. As the sensors were calibrated by the manufacturer, the purpose of pencil lead break testing is to test whether or not the two sensors used have the similar properties. As breaking the pencil lead on the skin will create pain to the participant, the two sensors were fixed on a flat wooden table by using the medical tapes in order to ensure the AE signal created by the pencil lead break is based on similar sensor attachment method, and the conductive gel was applied to smooth the contacting surfaces between the sensors and table. A 0.5 mm mechanical pencil lead was broken amid the transducers with the same distance (7.5 cm).

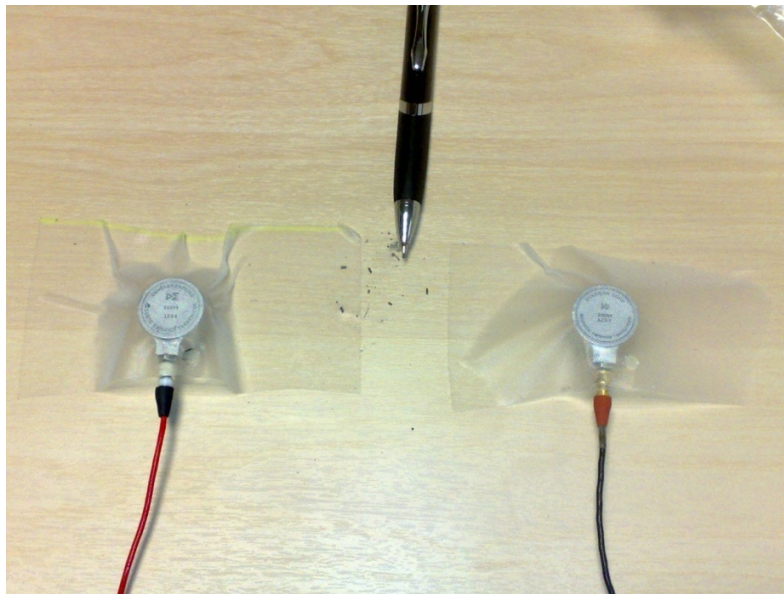


Figure B-1 AE sensors testing based on pencil lead breaking

Figures B-2 and B-3 illustrate the results of the same AE signal acquired by the two sensors in time and frequency domain. The signal was simulated by using the testing method shown in Figure B-1. From the time domain waveforms, it is clear that two similar signals were

acquired by the two sensors. From the frequency domain representation, although the values of peak magnitude were slightly different among the two channels, the overall frequency response and the frequency of peak magnitude occurred are similar. This means that the two transducers have the similar properties in both time and frequency domains.

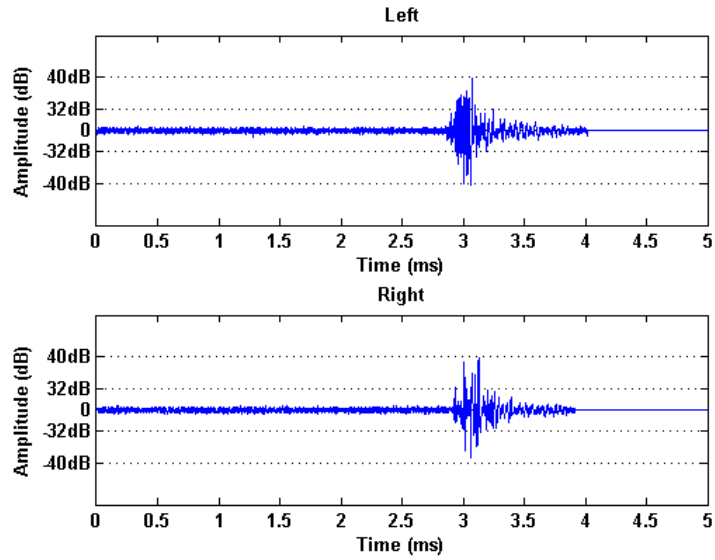


Figure B-2 Sensor testing response – time domain

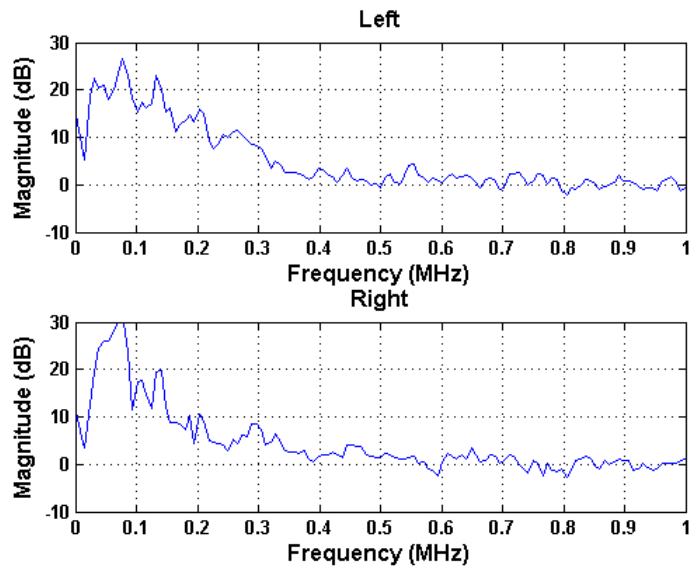


Figure B-3 Sensor testing response – frequency domain

APPENDIX C SPECIFICATIONS OF GONIOMETER SYSTEM

C.1 SPECIFICATION OF SG150 ELECTRO-GONIOMETER

Number of channels: 2.

Weight: 19 g.

Minimum permissible bend radius: 18 mm.

Measurement output: flexion/extension.

Measure range: $\pm 150^\circ$.

C.2 SPECIFICATION OF K800 DATA ACQUISITION UNIT

Analogue channels: 8.

Digital channels: 5.

ADC: 13 bit.

Digital circuitry sampling rate: 5 kHz.

Output: Analogue.

Power supply per channel: + 5.0 Vdc.

Current supply per channel: < 25 mA.

Input voltage: ± 12 mV.

Analogue channel input impedance: $1M\Omega$.

Accuracy: $\pm 3^\circ$ measured over $\pm 90^\circ$.

Bandwidth: 5 KHz.

APPENDIX D GONIOMETER CALIBRATION

The electro-goniometers were calibrated using the linear regression method [96]. During the calibration, the inputs for both channels of the goniometer is a vector of the angles in degrees between -130° and 130° with 10° intervals, and the goniometer output voltages are represented by unit of volts. From the calibration result shown in Figure D-1, it can be seen that similar goniometer responses are observed from the two channels, and the characteristics of the left and right channels can be approached by using equations D-1 and D-2, respectively:

$$U_L = 0.028\theta_L + 0.42 \quad (D-1)$$

$$U_R = 0.026\theta_R + 0.75 \quad (D-2)$$

where, U_L and U_R are referred to as the output voltage of goniometer for the left and right channel and θ_L and θ_R are the input angles. These two equations were used to obtain the actual angles during data acquisition. Based on the equations D-1 and D-2, the deviations of

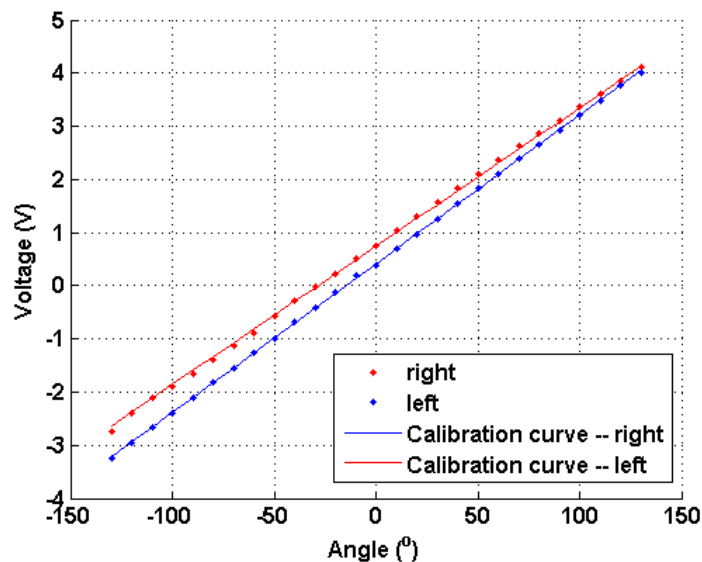


Figure D-1 Calibration curve of electro-goniometers

the calibration result can be measured, with the maximum difference = $\pm 0.9^\circ$ for channel left and = $\pm 2.1^\circ$ for channel right. As the angle measurement methods applied in this project are based on the movement phase, these errors could be considered as acceptable.

APPENDIX E GENERAL HEALTH AND WELL-BEING QUESTIONNAIRE

Personal information

Forename:

Middle initial:

Surname:

Date of birth:

Gender:

Bodymass:

Height:

BMI:

Health information

1. Do you have any health conditions? If **yes**, please give details:

2. Do you experience any of following in your knees

(a). Difficulty moving. **(b)**. Stiffness. **(c)**. Locking. **(d)**. Swelling. **(e)**. Pain. **(f)**. Tenderness. **(g)**. Grating. **(h)**. Clicking.

If **others**, please give detail:

3. For how long have you been experienced these?

4. How long do these usually last?

(a). Constant. **(b).** Seconds. **(c).** Minutes. **(d).** Hours. **(e).** Day. **(f).** Days. **(g).** Weeks. **(h).** Months. **(i).** Even longer.

5. How would you describe the level of these feeling?

(a).Slight annoyance. **(b).** Mild. **(c).** Moderate. **(d).** Severe.

6. Does anything make these worse? If **yes**, please give details:

7. Are you currently using any other methods to reduce these?

If **yes**, please give details:

8. Additional participant information.

**APPENDIX F QUANTITY OF AE EVENTS
FROM EACH KNEE IN EACH PHASE AND
EACH MOVEMENT CYCLE**

Subject ID/phase	AA (movement 1-10)	AD (movement 1-10)	DA (movement 1-10)	DD (movement 1-10)
H1-1	9 2 0 3 1	6 15 16 6 3	3 2 8 3 3	2 0 5 2 9
	6 2 2 4 12	0 5 1 3 3	3 5 11 8 8	9 9 10 16 9
H1-2	2 9 1 2 1	6 2 1 4 3	4 2 1 1 2	5 4 3 3 3
	4 1 4 6 2	3 0 5 1 6	4 0 3 2 8	3 1 1 2 4
H1-3	12 2 1 2 3	6 1 2 3 1	1 4 2 0 0	5 8 3 3 4
	2 3 2 3 2	4 3 4 4 3	1 2 1 4 1	3 3 1 2 2
H1-4	1 1 2 2 0	2 4 0 2 5	1 1 2 0 5	1 1 1 0 5
	6 1 2 1 1	2 2 2 2 7	2 2 4 1 1	2 1 0 0 3
H1-5	3 0 1 0 0	0 0 0 0 0	0 0 1 0 3	3 3 4 7 2
	0 0 0 2 2	0 0 0 1 0	0 3 1 1 2	2 8 1 8 17
H1-6	7 3 5 6 4	1 0 0 3 2 2	1 2 1 0 4 5	4 5 9 9 4
	2 2 4 4 6	2 6 4 7 1 2	6 3 6 4 7	8 4 2 3 4
H1-7	3 1 1 0 0	1 2 3 3 1	7 2 4 8 4	6 5 8 7 7
	1 0 0 0 1	0 0 4 3 2	5 5 7 3 3	6 6 2 7 7
H1-8	4 6 3 2 3	3 5 1 2 3	5 3 5 4 5	5 5 7 5 2
	6 5 2 5 4	6 0 4 2 2	2 2 4 3 8	2 2 7 4 5
H1-9	8 5 7 8 4	0 3 4 4 4	4 3 5 0 0	2 4 7 7 9
	7 4 1 3 2	0 2 0 1 0	0 1 1 0 0	4 7 3 4 7
H1-10	1 1 1 1 0	2 0 2 2 2	4 4 9 5 6	1 0 3 3 0
	1 2 1 2 1	7 3 6 4 2	10 10 12 11 14	3 7 5 4 4

Table F-1 Number of AE events for 10 individual movements in group H1

Subject ID/Phase	AA (movement 1-10)	AD (movement 1-10)	DA (movement 1-10)	DD (movement 1-10)
H2-1	10 10 5 4 1 12 6 2 3 1	4 4 8 5 6 6 9 5 4 5	4 2 3 4 2 7 7 13 15 9	8 7 11 13 20 12 9 7 10 15
H2-2	5 3 4 9 4 11 4 3 3 3	25 11 14 16 31 23 12 16 16 13	19 3 18 47 35 20 13 17 33 30	24 37 22 35 19 12 29 19 22 29
H2-3	8 5 3 2 2 8 1 0 0 2	4 0 1 0 0 0 0 0 4 0	13 12 11 8 9 12 5 7 3 11	16 17 18 7 9 23 19 35 20 23
H2-4	24 10 6 9 10 18 11 17 16 12	5 8 4 5 7 6 6 4 4 6	2 2 0 0 4 6 9 3 3 4	29 24 25 18 26 32 43 19 29 30
H2-5	11 4 3 3 2 17 4 0 2 0	0 1 0 2 0 1 1 2 0 0	0 0 1 1 1 2 0 2 3 0	25 13 13 15 11 16 13 17 10 11
H2-6	17 8 6 9 8 17 14 18 17 17	5 9 8 9 4 2 6 4 1 1	6 8 8 5 6 4 7 5 7 5	16 33 15 19 14 7 15 9 17 17
H2-7	13 5 7 8 6 7 9 5 7 10	9 16 14 16 6 22 16 15 15 19	15 7 15 10 12 9 14 13 14 10	12 20 14 11 17 18 11 12 10 13
H2-8	17 15 15 11 12 20 15 10 14 16	4 5 7 4 3 15 9 8 3 6	6 7 9 7 7 12 14 8 10 10	27 22 20 20 18 26 20 16 20 19
H2-9	23 10 8 10 10 18 9 13 2 7	6 5 2 1 0 4 6 4 9 4	4 4 9 11 4 2 7 8 16 9	37 19 24 3 5 23 17 31 11 11
H2-10	18 6 7 6 7 12 5 9 5 4	0 2 1 0 1 2 3 3 1 2	6 11 6 5 8 9 10 6 11 10	5 1 6 7 6 10 8 8 14 12
H2-11	1 2 1 4 4 1 5 1 1 4	15 16 7 6 4 8 18 16 13 17	13 9 6 9 9 16 16 18 13 12	19 19 20 17 16 22 15 20 14 16

Table F-2 Number of AE events for 10 individual movements in group H2

Subject ID/Phase	AA (movement 1-10)	AD (movement 1-10)	DA (movement 1-10)	DD (movement 1-10)
H3-1	20 11 10 17 19 30 16 11 16 11	4 11 5 2 2 8 2 1 2 9	9 15 26 35 27 15 22 30 15 28	24 40 25 28 20 20 32 32 48 28
H3-2	27 17 14 17 7 28 23 15 11 32	1 3 9 16 3 8 10 5 8 8	44 33 25 36 26 32 43 35 27 32	37 35 35 20 32 29 37 32 29 25
H3-3	44 41 34 41 43 40 31 32 27 40	18 9 11 13 16 10 8 10 5 5	7 4 5 4 6 8 6 12 1 8	24 30 28 20 35 45 42 28 31 30
H3-4	19 11 16 16 14 34 16 16 11 23	13 13 9 15 19 14 38 24 22 23	2 22 5 34 20 12 4 19 15 19	51 28 50 30 35 41 54 38 70 36
H3-5	32 14 14 17 12 17 22 20 28 32	14 39 12 21 9 23 31 29 11 16	10 10 15 12 12 10 27 22 20 17	34 27 31 33 41 38 40 39 39 34
H3-6	38 13 11 15 15 50 21 75 28 51	8 7 9 7 5 13 9 6 12 8	8 8 5 2 2 4 6 1 4 8	41 63 44 60 49 49 52 69 52 53
H3-7	12 5 11 17 20 26 27 37 43 36	12 9 10 14 9 11 15 14 22 13	30 23 15 30 19 26 26 26 25 31	39 28 39 20 23 25 18 19 22 23
H3-8	51 45 32 35 40 59 51 43 41 44	7 15 9 7 14 10 15 16 20 13	5 5 11 5 7 10 5 5 5 14	54 56 42 48 64 66 59 62 57 60
H3-9	49 46 42 39 29 35 31 29 28 26	25 40 43 34 32 34 44 35 30 31	24 42 34 20 39 36 22 19 32 17	34 26 18 23 22 21 17 20 16 27
H3-10	63 41 57 56 57 61 48 51 41 40	31 18 29 18 17 23 11 43 14 15	5 9 5 11 5 4 10 8 9 4	20 25 23 15 16 33 23 21 22 25
H3-11	11 4 18 9 6 16 14 15 11 7	17 17 13 15 11 12 6 10 10 11	7 10 11 10 7 12 8 2 6 6	32 18 23 31 51 41 44 31 46 44
H3-12	38 22 19 14 15 32 20 18 16 16	47 21 15 28 21 41 20 28 22 25	4 23 21 22 33 36 20 25 32 18	30 20 16 23 10 16 14 25 19 24
H3-13	15 74 9 15 17 14 23 13 18 14	17 10 16 17 17 35 15 6 13 16	50 48 16 54 27 44 39 29 35 34	38 30 39 43 51 40 41 43 43 19

Table F-3 Number of AE events for 10 individual movements in group H3

Subject ID/Phase	AA (movement 1-10)	AD (movement 1-10)	DA (movement 1-10)	DD (movement 1-10)
OA1-1	42 44 47 37 45 69 36 44 44 36	5 11 6 2 8 10 6 4 4 3	4 4 5 4 6 9 5 6 5 10	68 71 57 62 54 57 89 52 57 68
OA1-2	27 21 23 39 21 44 35 22 32 20	48 44 74 65 59 59 79 78 76 73	21 51 27 26 44 50 53 46 55 39	64 54 75 66 63 72 79 85 87 104
OA1-3	35 24 38 31 33 38 16 30 30 32	7 66 86 89 88 86 89 79 111 80	51 32 62 60 102 42 44 59 54 67	24 28 47 44 32 103 73 115 32 46
OA1-4	63 42 49 53 53 64 44 43 56 46	38 39 43 32 51 61 43 51 58 49	36 26 22 25 23 37 30 43 41 27	39 37 70 64 37 63 51 48 53 48
OA1-5	72 83 83 62 58 85 70 79 86 72	18 23 36 21 17 21 19 12 12 7	9 7 5 6 2 5 11 10 11 15	92 110 101 115 118 128 117 118 119 135
OA1-6	123 120 126 140 136 128 103 109 99 146	11 17 19 32 12 43 12 16 13 33	6 16 19 15 17 31 35 24 19 13	90 83 61 62 67 82 110 76 67 63
OA1-7	60 47 32 32 30 54 41 46 45 34	21 30 31 12 19 14 48 70 29 17	22 15 15 9 3 15 16 21 23 17	75 76 74 68 64 73 88 80 73 74

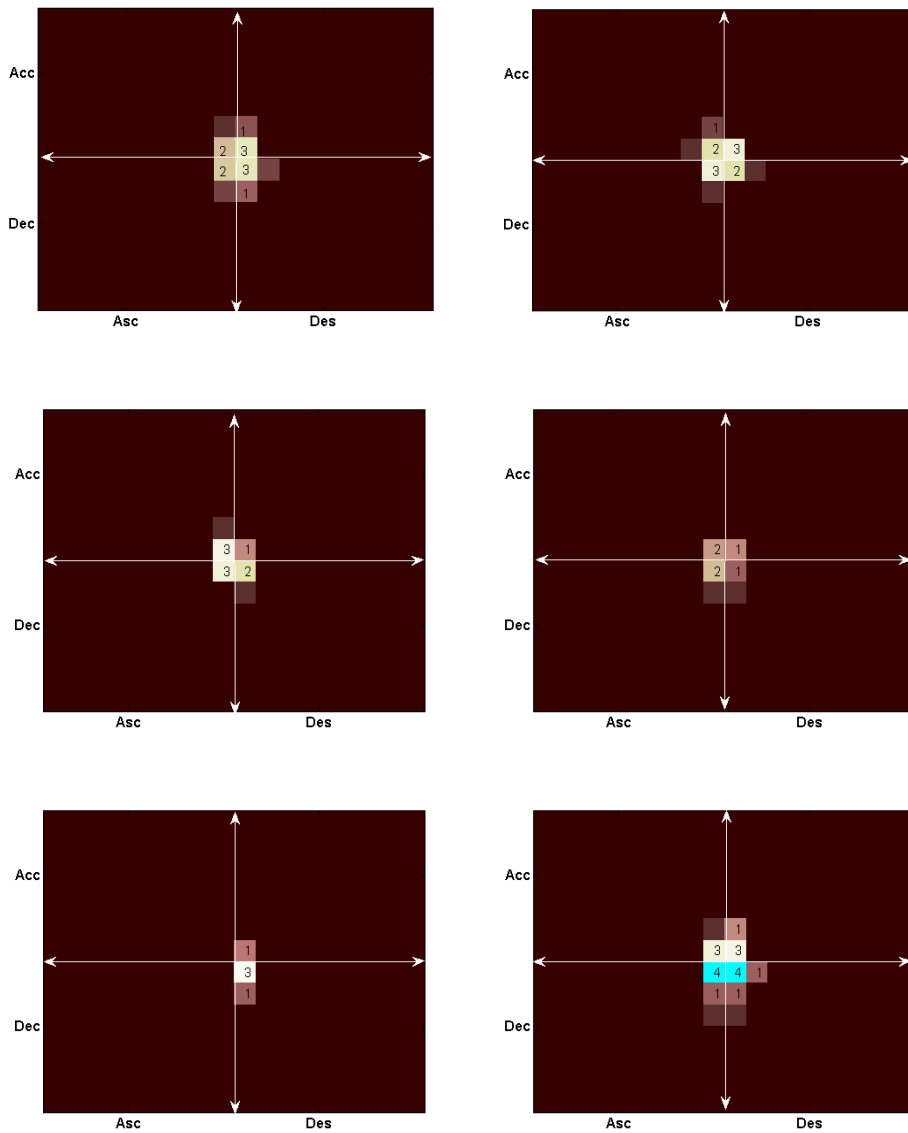
Table F-4 Number of AE events for 10 individual movements in group OA1

Subject ID/Phase	AA (movement 1-10)	AD (movement 1-10)	DA (movement 1-10)	DD (movement 1-10)
OA2-1	41 38 77 105 83 64 39 41 61 45	67 62 61 95 72 70 86 92 91 84	82 82 60 86 66 65 75 88 86 91	81 112 98 111 67 90 94 60 76 64
OA2-2	111 92 87 109 86 129 100 109 99 88	42 26 49 51 37 45 59 41 47 35	52 46 31 35 44 38 40 33 26 22	124 130 136 136 143 156 171 157 137 105
OA2-3	113 143 117 107 98 155 117 116 120 109	93 57 66 63 55 50 42 62 65 51	104 143 118 102 126 115 113 43 61 127	107 70 66 75 43 86 73 143 115 63
OA2-4	118 94 93 94 71 117 92 92 104 95	42 53 60 59 49 80 72 56 62 57	35 45 35 30 29 30 32 31 21 33	88 114 136 122 118 102 106 118 145 146
OA2-5	74 47 48 39 44 78 46 29 41 32	43 43 51 46 26 39 49 48 53 45	18 18 19 17 9 15 32 13 7 25	81 124 140 152 114 85 88 116 114 126
OA2-6	129 114 117 93 85 115 99 86 104 66	134 125 107 140 135 123 148 116 150 156	91 85 103 152 80 87 107 95 70 79	162 140 148 113 138 141 129 131 143 133
OA2-7	113 95 100 98 81 97 101 95 100 88	108 129 115 151 122 111 107 105 121 149	108 70 98 106 76 91 102 73 55 70	181 182 129 121 111 110 103 113 146 144
OA2-8	115 121 103 102 92 124 101 60 67 83	110 91 108 104 91 127 131 175 119 135	38 56 50 50 60 53 78 43 60 76	170 124 180 154 179 150 138 187 145 130
OA2-9	115 106 104 107 93 119 110 96 98 62	98 59 45 46 66 87 85 117 77 104	63 62 31 43 76 71 63 43 61 83	158 93 116 129 144 125 99 144 110 107
OA2-10	76 61 50 59 69 101 78 77 47 48	43 35 43 37 47 58 42 64 47 44	64 43 31 31 64 81 55 43 5 66	67 75 65 69 54 52 68 85 103 43
OA2-11	94 60 65 44 39 53 50 43 58 59	100 70 68 95 90 94 102 89 117 81	38 22 22 15 43 25 19 23 16 47	86 62 55 60 36 58 64 59 65 32
OA2-12	67 50 50 45 41 76 55 47 71 44	57 41 79 51 83 99 13 73 83 101	22 45 34 33 58 24 38 52 48 87	104 122 102 101 85 130 113 107 111 75

Table F-5 Number of AE events for 10 individual movements in group OA2

APPENDIX G AE FEATURE PROFILES FOR ALL KNEES STUDIED

Figure G-1 AE feature profiles of group H1 knees



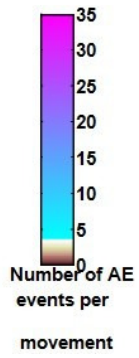
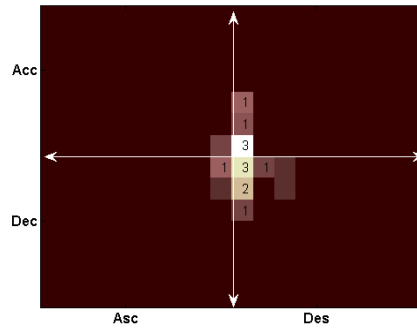
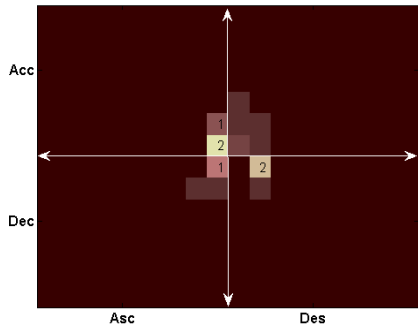
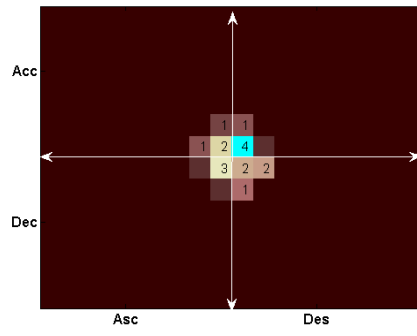
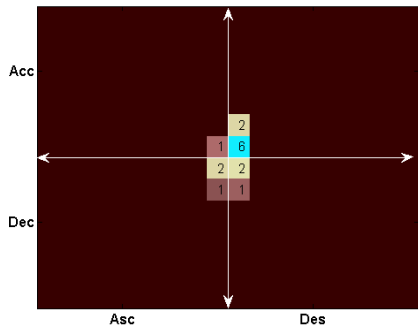
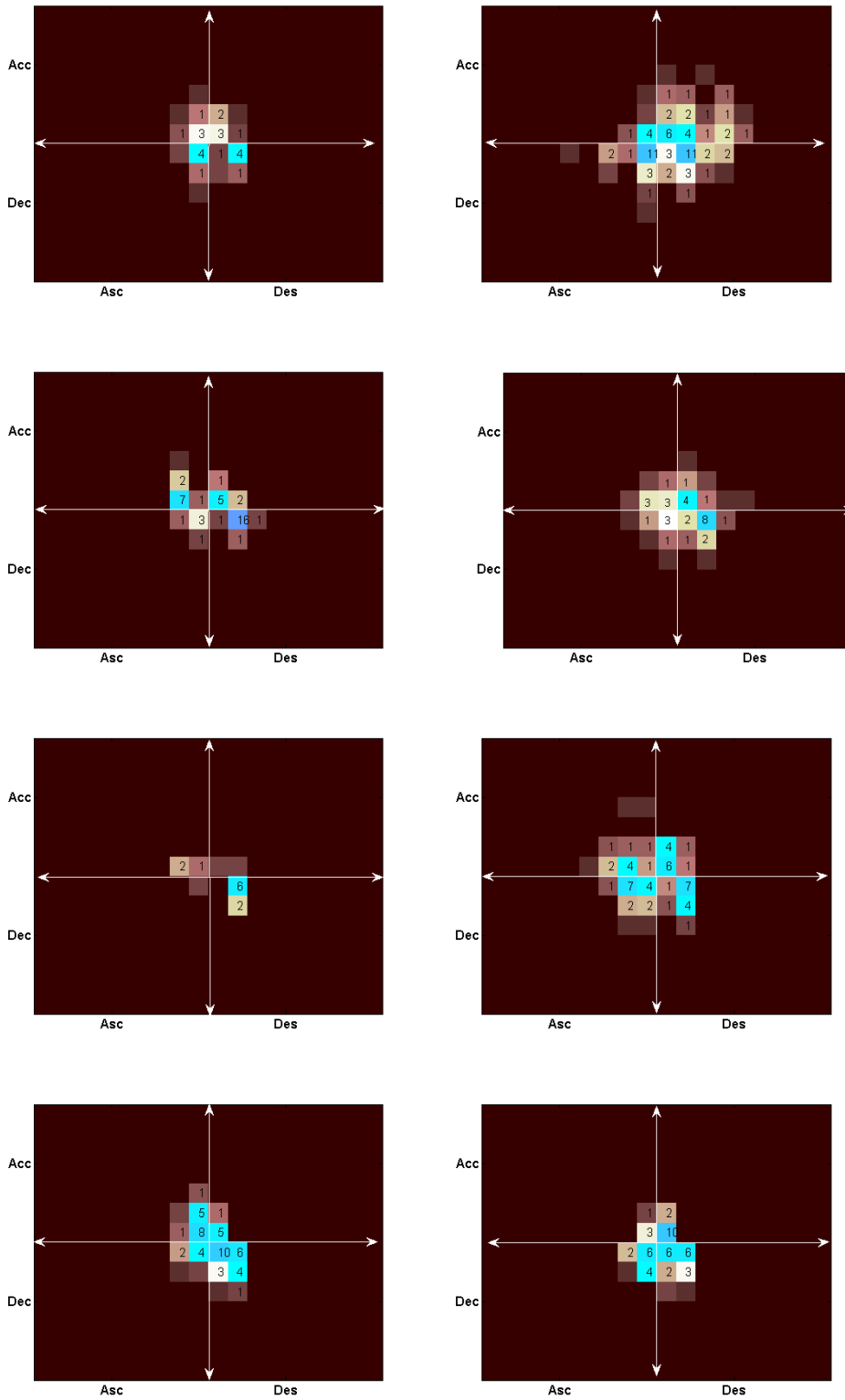


Figure G-2 AE feautre profiles of group H2 knees



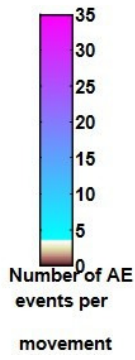
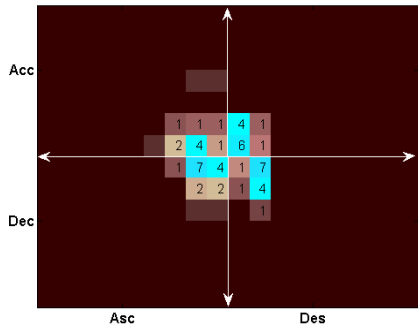
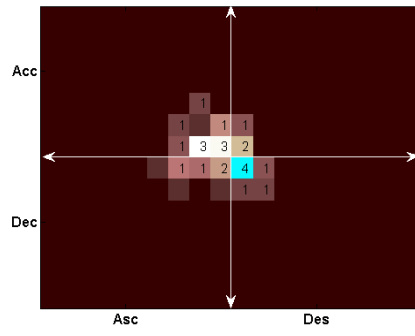
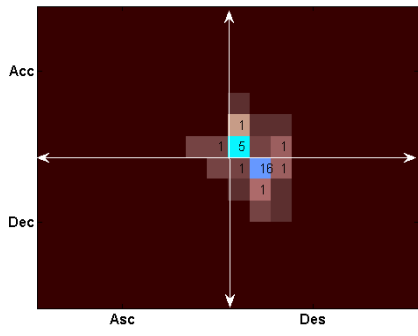
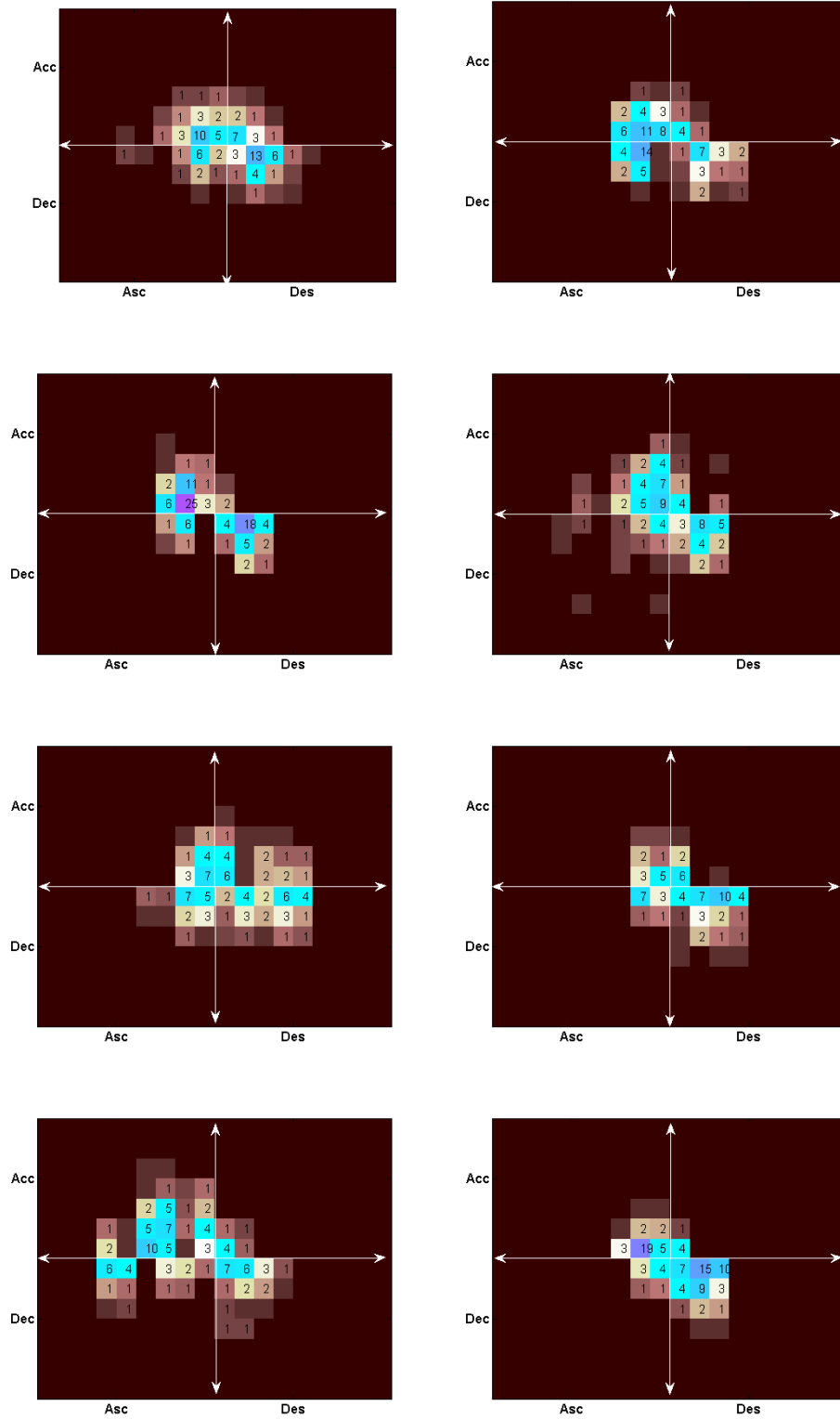


Figure G-3 AE feature profiles of group H3 knees



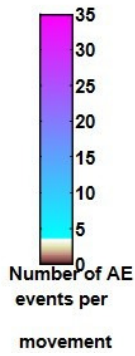
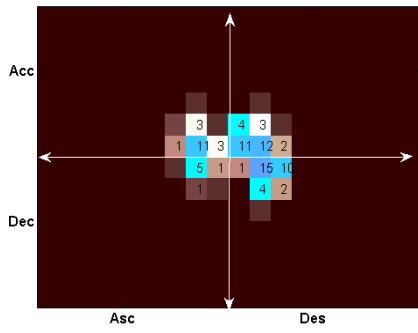
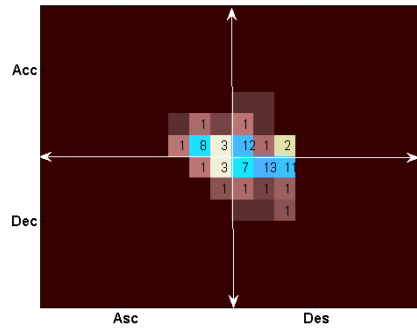
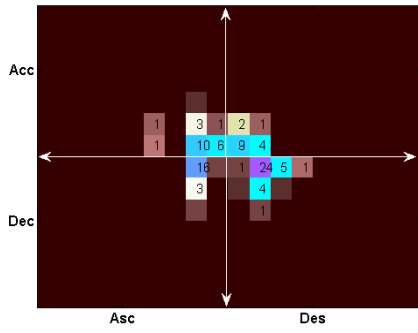
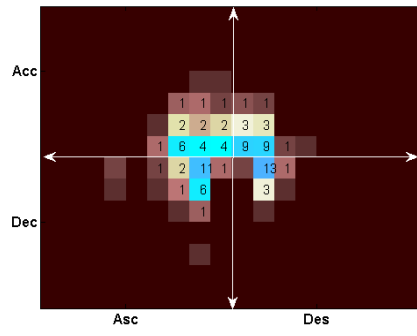
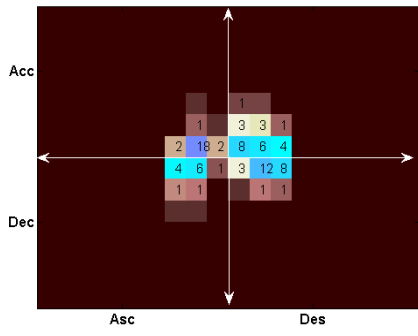


Figure G-4 AE feature profiles of group OA1 knees

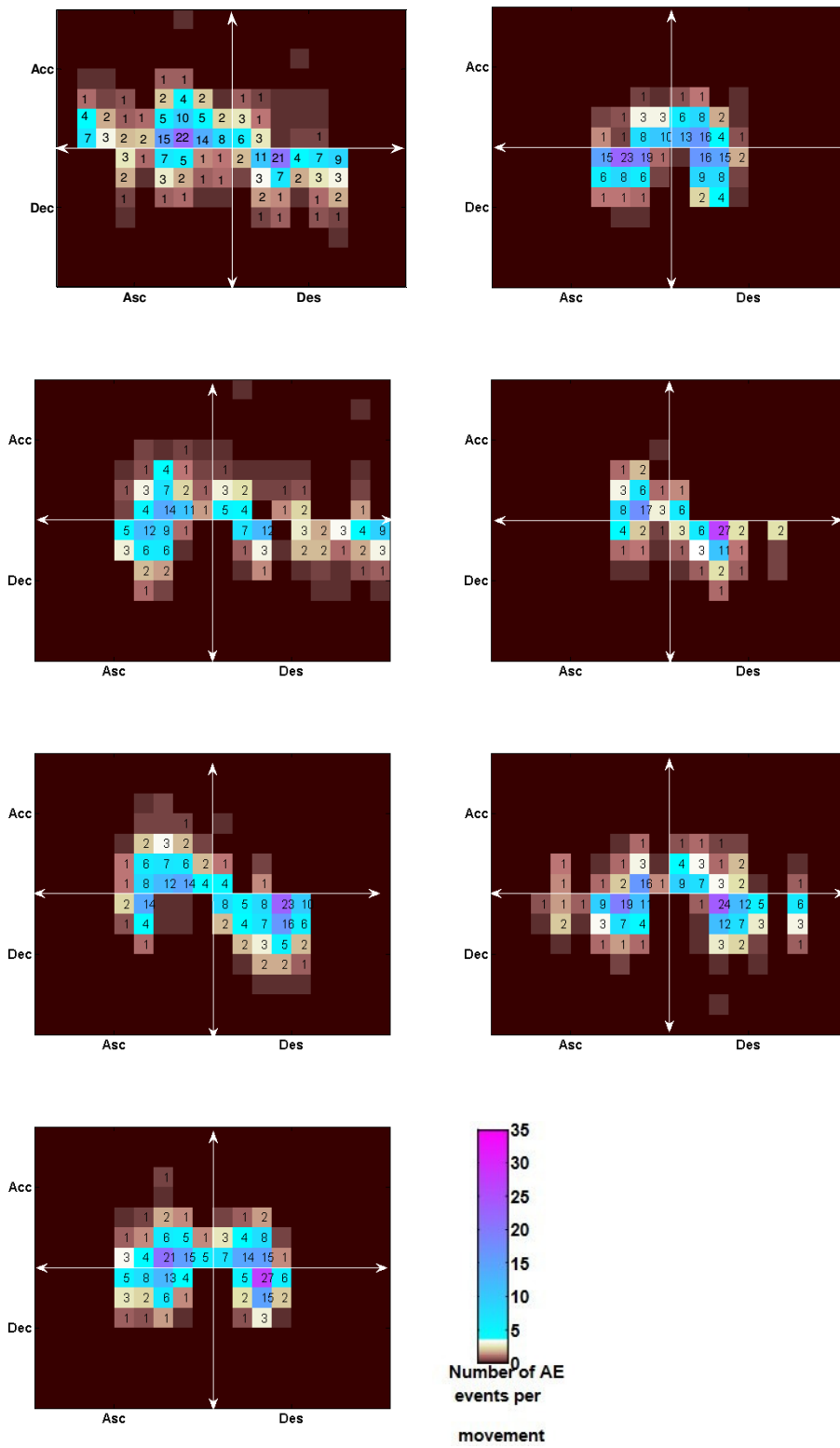
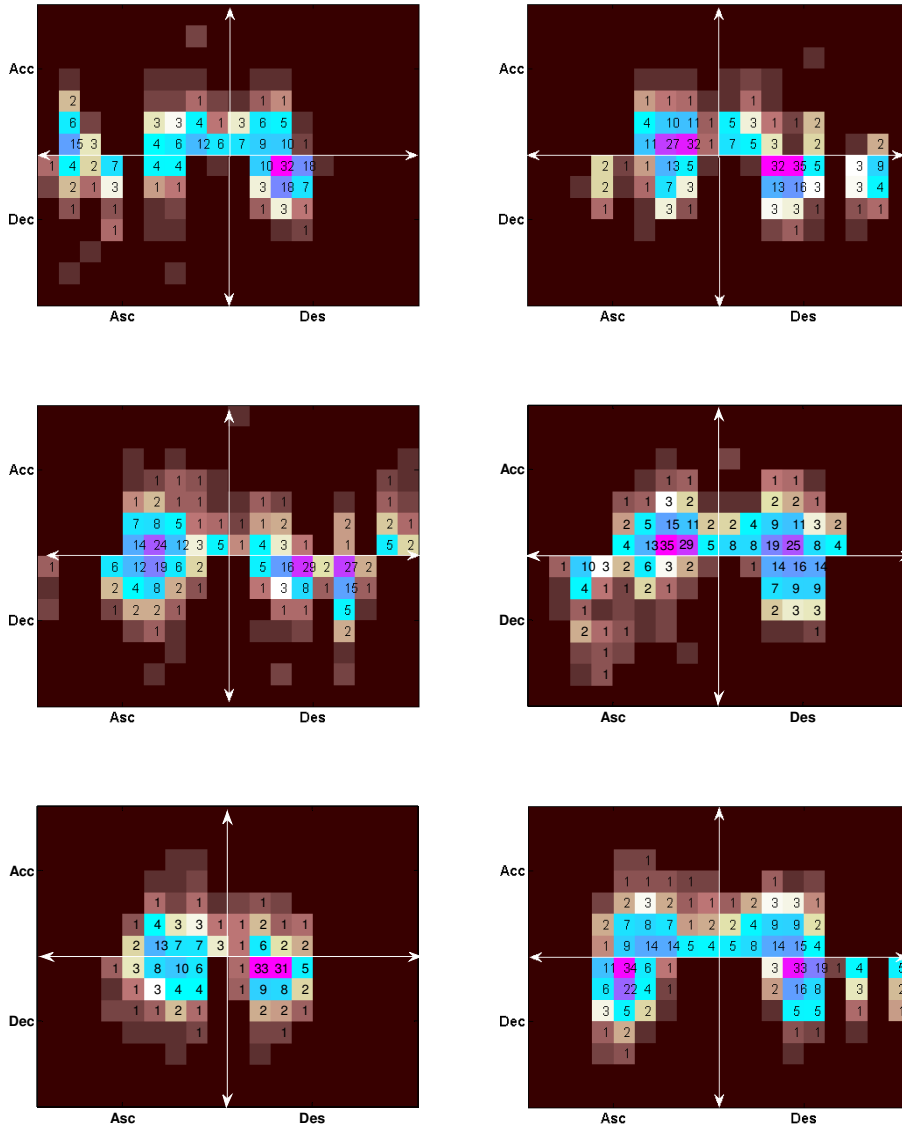
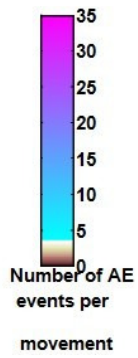
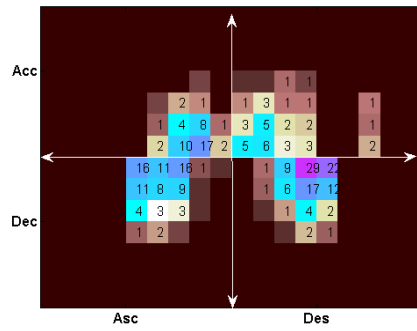
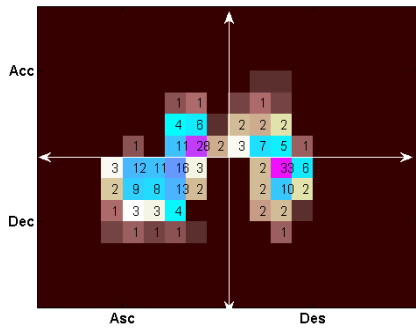
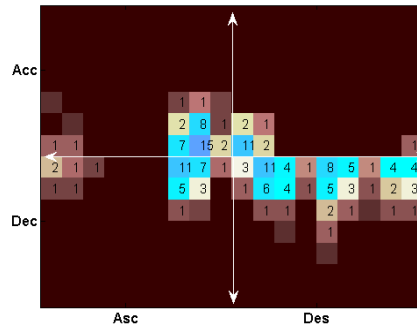
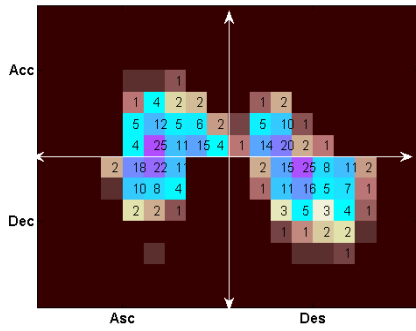
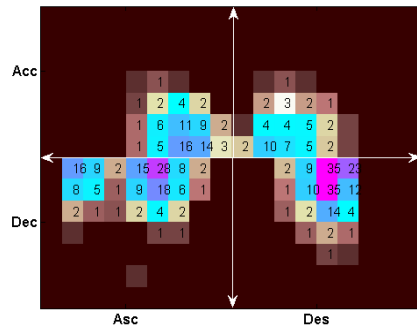
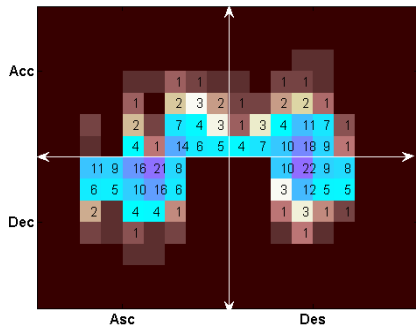


Figure G-5 AE feature profiles of group OA2 knees





APPENDIX H PUBLICATION LIST

- [1]. **Chen, H., Mascaro, B., Shark, L-K and Goodacre, J.** *Signal analysis and classification of joint movement based acoustic emission from health and osteoarthritis knees.* 1st biosensing technology conference, 2009.
- [2]. **Shark, L-K., Chen, H and Goodacre, J.** *Discovering differences in acoustic emission between healthy and osteoarthritic knees using a four-phase model of sit-stand-sit movements.* J Open Med Infor: Special issue on "Intelligent signal and image processing in eHealth", 2010; (4): 116-25.
- [3]. **Shark, L-K., Chen, H and Goodacre, J.** *Knee acoustic emission: a clue to joint ageing and failure.* Rheumatology, 2010, 49: Supl(1), i78-80 .
- [4]. **Shark, L-K., Chen, H and Goodacre, J.** *Knee acoustic emissions: a potential biomarker for quantitative assessment of joint ageing and degeneration.* Med Eng Phy, 2011, 33: 534-45.